5. SURFACE CHARACTERIZATION OF ORIGINAL AND MODIFIED CBs

In order to characterize the modification produced on the surface of the CB's during the presented treatments at LPP and APP, several studies were carried out concerning the CB morphology, surface structure, surface chemistry and energy. These parameters are considered to be the ones which have a very high influence in the final properties and capabilities of the carbon powders such as CB. As example of these behavior some final applications will be also tested in chapter 6 (polymer reinforcement) and chapter 7 (CB as oxygen reduction catalyst in Fuel Cells).

5.1 CB Morphology

As it has been presented in chapter 2, many techniques have been developed over the years in order to be able to characterize the parameters which are responsible for CB behavior. Specific surface area and microporosity have been used since very long ago as two of the parameters that play a key role on the final properties of the CB (D. Rivin 1972 and J. Janzen 1982). Although some authors do not accept surface area measurements as a true value due to the artifacts assumed by the mathematical models, it is true that it is related with the particle (aggregate) size and that can be very useful when comparing an original with a modified CB. Following, the results for low pressure nitrogen isotherms as well as some obtained parameters such as specific surface area by BET, STSA and microporosity are presented as a comparative way for non modified and modified CB grades.

5.1.1 Nitrogen Adsorption Isotherms (@ 77K)

As it has already been stated, specific surface area has been for a long time one of the most characteristic parameters to define CB grade as it was defined as being very close related to the final performance of this powder. Because specific surface area defines the amount of CB surface exposed to certain media it is usually determined by the adsorption of molecules with well-known cross-section area. Iodine and nitrogen adsorption are the most utilized techniques to characterize this parameter at industrial level. However, possibility of I_2 to react with some CB surface groups and therefore give a smaller specific surface area value, has given the nitrogen adsorption a higher reliability (W.M Hess and C.R. Herd 1993). It should also be mentioned that N_2 adsorptions isotherms have not only been used to determine specific surface area, but in some cases it have also been reported to be able to establish energy differences between several regions on CB, as well as to determine the dispersive surface energy of the filler (A.Lapra et al 2004, D. Pantea et al. 2002 M. Kurk et al 2002 and M. Heuchel et al. 1993). Further information

about energy surface analysis of CB will be given in further on in this chapter with more detail.

Another important parameter close related to the specific surface area is surface microporosity. Depending on the molecule size used to calculate specific surface area, it can penetrate in the porous of the surface of the carbon. In the case of I_2 and N_2, the molecules are able to enter all the porous (including the ones at the micro range) giving a total measurement of the surface. During a long time larger molecules such as CTAB (cetyltrimethyl ammonium bromide) have been used in order to calculate the external surface area of the CB as these large molecules can not enter in the porous and reach the surface inside. Other approaches using the data obtained from the N_2 adsorption isotherms can also be used to determine the meso, macro and microporosity of carbon surfaces as will be presented (P.A Webb at al.1997).

In this work, nitrogen adsorption at nitrogen liquid temperature (77K), has been used to study the changes produced in the specific surface area and microporosity during plasma modification. The study has been carried out in other to be sure that observed effects in posterior experiments could not be attributed to an increase or decrease of the specific surface area of the utilized carbon black but only to the modification itself.

For this purpose, experiments where carried out on a static volumetric adsorption analyzer (Gemini V from Micromeritics). The mass of a given CB used for the measurements was chosen depending on its specific surface area and was between 0.1g and 0.3 g. Before the measurements the samples were degassed under a nitrogen flow at 250ºC, using the Flow Prep modulus from Micromeretics to ensure the evaporation of adsorbed water. A minimum surface to give of a total N_2 adsorption above $4m^2$ should be present in each test in order to ensure reproducibility. Free volume of the tubes with the samples were determined by helium measurements before the nitrogen adsorption run. A minimum of 13 points were obtained in a range of 0.3 to 0.3 P/Po for each sample as it is the range used to calculate specific surface area by means of BET approach. However as it will be presented, this range can be narrower when high microporosity is present on the surface of CB, this effect has to be taken into account when evaluating collected data. Range used for each CB in order to adjust the mathematical models is presented later on in Table 5.3. Curves where repeated 3 times obtaining a relative error of 3%.

As it will be further explained the BET isotherm model was used to calculate specific surface area as already mentioned above, while the t-plot approach was used to the determine the Statistical Total Surface Area (STSA) which is the total area excluding mircoporosity. This value is also important as the surface inside microporous may not always get in contact with the external molecules as for example long polymer chains.

However, because mentioned approaches are based on mathematical approximations it is important also to observe the raw data obtained from the nitrogen adsorption isotherms. Following the results are presented for LPP and APP modified CB's. In order to give an

overview of the studied parameters obtained from the nitrogen adsorption isotherms using the Gemini V, the adsorption isotherms original carbons N.134, XPB171 and Vulcan are presented next in Fig.5. 1. From the figure is easy to observe that XPB presents a much higher adsorption capacity than Vulcan and N-134 which are closer to each other. The higher slope presented by XPB171 also indicates a higher adsorption capacity. However it is here difficult to observe changes in microporosities which will be presented later.

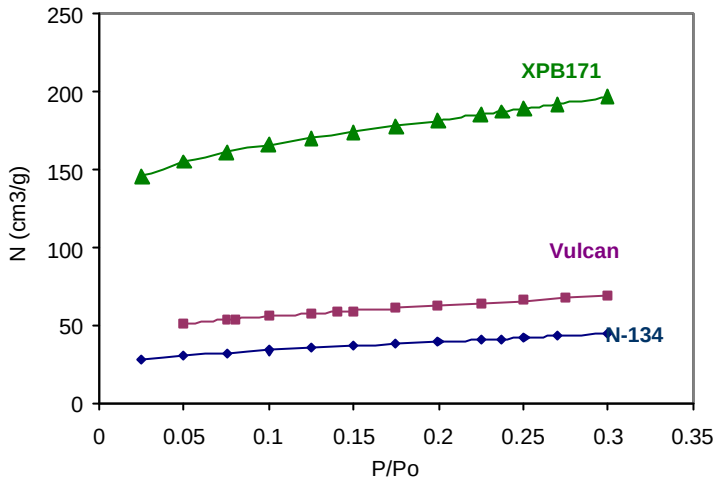

Fig.5. 1 N_2 Adsorption Isotherms for N-134, XPB171 and Vulcan CB's

When the adsorption curves for the different N-134 used types are observed (Fig.5. 2), some differences can also be seen. N-134 presents a higher adsorption than N134e and N-134g. However, it can also be observed that while N134 and N-134e present a similar trend and slope, the situation is different for N-134g. In this case changes in slope are observed which indicates that not only a lower monolayer coverage but also it can also indicate a change in surface roughness, fractal dimension and energy (A. Schroeder et al. 1999 and M. Kurk et al 2002). As it can also be observed, the maximum curve separation can be found in the data obtained in the region above 0.3 P/P_o while for lower values all three curves seem to convert. Adsorption values at low P/P_o are related to high energy sites (crystallite edges), therefore the curves seem to indicate that main difference between N-134 and N-134g are found in the low energy sites, while on the other hand, high energy sites seem to be present in both cases at similar level. As a matter of fact it has been described that for very low P/P_o between 0.1 and 10^{-5} adsorption on graphitized CB can be higher than for original grades (H. Darmstadt et al. 2001, M Kurk et al. 1999)

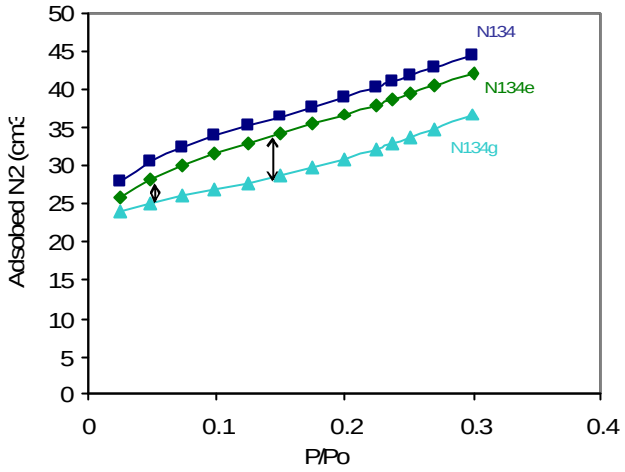

Fig.5. 2 N_2 Adsorption Isotherms for N-134 CBs indicating maximum differences at high P/Po levels (low energy sites)

On the other hand when results for N134e are examined, a non expected effect is observed. It is well-known that impurity extraction will expose crystallite edges which where previously covered and consequently a higher surface energy is normally observed after extraction. Therefore, the obtainment of higher nitrogen adsorption capacity could be expected, however, the results indicate an opposite trend. Although this effect is difficult to explain only looking at the isotherm data, further analysis will help to understand this phenomenon which is related to a change in the microporosity of the surface upon extraction.

Next, isotherms are presented for LPP and APP treatments. Treatment parameters for LPP are presented at table Table 5. 1.

Table 5. 1 Modification Parameters for LPP treatments

Reactive Gas	Generator Power (W)	Duration (min)
Oxygen	**40**	**15**
Nitrogen	**40**	**30**
Ammonia	**40**	**30**

For APP treated samples, only one cycle treatment was applied and in the case of NH_3 flow was 2L/h.

Obtained isotherms after plasma treatments are presented next. In all cases isotherms were type 2 as described by the ASTM norm.

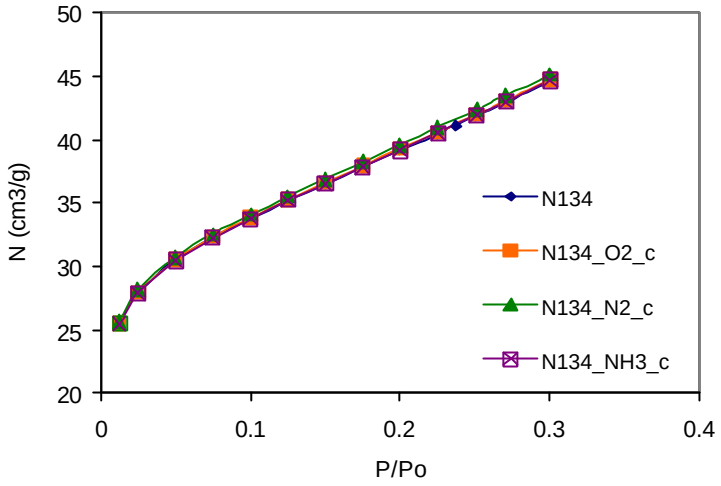

Fig.5. 3 N_2 Isotherms for N-134 before and after LPP Modification

In the case of N-134 modification with LPP isotherms before and after modification are practically identical indicating that N_2 adsorption capacity has not changed after the treatment. Whether the adsorbed impurities help to preserve this property will be discussed in more detail later on, as well as the effect of the plasma treatment on the surface impurities. However, some interesting information is given here in advance as it is thought to be relevant to explain these results. Due to the low pressure conditions and plasma attack to the CB surface an ablation process of the adsorbed impurities could take place during the modification. Therefore, an extraction after plasma treatment was performed to study this phenomenon. Results are presented later in this chapter, where it is observed that LPP modification does not diminish the amount of impurities on the CB. Consequently, it is thought that the modification due to the plasma reaction does not take place on the CB surface itself but on the impurities molecules.

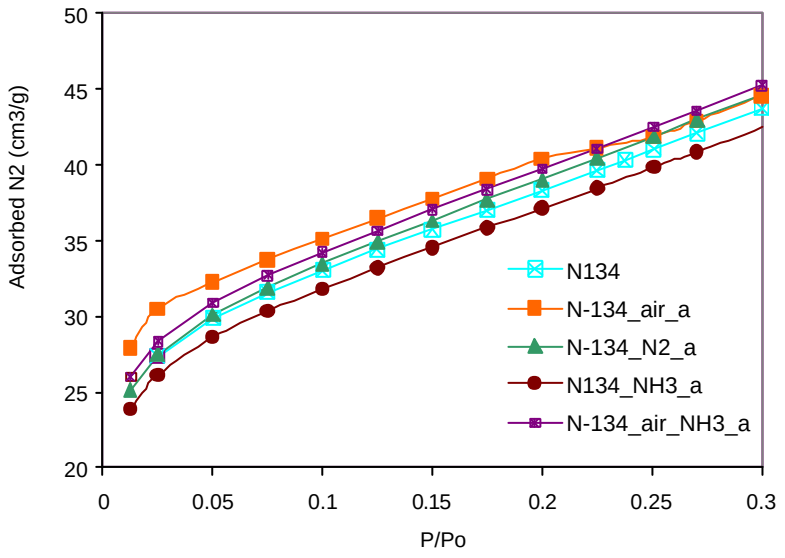

Fig.5. 4 N_2 Isotherms for N-134 before and after APP Modification

On the other hand, when samples are analyzed after APP treatment although not dramatic, some differences can be observed in the N_2 adsorption isotherms.

While almost no differences are observed for nitrogen APP treated N-134 changes are observed for the air plasma treated N-134, in this case a higher nitrogen adsorption is observed although at high relative pressure adsorption is equivalent. This could be related to the Van der Waals interaction that takes place in this multilayer adsorption zone, indicating that a first layer of nitrogen covers all new surface groups. Contrary to the previous case, atmospheric air plasma treatment does produce a reduction of the amount of the surface impurities level (being 80% lower), which could be related to this change in adsorption capacity.

Very similar results where obtained when N134g was modified by means of oxygen LPP. In this case the N134g_O_2_c also shows a higher adsorption capacity at low relative pressures while level is decreased to the one of N134g above 0.25 P/Po. This could indicate that both atmospheric air plasma on N134 as well as oxygen LPP on N134g, do provide a modification on the CB real surface. Moreover, in Fig.5. 5 it can be observed that all isotherms follow the inverted slope similar to N134g, which indicates a lack of low surface energy zones and a higher density of high energy sites especially for the oxygen plasma treated sample.

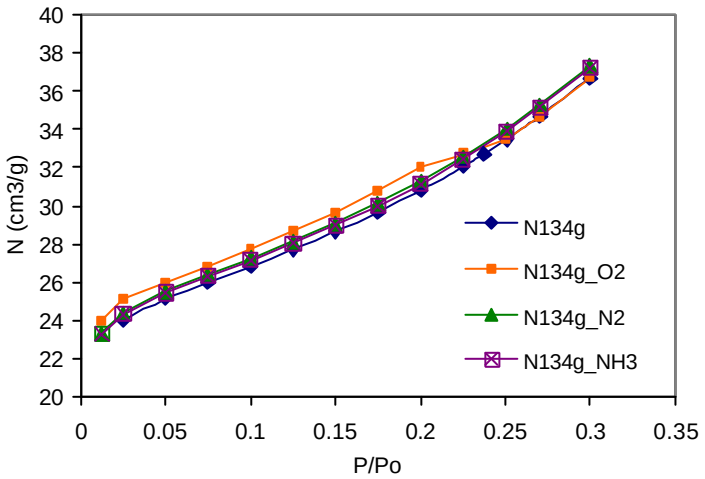

Fig.5. 5 N_2 Isotherms for N-134g before and after LPP Modification

It could be expected that N134e behaviour was similar to the one presented for N134g due to the lack of surface impurities on the CB. However, in this case all plasma modified samples present a very similar nitrogen adsorption capability slightly higher than the one presented by the original N134e which would correspond to a behaviour in between too extreme cases N134 and N134g. The results show that not only surface chemistry is

important but also surface structure to determine a final composition of the CB after modification, and probably the combination of these two factors are the driving force for the final properties of the material. Further studies presented during this work will be focused to clarify which is the role of each parameter during modification.

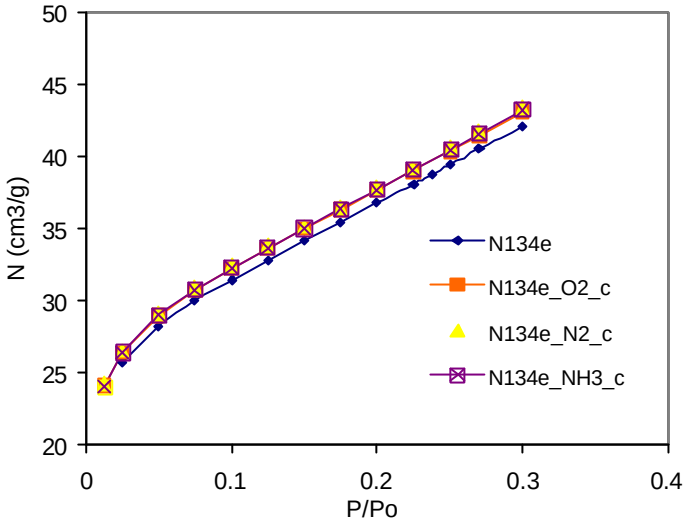

Fig.5. 6 N_2 Isotherms for N-134e before and after LPP Modification

Following the curves for XPB171 both at LPP and APP conditions are presented. In this case similar trends are observed in both cases. Contrary to the already presented results for N134, modification with air APP as well as with oxygen LPP gives a final material with lower nitrogen adsorption. This effect is slightly more visible in the case of LPP which curve is still different at very low P/Po indicating a probable change in the microporosity of the material. This effect although it could seem controversial with the previous results obtained with N134 can be explained due to the large porosity of the material. The oxygen plasma attack may convert some microporous in macroporous decreasing the total surface but increasing the total external area, but it can also occur that the oxygen groups are located in the entrance of the microporous blocking the entrance of the nitrogen molecules. This effect was already observed when active carbon was modified by oxygen LPP by the group of J.P Bodou et al. (J.P. Bodou et al. 2000). As a conclusion, surface initial structure seems to play a key role in defining the final properties of CB after modification.

On the other hand nitrogen and ammonia plasma at low pressure seem to increase in a similar way the nitrogen adsorption with no changes in the microporosity region. This effect is not observable for the nitrogen and ammonia atmospheric samples, but it has to be pointed out that for these two cases the difference is much narrower than for the oxygen containing samples and therefore results should carefully studied.

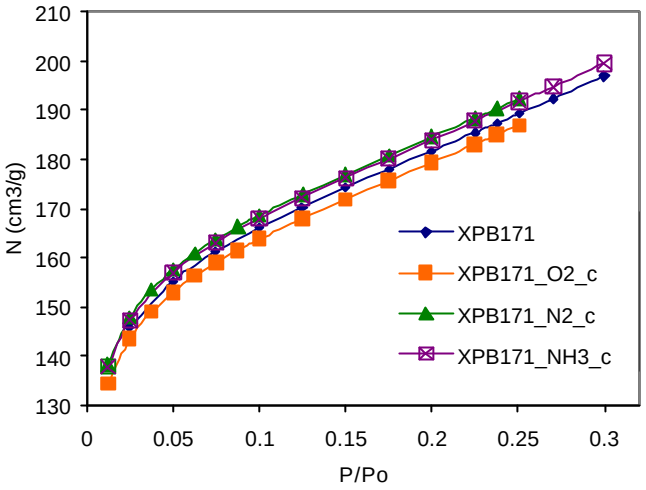

Fig.5. 7 Isotherms for XPB171 before and after LPP Modification

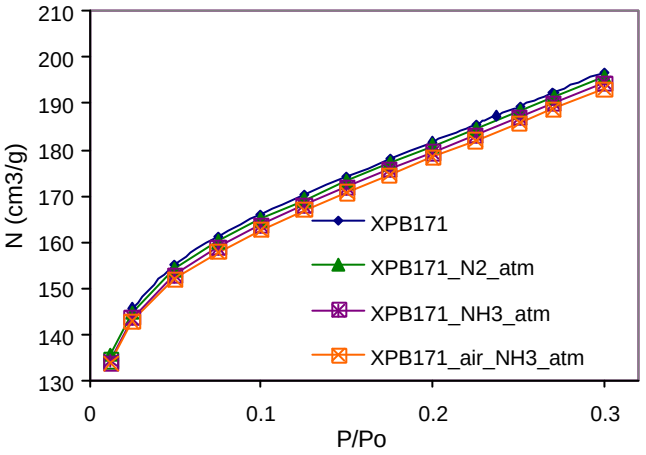

Fig.5. 8 Isotherms for XPB171 before and after Atmospoheric Plasma Modification

Finally, Fig.5. 9 shows the isotherms for Vulcan after low pressure plasma modification. The results follow the same trend as for XPB 171with higher adsorption for both nitrogen and ammonia plasma which could not be observed in N134 probably due to the presence of the impurities, but could be also observed for both N134g and N134e.

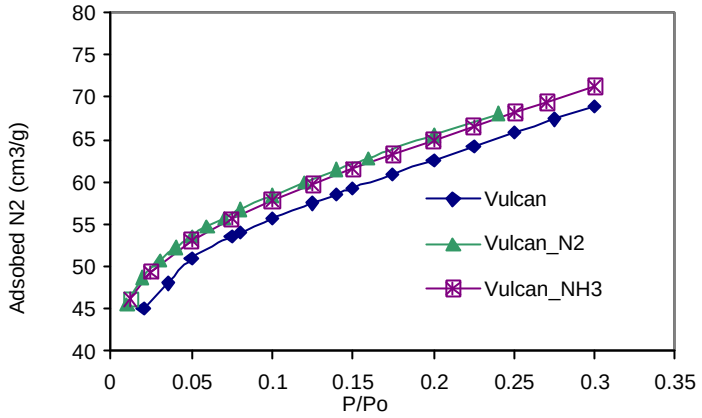

Fig.5. 9 Isotherms for Vulcan before and after LPP Modification

Summarizing the results obtained by studying the nitrogen adsorption isotherms it can be said that as expected, evident differences in nitrogen adsorption were seen between the different selected CBs N134, Vulcan and XPB171 (XPB171> Vulcan> N134 which is to a large extend related to its specific surface area and particle size as will be also presented next. Studying N134 it has been observed that both extraction and graphitization treatments do affect the nitrogen adsorption capacity as lower adsorption levels are observed (N134>N134e>N134g). The disappearing of the surface impurities in N134e and the replacement of amorphous carbon by graphitic planes with lower energy and flatted in the case of N134g are responsible for these results.

Although no changes were observed for the isotherms obtained after LPP treatment on N134, it was possible to observe differences between the curves both after graphitization and extraction. Changes are also observed for the APP treatments on N134, this effect is more relevant after the air plasma treatment and is probably caused by the removing of a large extend of surface impurities during this type of treatment as will be shown in later in section 5.4.4.

A first hint about the dependence of oxygen plasma reactivity on the surface structure of the carbon black has also been observed. Higher adsorption was shown after oxygen LPP for N134e and N134g (containing very few microporous) while XBP171 which presents a very high microporosity (half of its surface approximately) decreased its nitrogen adsorption capacity after the same treatment. This result is in good agreement with chemical composition analysis that will be presented further on in this chapter.

5.1.2 BET and STSA

For all presented cases, specific surface area value was determined by means of the BET approach. This mathematical model includes the possibility of multilayer formation on the analyzed surface which happens to be the case for CB as was also shown by other

studies. When Langmuir model was applied it was observed that for all carbons BET theory was better than the former, as observed due to a better correlation coefficient. Fig.5. 10 and Fig.5. 11 show an example which is common for all obtained results. This effect is because Langmuir theory does not take into account the possibility to obtain multilayer adsorption, consequently the values obtained using this theory are much higher (and probably excessive) for the measured carbons as can be observed in Table 5. 2. This effect was already observed by (V Gomez-Serrano et al. 2001)

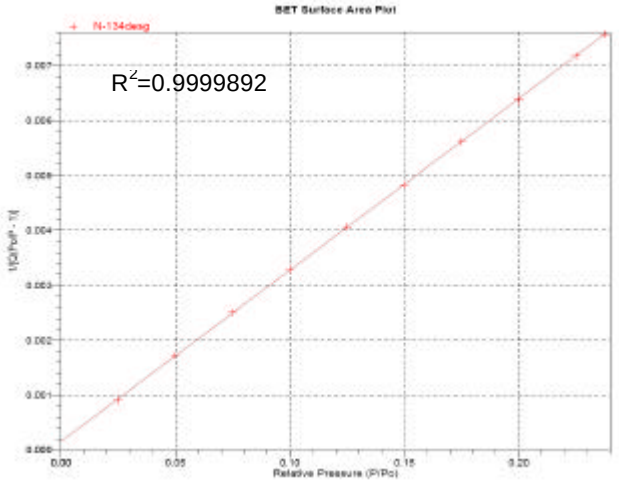

Fig.5. 10 BET regression for the nitrogen adsorption data on CB

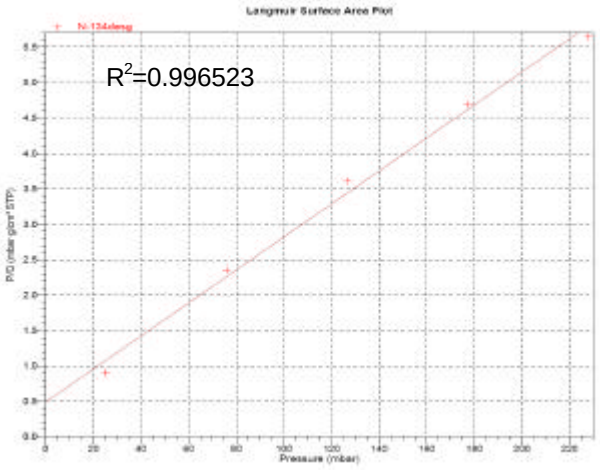

Fig.5. 11 Langmuir regression fort he nitrogen adsorption data on CB

Table 5. 2 Specific surface area determined by BET and Langmuir approaches

CB grade	BET specific surface area (m^2/g)	Langmuir Specific surface area (m^2/g)
N-134	**138.74 ± 0.23**	**186.84 ± 9**
Vulcan	**220.63 ± 0.9**	**253.93 ± 5**
XPB 171	**656.49 ± 3.1**	**836.85± 23.15**

BET regression for specific surface determination does not only allow to calculate specific surface area but also other interesting parameters form the used equation (eq. 5.1).

$$\frac{P}{V_a(Po-P)} = \frac{1}{VmC} + \frac{C-1}{VmC}\left(\frac{P}{Po}\right) \qquad \text{eq.5.1}$$

where C corresponds to: $$\exp\frac{q1-qL}{RT} \qquad \text{eq.5.2}$$

q_1 equal to the heat of adsorption of the first layer
q_L equal to the heat of liquefaction of the adsorptive
Va: N_2 volume adsorbed in a monolayer.
Vm: N_2 volume adsorbed at the measurement point
P: Pressure at the measurement point
P_0: Vapor pressure of adsorptive specie

In Table 5.3 specific surface area and C and V_a values are presented. In this table the P/Po range used to evaluate specific surface is also presented. In order to select this range one of the main facts is that intercept should be never negative, as otherwise C or V_a would have a negative value with no physical sense. Because adsorption heat trends to be higher for microporous geometries, normally higher C values also indicate a higher microporosity which usually reduced the linearity region to P/P_o near 0.15.

Two other values can also be found in this table, STSA and microporosity. These two parameters were calculated using the t-plot approach of Lippens and de Boer which has been widely used for this purpose by other research groups (R.H. Bradley et al. 1996, M. Kurk et al 1996 refs), where t represents the thickness of the adsorbed layer represented in Angstroms. The t-plot corresponds to the representation of the adsorbed amount versus the thickness. In

Fig.5. 12 and Fig.5. 13 examples of the extrapolation plot used to estimate the mentioned values are presented both for a high microporous material XPB171 and for a non-microporous material, evident differences are observed.

As it can be seen in the mentioned examples, for non microporous material t-plot it gives a straight line which goes through the 0.0 point. On the other hand extrapolation of the linear region of the t-plot obtained for microporous materials gives a positive intercept equivalent to the microporous volume. However, the limitation of this method is the lack of information about the microuporous diameter distribution. Nevertheless, it is very useful to compare CB samples before and after being modified. As presented results correlates with the expected values as for it has been presented before, XPB171 is a high microporous material while N134g does present a very flat surface with almost no microporosity

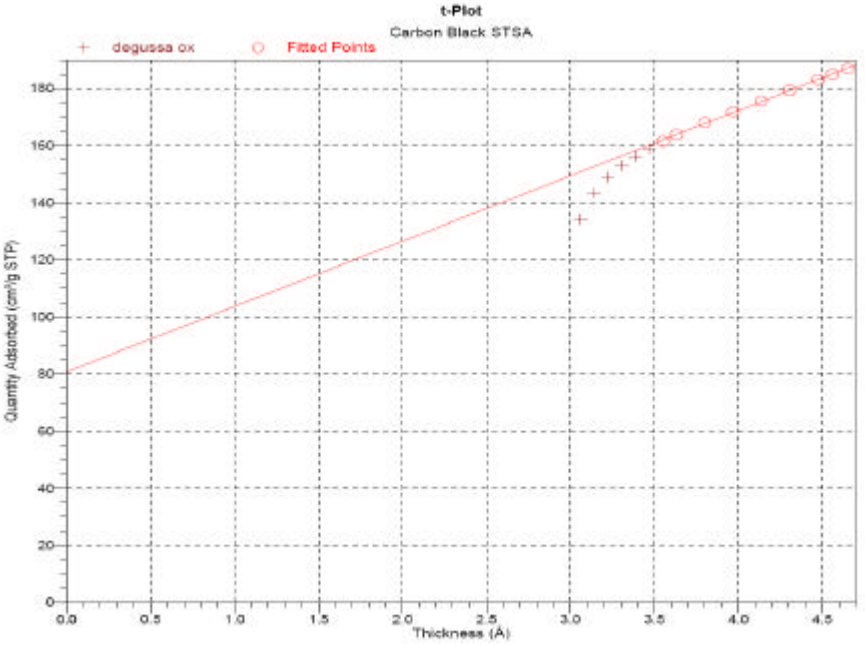

Fig.5. 12 t-Plot used for STSA and microporosity calculation for XPB171

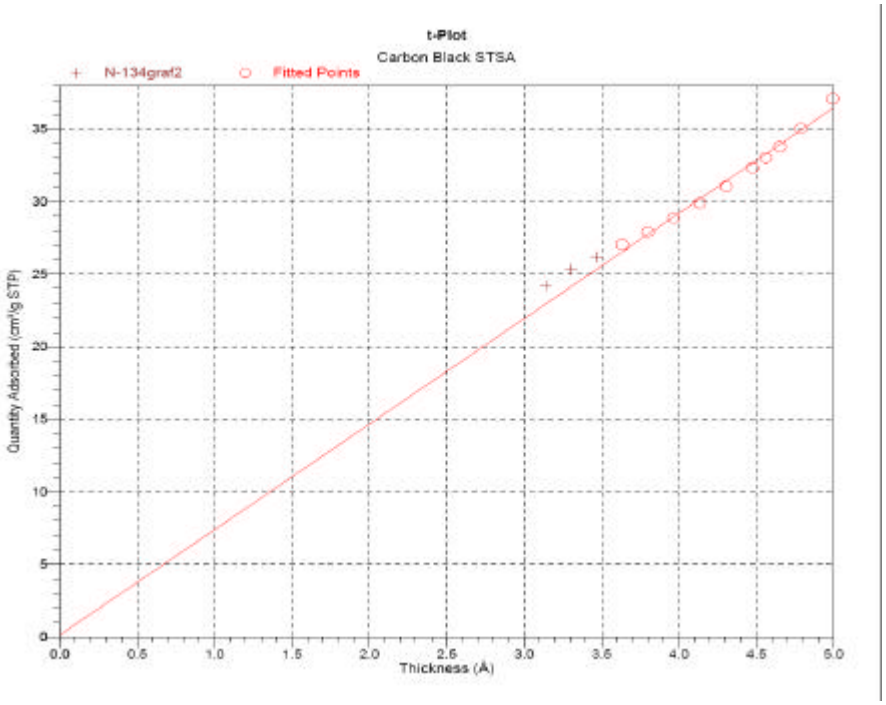

Fig.5. 13 t-Plot used for STSA and microporosity calculation for N134g

.

Table 5. 3 Data obtained from the nitrogen adsorption isotherm analysis using BET and t-plot approach

CB type	BET (m^2/g)	STSA (m^2/g)	Microporosity (m^2/g)	C	Na	P/Po Linearization Range
N134	138.54	121.92	16.62	198.21	31.97	0.03-0.24
N134_O_2_c	138.30	122.77	15.53	239.79	31.77	0.03-0.24
N134_N_2_c	139.13	125.35	14.77	210.26	32.19	0.03-0.24
N134_NH_3_c	138.59	123.20	15.38	217.10	31.83	0.03-0.24
N134_N_2_a	138.51	127.32	11.18	192.39	31.81	0.03-0.24
N134_(N_2+NH_3)_a	131.80	120.60	11.20	189.91	30.27	0.03-0.24
N134_air_a	135.92	121.42	14.50	215.66	31.22	0.03-0.24
N134_air_(N_2+NH_3)_a	140.43	124.68	15.75	225.04	32.26	0.03-0.24
N134g	108.45	108.45	-----	474.033	24.91	0.03-0.24
N134g_N_2	109.82	97.36	12.46	445.83	25.23	0.03-0.24
N134g_O_2	115.33	115.33	------	270.49	26.49	0.03-0.24
N134g_NH_3	109.31	109.31	------	472.17	25.11	0.03-0.24
N134e	131.14	122.94	8.20	158.29	30.12	0.03-0.24
N134e_O_2_c	133.60	123.48	10.11	187.59	30.69	0.03-0.24
N134e_N_2_c	134.25	124.29	9.96	187.63	30.83	0.03-0.24
N134e_NH_3_c	134.07	124.17	9.90	180.40	30.79	0.03-0.24
XPB171	656.49	347.38	309.10	797.27	150.80	0.03-0.14
XPB171_O_2_c	649.12	353.72	295.40	698.00	149.11	0.03-0.14
XPB171_N_2_c	668.10	305.47	362.62	714.05	153.47	0.03-0.14
XPB171_NH_3_c	660.10	356.01	304.08	942.19	151.63	0.03-0.14
XPB171_N_2_a	648.28	348.66	299.59	1874	147.63	0.03-0.14
XPB171_(N_2+NH_3)_a	643.50	348.02	295.49	1726.97	146.56	0.03-0.14
XPB171_air_(N_2+NH_3)_a	643.97	344.99	298.87	713.92	147.93	0.03-0.14
Vulcan	222.27	153.26	60.01	396.14	51.02	0.03-0.17

Vulcan_O_2_c	**220.37**	**156.92**	**63.45**	**375.12**	**50.62**	**0.03-0.17**
Vulcan_N_2_c	**233.72**	**161.76**	**71.95**	**385.44**	**53.69**	**0.03-0.17**
Vulcan_NH_3_c	**231.46**	**152.04**	**79.42**	**4.2.77**	**53.17**	**0.03-0.17**

As it can be observed in the table above, different linearization ranges where used for the BET regression depending on the CB sample. As explained, this range is restricted mainly by the obtainment of a positive intercept in the Y axis which makes possible the calculation of C and V_a parameters. As it is also usual, low microporous materials such as N134 enable the BET regression to be done in a wider pressure range while high microporous materials such as XPB171 limit the range up to 1.4 P/P_o.

As it could be also seen directly form the nitrogen isotherms N134e and N134g present a lower specific surface area. Graphitization produces a specific surface area reduction (calculated by means of BET linearization) about 20% of the original area while at the same time no microporous are detected. On the other hand, the extraction procedure does not have such a large impact on specific surface area although a 5% decrease is observed. However, what is very interesting in this case, is that the specific surface decrease is due to a low microporosity value (50% lower than original N134) while external surface presents the same values as for the original N134. This effect would clarify the unexpected lower specific surface value for the extracted material. In advance it could be thought that extraction of impurities should not affect or even increase the specific surface area of the CB due to an enhancement of its surface energy. But results seem to indicate that impurities form a microporous layer due to the partial aromaticity and unfinished nature of these materials at the surface of CB. Once extracted, the material has a similar surface area but microporosity decreases due to the lack of the impurity microporous layer.

On the other hand, no dramatic changes where observed on the plasma modified N134 grades. It is possible to observe that larger variations are observed for N134g and N134e than for the original N134 which is in agreement to the conclusion obtained from the visual study of the nitrogen adsorption isotherm. The same can be said for the results obtained after oxygen plasma treatment for Vulcan and XPB171 were slightly decrease in the specific surface are is detected. On the other hand it is also interesting to observe that N134g after nitrogen LPP has developed some microporosity, the reason could be an ablation effect of the nitrogen active species that could lead to the formation of new structures. This hypothesis will be further developed during this work.

It is obvious that differences produced by graphitization or extraction affect much more the specific surface area than the plasma treatments both at atmospheric or low pressure. However, as it will be seen in the next section of this chapter, no evident changes in surface specific does not mean that the surface has not been modified, but gives a very good first idea about the extend of this treatment. It can be concluded that plasma

treatment affects the very first layers of the CB surface without being an aggressive treatment as many others that have been presented in chapter 4 (S. J. Park 2003). This is a very interesting result and moreover when studying CB behavior in final applications the influence of variation in specific surface or microporosity is kept to the minimum.

For 5 CB (XPB171, XPB171_(N_2+NH_3)_a, XPB171_(N_2+NH_3)_a, N134 and N134e_NH_3_c) samples the test was performed in a ASAP 2000 apparatus from micromeritics, the difference between the two equipments is that the former can not reach very low relative pressures (P/Po under 0.05) were much of the information about CB energy and porosity is given. However, this is also a much longer time consuming technique. This automatic instrument is equipped with 1000, 10 and 1 Torr transducer and allows an accurate measurement for nitrogen adsorption at very low relative pressure starting from 10^{-6} to 10^{-7} mbar. The samples were selected due to they relevant role in the oxygen reduction catalyst as will be presented in chapter 7. In this application microporosity has been reported to play a very important role in the final activity of the catalyst (ref). Therefore ,some of the most active materials where studied to evaluate microporosity and porosity changes more precisely during plasma treatment.

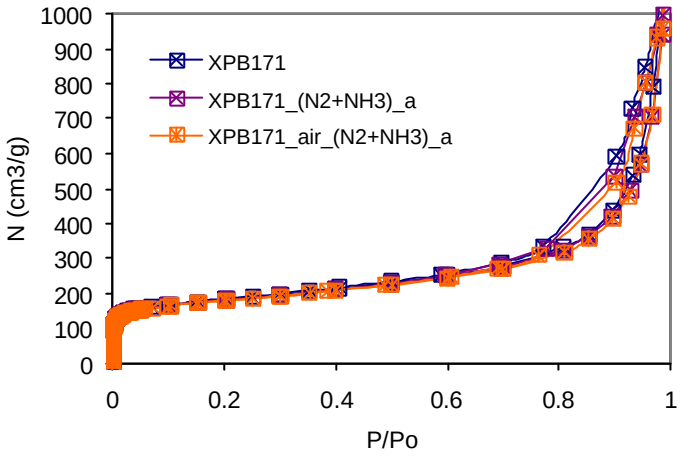

Fig.5. 14 Nitrogen Isotherms for XPB 171 grades using ASAP 2000

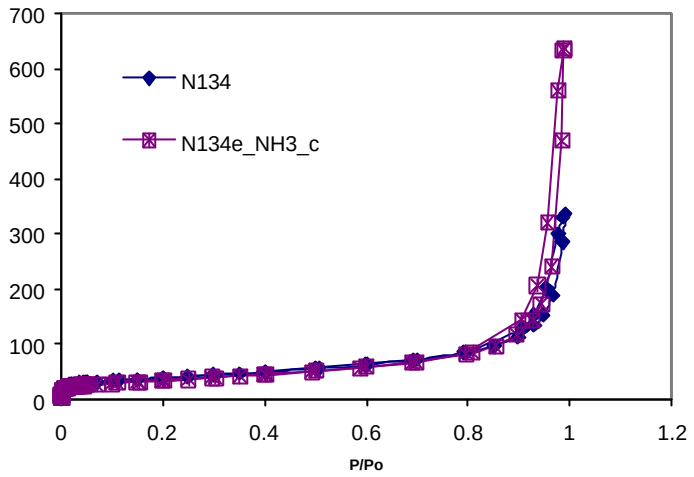

Fig.5. 15 Nitrogen Isotherms for N-134 grades using ASAP 2000

Fig.5. 14 presents the nitrogen adsorption isotherms for the XPB171 and Fig.5. 15 the ones for N134 grades. In both cases it can be observed that the number of points obtained at very low P/P_o values are much higher than the ones obtained in the previous experiments, consequently results are more precise when calculating microporosity levels.

Table 5. 4 presents both the values obtained with the Gemini V (G) and the ASAP 2000 (A). Although the numbers are not exactly the same error is always in a 5% margin which could be considered reproducibility error and a general trend was followed for all CB types. Again, the decrease in microporosity after the extraction was confirmed as could also be observed in the region for low P/Po presented for N134 in Fig.5. 16.

Table 5. 4 Comparison between Gemini V and ASAP 2000

CB type	BET (m^2/g)	STSA (m^2/g)	Microporosity (m^2/g)	C	Na	Apparatus
N134	**138.7**	**121.92**	**16.81**	**198.21**	**31.97**	**G**
N134	**140.24**	**123.60**	**16.63**	**206.07**	**32.2**	**A**
N134e_NH_3_c	**134.07**	**124.17**	**9.90**	**180.40**	**30.79**	**G**
N134e_NH_3_c	**126.73**	**120.50**	**5.23**	**157.36**	**28.99**	**A**
XPB171	**656.49**	**347.39**	**309.10**	**797.27**	**150.80**	**G**
XPB171	**666.65**	**348.37**	**318.27**	**717.91**	**153.14**	**A**

XPB171_(N_2+NH_3)_a	**643.50**	**348.02**	**295.49**	**695.97**	**146.56**	**G**
XPB171_(N_2+NH_3)_a	**648.70**	**342.29**	**306.41**	**705.69**	**153.27**	**A**
XPB171_air_(N_2+NH_3)_a	**643.97**	**391.43**	**252.54**	**713.92**	**147.93**	**G**
XPB171_air_(N_2+NH_3)_a	**643.97**	**344.99**	**298.87**	**786.27**	**149.39**	**A**

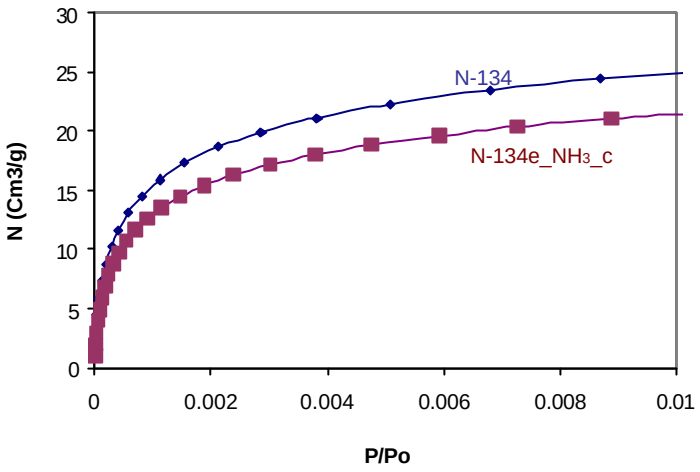

Fig.5. 16 N_2 Adsorption at low P/Po range for N-134 grades

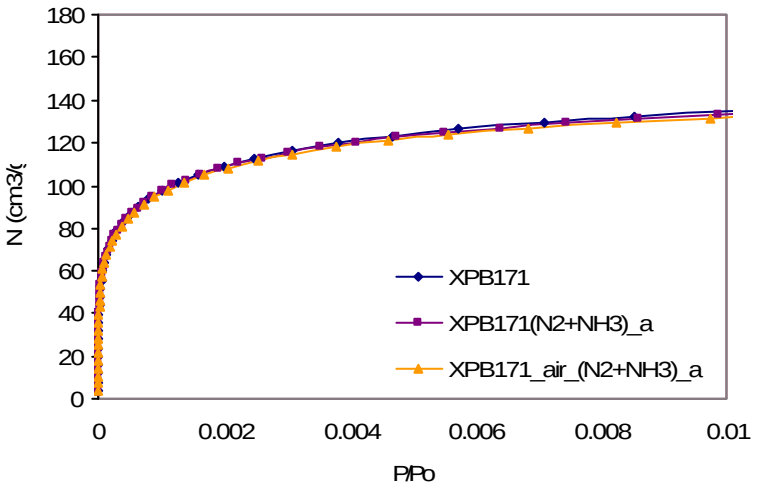

Fig.5. 17 N_2 Adsorption at low P/Po range for N-134 grades

As it has been said in this case not only specific surface area and microporosity were calculated but also porosity distribution in the meso and macro range. A porous sample including the former previous range presents and hysteresis in the adsorption desorption curves as the one that can be observed in Fig.5. 14 and Fig.5. 15 in the range between 0.5 and 1 P/Po. Normally the larger the area between the two curves the higher the volume and area that form the meso and macro porosity. Some differences can be observed by only looking at the nitrogen adsorption however, BJH adsorption and

desorption were used in order to evaluate more precisely the differences between the CB's.

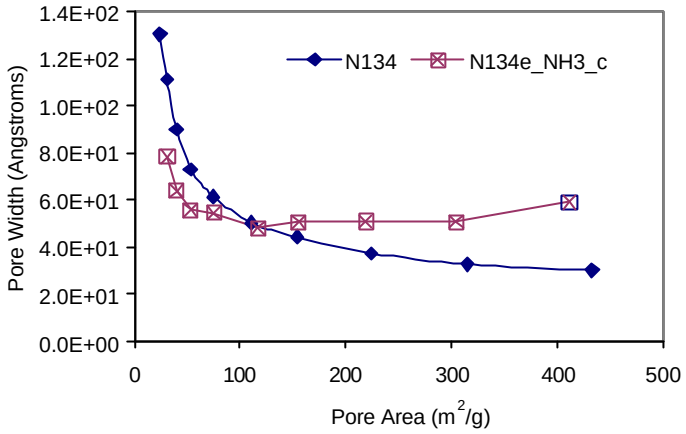

Fig.5. 18 Mesopore and macropore distribution for N134 grades

In Fig.5. 18 porous distribution of N134 CB's are presented. The results confirm the hypothesis that has been presented related to the microporosity nature of the impurity layer. Once again it is observed that N134 original CB presents a higher volume of low diameter porous, although this figure does not include the microporous range, a very clear trend toward microporosity region can be observed for N134. On the other hand, the situation is different for N134e_NH_3_c which presents a more regular distribution in the meso and macro porous range higher than for original N134, while volume in the microporous range could be extrapolated lower than for the former CB. When analyzing the same results for the XPB171 grades presented in Fig.5. 19 it can be observed that in this case no clear differences in the very narrow pores in the limit of microporosity can not be observed (as stated before from the obtained results from t-plot), however, changes are observed in the macroporous zone in which a decrease of meso and macro porous volume is observed for both APP treated samples.

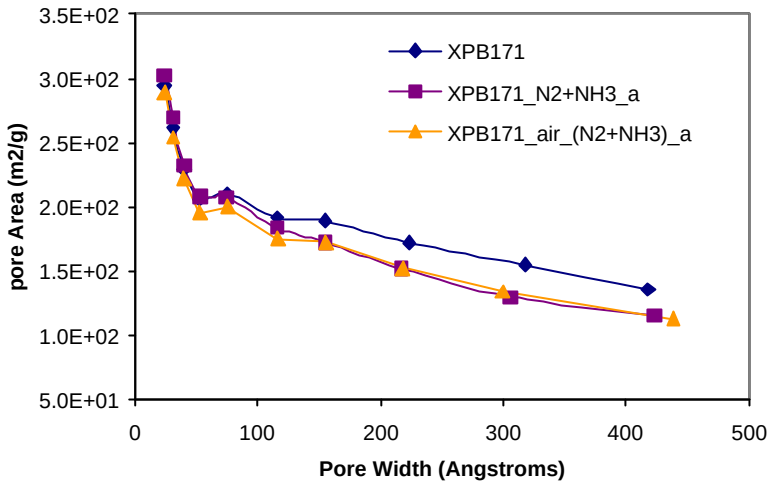

Fig.5. 19 Mesopore and macropore distribution for XPB 171 grades

5.2 CB Surface Crystallinity

Besides specific surface area, CB surface structure has been reported to play a very important role in the interaction of the CB with the surrounding media. It has been here already presented the model developed by Sid Richardson CB Co. in chapter 2, in which CB surface presents both crystalline and non-crystalline regions. This approach was confirmed by Schröder et al. using low pressure static ethene adsoption isotherms but also by other techniques such as Scanning tunneling Microscope STM and Raman Spectroscopy as it was previously presented.

But the presence of different structures was already mentioned a long time ago. First X-ray diffraction (XRD) techniques (J. Biscoe et al. 1942 and E. Franklin 1950) and later scattering techniques such as Wide Angle X-ray Scattering (WAXS) (G.J. Schneider et al. 2005) and Raman Spectroscopy (T.C. Gruber et al 1994, W. Zerda et al. 1998) have been used in order to study the crystallite parameters such as L_c and L_a presented in Fig.5. 20. Whether results obtained for these parameters (L_c and L_a) are representative and comparable when using XRD and Raman techniques has been a point of discussion, for example the group of A. Cuesta and coworkers, recommended measuring these parameters by using XRD as the Raman approach could give errors as large as 100% (A. Cuesta el al. 1998). However, as it is the present case, for comparative measurements should be in both cases very helpful.

On the other hand, although crystalline parameters are not so easy to obtain from STM and SAXS they do give information about surface topology and roughness (J.B Donnet et al. 1992, and Göritz et al. 1999).

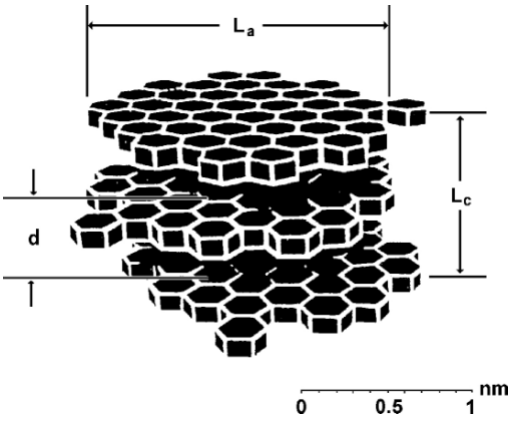

Fig.5. 20 Scheme of a crystallite on the CB surface (Sweitzer et al. 1956)

In this work, crystallinity variation of plasma treated CB's was studied by means of two different techniques: XRD, WAXS. For some given samples topology was also studied by means of SAXS and STM measurments.

5.2.1 X-Ray diffraction (XRD))

In order to study changes on the surface structure (L_c and L_a) N-134 and N-134g before and after several plasma treatments were studied. Spectra were collected using a Bruker D5000 instrument, with monochromatic ? (Cu ? = 0.154 nm. Each sample was measured 3 times filling a standard holder with the powder, reproducibility error was found to lower than 10%.

Two peaks are expected to appear in the X-Ray diffractogram for CB. One corresponds to the d_{002} (interplanar spacing), while the other corresponds to the d_{001} related to the size of the crystallite. Using Cu ? = 1.54 nm and the obtained the distances d_{002} and d_{001} can be obtained using the Bragg equation:

$$2\,d \sin\theta = n\,\lambda \qquad \text{eq.5. 1}$$

where d is the distance between crystallographic planes, and θ is half the angle of diffraction, n is an integer, and λ is the wavelength of the X-ray.

Finally L_a and L_c can be obtained by means of the Scherrer equation (M.A. Short et al.1963) eq.5.2

$$Lc = \frac{K \cdot l}{B \cos q} \qquad \text{eq.5. 2}$$

were K is the Scherrer constant (=0.94), ?=1.54 nm, B the half-height width of the d_{002} diffraction line and ? the Bragg angle. Although as it has been presented this technique was one of the first being used to study the crystalline structure on the surface of CB is still very widely used nowadays (W.T. Zerda et al. 2002, H. Darmstadt et al. 2002 and K. Huang et al 2005). One of the most accepted results using this type of technique is that crystallite length (L_a) trends to diminish when decreasing particle size however stacking height (L_c) does not seem to be dependent on this parameter (J.B. Donnet et. al 1992b, T. Ungar et al 2002)

This method has also been used in order to study the effect of wet chemistry modification of CB using H_3PO_4, KOH and C_6H_6., where it was found that the presented treatments modified mainly the L_c parameter with minor changes on interspacing d_{002}(S. J. Park et al. 2001).

In this work N-134 grades were selected in order to study the changes produced on CB surface microstructure both during LPP and APP treatments. Although L_c could be calculated from the obtained XRD diffractogram, signals were in almost all cases too low to obtain a correct measurement for L_a. This problem has been commonly describe din literature and could be a reason to perform Raman spectroscopy to have complementary information.

As it can be seen in Fig.5. 21, the diffractogram does show some changes for the diffraction corresponding to the d_{002}, as general information, a decreasing of the area of the peak can be observed for the treated CB's specially for the one submitted to the oxygen plasma. The curve for N134e has not been included in the figure due to its similarity to the original N134 which could probably cause confusion.

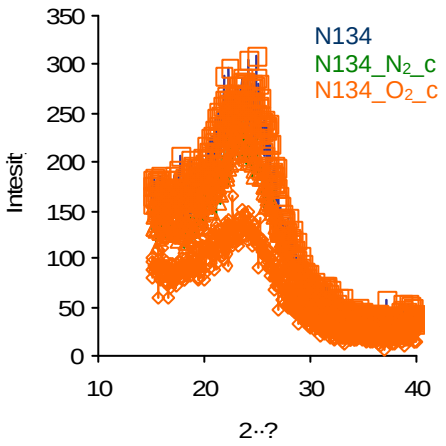

Fig.5. 21 XRD diffraction d_{002} for N134 before and after low pressure plasma modification

More accurate information about the d_{002} diffraction peak can be found In Table 5. 5, showing interspacing for the graphitic layers and L_c values. The results presented confirm that as previously said, the area changes after plasma treatment, although this parameter

is not directly related to a measure of crystallinity it is indeed an indication that some difference on the structure is present. When studying the interspacing for d_{002} it can be seen that N134 presents the minimal value while the sample treated with nitrogen plasma presents the broader distance between the planes. When analyzing the values for L_c it can be seen that both N134 and N134e present very similar values, slightly higher for the extracted CB, however the distance is shorter for the plasma treated carbons especially for the oxygen treated one. As it will be presented next, the shift of the 2? values toward lower values is also an indication of a decrease in the cristallinity order of the structure. On the other hand, in any case it was possible to obtain a good enough peak for the d_{001} diffraction which did not enable to calculate L_a distance.

Table 5. 5 XRD parameters obtained for N134 CB before and after LPP modification

	2?	d_{002} (Å)	B	L_c (Å)	Area d_{002}
N134	**24.25**	**3.667**	**6.100**	**13.91**	**754**
N134e	**23.95**	**3.712**	**6.812**	**14.13**	**814**
N134_N_2_c	**23.6**	**3.766**	**6.152**	**13.77**	**592**
N134_O_2_c	**23.8**	**3.706**	**6.844**	**12.44**	**485**

The cristallinty of the APP treated samples under air and nitrogen reactive gases was also studied. The correspondent diffractogram for both d_{001} and d_{002} are presented in the figure below (Fig.5. 22). A very similar trend to the one observed for the cold plasma treatment can also be observed.

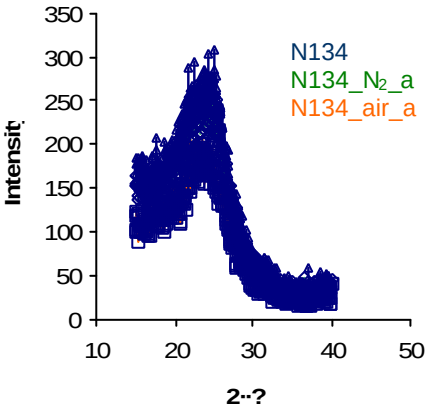

Fig.5. 22 XRD diffraction d_{002} for N134 before and after APP

Table 5. 6 shows the crystallinity parameters after the APP treatment. As it can be observed differences are not so evident as for the samples treated in the LPP reactor. The main difference is a decrease of Lc for the attmospehric nitrogen treated N134.

Table 5. 6 XRD parameters obtained for N134 CB before and after APP modification

	2?	d_{002} (Å)	B	L_c (Å)	Area d_{002}
N134	**24.25**	**3.667**	**6.100**	**13.91**	**754**
N134_N_2_a	**24.08**	**3.695**	**6.223**	**13.36**	**770**
N134_O_2_a	**24.35**	**3.652**	**6.399**	**13.86**	**640**

In order to have a better information about the action of LPP on the surface of the CB crystallites, N134g was also studied by means of XRD. Due to the graphitization process crystallites are expected to be bigger and thus a more significative signal should be detected. It is expected that changes after the plasma treatment can be also observed with higher accuracy.

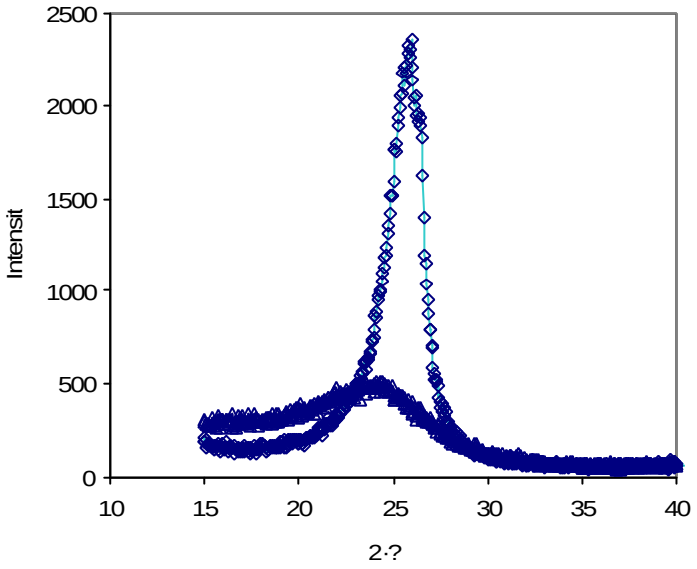

Fig.5. 23 XRD d_{002} diffraction for N134 and N134g

As it can be observed in Fig.5. 23 the diffractogram for the N134g does present a narrower and larger peak for the d_{002} peak. This effect is due to the higher crystalline degree on the surface which indicates that the graphitization process was successfully achieved. Moreover, when comparing both d_{002} interspacing as well as L_c before and after graphitization, the effect is also observed; d_{002} becomes smaller indicating a higher proximity of the graphitic planes while L_c, the stacking dimension becomes three times larger (Table 5. 7). Also a shift of the 2? to slight larger angles have also been reported by Schneider et al. were the same values for d_{002} and L_c before and after graphitization for N115 and N234 were also obtained (G. Schneider et al. 2005 and J.A. Ayala et al. 1991)

Table 5. 7 XRD parameters obtained for N134g CB before and after LPP modification

	2?	d_{002} (Å)	B	L_c (Å)	Area d_{002}

N134	**24.25**	**3.667**	**6.100**	**13.91**	**754**
N134g	**25.92**	**3.434**	**2.077**	**40.98**	**1994**
N134g_N_2_c	**25.872**	**3.440**	**2.020**	**42.11**	**1598**
N134g_O_2_c	**25.650**	**3.470**	**2.132**	**39.93**	**1596**

The effect of cold plasma treatment both with N_2 (at 80W and 30 minutes) as well as O_2 plasma (at 60W for 30 minutes) was studied by means of XRD. In Fig.5. 25 the peak for d_{002} can be observed before and after plasma treatment. It can be clearly observed that the treated samples present a much smaller peak than the one corresponding to the initial N134g. The values obtained for the calculated parameters are presented in Table 5. 7. As it can be seen, interspacing in between the graphitic planes does not seem to be affected due to the plasma treatment, probably as a consequence of the high graphitization degree. However, the plasma treatment does seem to have an influence in the L_c value which trends to decrease after oxygen plasma treatment. This result confirms that oxygen plasma does attack graphitic planes as stated by other researchers using STM and AFM techniques (J.B. Donnet et al. 1994 and, J. I. Paredes et al. 2002) On the other hand, L_c does not seem to be affected by low pressure nitrogen plasma, in this case although very slight an increase can be observed. This effect was also observed after cold plasma modification of original N134 but in a larger extent. S.J. Park et al. postulated that N_2 plasma may have an ablation effect which could remove loosely attacked structures from the CB surface. As a result, a higher crystallinity was observed which was related to the elimination of lousy attached C structures on the surface of CB (S.J. Park et al. 2001).

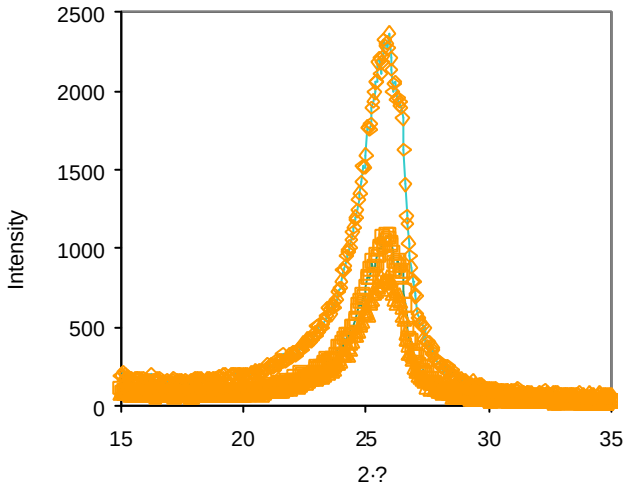

Fig.5. 24 XRD d_{002} diffraction for N134g before and after LPP modification

Although d_{002} peak gives information about interspacing and staking height it does not give information about the crystallite dimensions already said. Contrary to the cases presented above in which no difference could be observed for the d_{001} diffraction pattern, for n134g it is possible to observe changes.

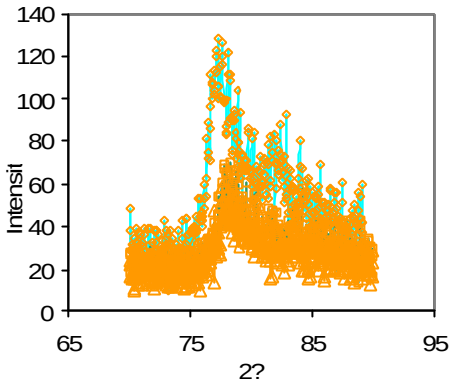

Fig.5. 25 XRD d_{001} diffraction for N134g before and after low pressure plasma treatment

5.2.2 Wide Angle X-Ray Scattering (WAXS

In order to confirm the obtained results for N134g which show a clear change in the surface structures of CB, Wide Angle X-Ray Scattering measurements were conducted in collaboration with Dr. Schneider and Prof. Dr. Göritz from University of Regensburg (Institut für Experimentelle und Angewandte Physik), Germany. Measurements were carried out with a Siemens D5000 diffractometer using monochromatic Cu Ka radiation and controlled by a Siemens DIFFRACT AT 3.2 measuring program. Samples were examined in reflection with a 2? step scan between 10º and 50º (0.1º step) at ambient temperature. L_c was also in this case calculated from the obtained data.

The results obtained from WAXS experiments, scattering intensity versus the scattering angle 2? are presented in Fig.5. 26 and Fig.5. 27. It can be observed how the same trend as the obtained for the XRD measurements is present; L_c increasing for N_2 LPP treated LPP and decreasing for the oxygen LPP treatment. Because this phenomenon seems to be a real effect of the plasma treatment an hypothesis is here presented. N_2 atoms may cause ablation of the surface when having enough energy as they are less reactive than oxygen species. Therefore, if a nitrogen specie with enough energy collides on the carbon surface in a crystallite edge it may increase the lateral exposed crystallinity and it can also cause the microposrosity observed during the specific surface area measurements. Contrary, oxygen species do not produce ablation but mainly react with the carbon surface, even if it presents a crystalline structure as it will be confirmed with further results. Therefore the L_c staking height is consumed by the reaction of the carbon at the very surface and the oxygen species.

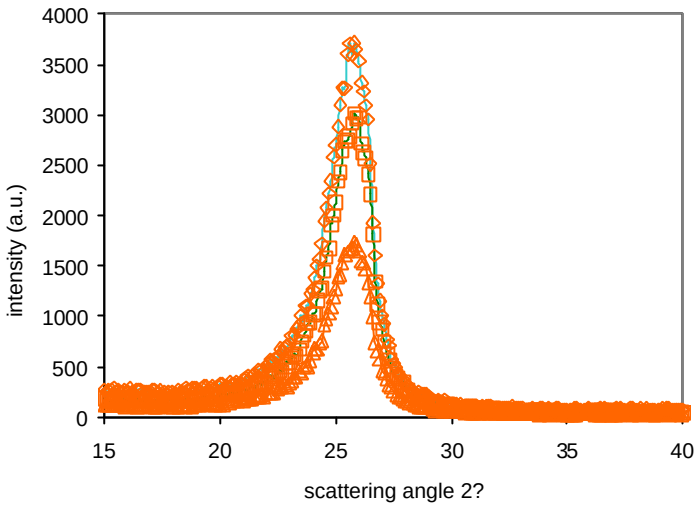

Fig.5. 26 WAXS d_{002} measurements for N-134g before and after LPP treatment

Table 5. 8 WAXS parameters obtained for N134g CB before and after LPP modification

	2?	d_{002} (Å)	B	L_c (Å)
N134g	**56.65**	**3.474**	**1.63**	**52.18**
N134g_N_2_c	**25.60**	**3.468**	**1.57**	**53.88**
N134g_O_2_c	**25.61**	**3.473**	**1.86**	**45.53**

Using WAXS enough sensitivity was obtained in order to measure parameter La from the d_{001} diffraction peak shown in Fig.5. 27. Here once again an evident difference is observed between the original and the two N134g LPP treated samples.

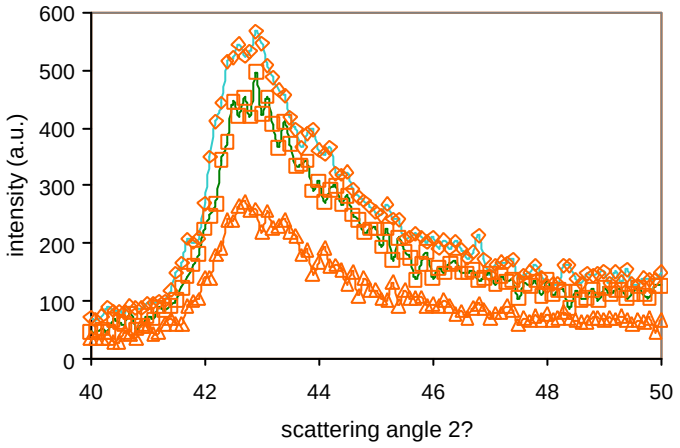

Fig.5. 27 WAXS d_{001} measurements for N-134g before and after LPP treatment

Table 5. 9 WAXS parameters obtained for N134g CB before and after LPP modification

	2?	B	L_a (Å)
N134g	**43.123**	**1.659**	**53.75**
N134g_N_2_c	**42.962**	**1.066**	**83.543**
N134g_O_2_c	**43.246**	**1.871**	**47.67**

As it can be seen above L_a also trends to increase due to the effect of nitrogen LPP modification while being reduced by LPP oxygen treatments. The effect can be explained by the same hypothesis proposed for L_c. Nitrogen energetic species by cause ablation of surface attached lousy structures presenting after the LPP treatments higher surface crystallinity, this effect was already stated by J.S. Park (J.P. Park et al. 2001) and explained by the same theory. On the other hand the reaction with oxygen species results in a lower crystallinity of the carbon black surface, at least for graphitized grades.

It can be then concluded that, although not relevant changes were detected during the specific surface area measurements, surface structure has been found to be affected by the plasma treatment. When comparing N134 at low and atmospheric plasma larger difference was observed for the first treatment.
N134g confirmed by means of both XRD and WAXS that even the structure of a surface containing only crystallites can be modified by the reactive species, both by reaction or ablation processes in a LPP.

However, crystallinity is not the only surface structure parameter that may alter surface behavior, roughness and fractal dimension may also play an important role. In the present case some CB's were also studied by means of STM and SAXS in order to have a better insight into those properties.

5.3. CB Surface Topology

5.3.1 Surface Roughness by Scanning Transmission (STM) Measurements

Previous presented results in this chapter indicate that plasma treatment of CB although does not alter the specific surface as measured following the BET approach, it can indeed change surface crystallinity. In order to further study such modification surface roughness and surface fractal dimension was studied by means of STM and SAXS respectively. Concerning the fractal dimension also the FHH approach which allows the calculation of the fractal dimension using the low adsorption isotherms was also used. This technique however, has been presented by other researchers as a non robust method very

dependent on the assumptions taken for calculations. In our case the data obtained during the specific surface measurements for the low pressure nitrogen isotherms where used to contrast our results with the previous given by other research groups.

To perform these studies at APP treated samples with nitrogen and ammonia where mainly studied. As presented these samples did not show relevant changes when being studied by XRD techniques but due to the importance of this type of modification (mainly in fuel cell and polymer reinforcement) and the possibility to obtain such material at industrial level, encouraged us to study them more carefully. N134 but also XPB171 have been analyzed due to their high performance or relative improvement after the plasma modification. Because some studies related this high activity with some surface parameters such as crystallite edges and microporosity it was considered convenient to focus these studies on the mentioned samples (F. Jaouen et al 2006).

STM measurements where conducted in a collaboration with The University of Regensburg at the ”Institut für Experimentelle und Angewandte Physik” (prof. D. Göritz) in a self designed and constructed STM apparatus. Measurements were carried out to study the topology of four different samples: N134, N134_N_2_a, N134_(N_2+NH_3)_a, last modification was also carried out including 5% hydrogen in the carrier gas. For the STM experiments the powders were prepared using a standard technique by ultrasonically dispersing the CB in a solvent (ethanol). The dispersion was dripped onto a recently cleaved HOPG surface and dried afterwards at 100ºC for 24 hr. at vacuum conditions.

All the surface topology pictures shown in this work have been measured in the constant current mode. In this mode of operation, the current is kept constant by a feed back loop, on order to control the tip-sample separation forcing the tip to follow the surface contours, by monitoring the vertical z position of the tip as a function of the lateral displacement (x,y), one can get a three-dimensional image of the carbon surface as the ones here presented.

Fig.5. 28 shows an STM picture obtained for N134, the length of the analyzed area corresponds to 153nm, and shows a quite rough surface which is characteristic for N134. The maximal height difference that can be observed in these measurements is about 140nm.

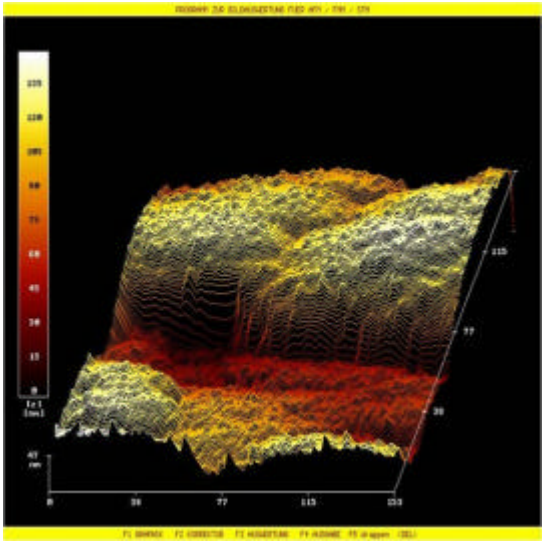

Fig.5. 28 STM picture for N134

Fig.5. 29 shows an STM result for a N134_N_2_a for a 24 nm length and 48nm left and right respectively. In this case the maximum height difference corresponds to 35nm and 50 nm for each picture.

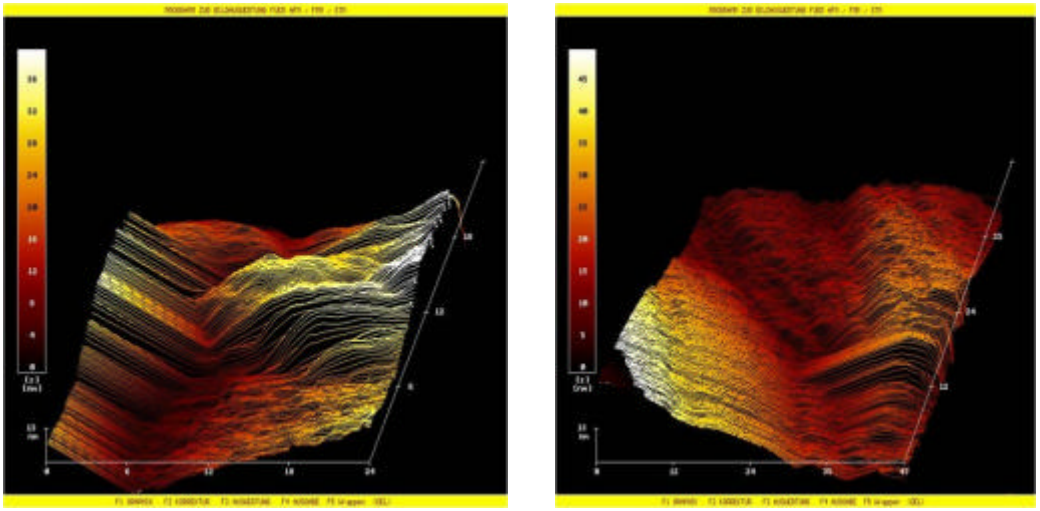

Fig.5. 29 STM pictures for N134_N_2_a

The images obtained for the N134_(N_2+NH_3) (Fig.5. 30) are very similar to the ones obtained for the previous sample. In this case a maximum height difference in an 88nm zone is about 50nm, a rather flat surface is observed when a 24nm length for the same sample is analyzed.

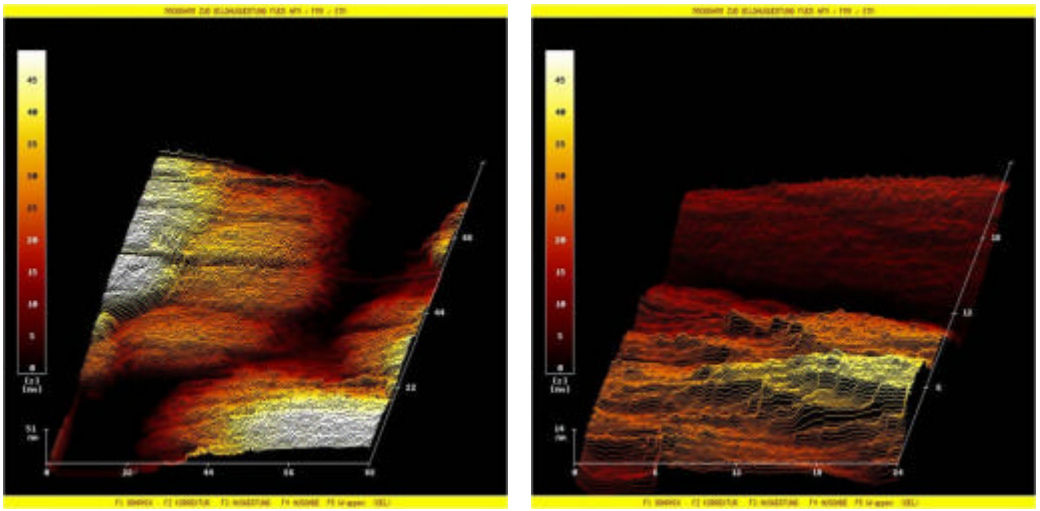

Fig.5. 30 STM picture for N134_(N_2+NH_3)_a, 88 and 24 nm left and right respectively

Finally, Fig.5. 31 shows also a N134 modified using APP with a mixture of nitrogen and ammonia as the previous presented. In this case however, a small amount of hydrogen was included in the carrier gas that introduces the CB in the APP system. The presence of hydrogen was though to favor hydrogenation of CB surface and therefore decrease crystallinity and flatness of the surface. However, as it can be seen in the obtained pictures by STM no evidence of a higher roughness on the surface was obtained, this result was confirmed by SAXS measurements that will be presented shortly.

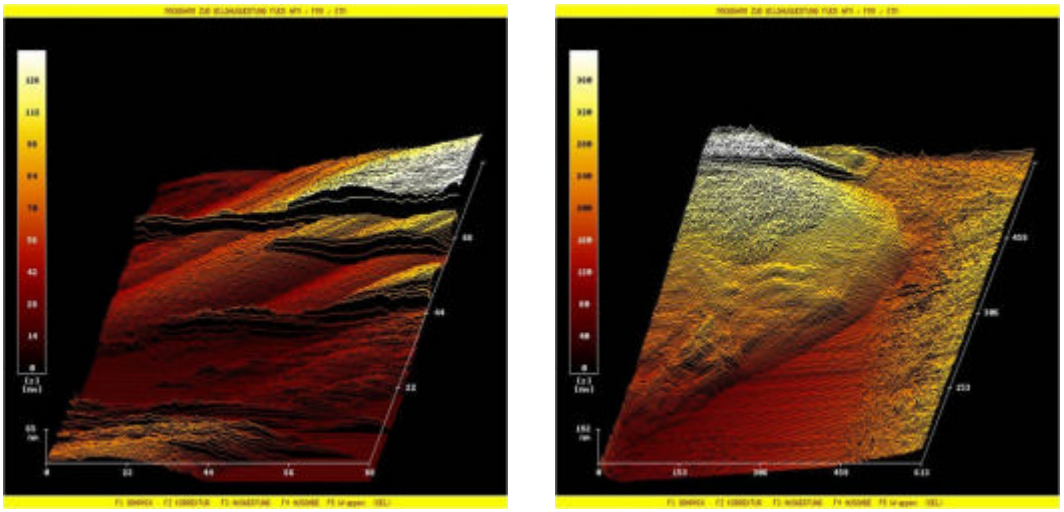

Fig.5. 31 STM picture for N134_(N_2+NH_3)_a with 5% hydrogen, 88 and 613 nm respectively

As a conclusion of the presented results it can be said that APP treatment with nitrogen species containing gases such as nitrogen or ammonia slightly flattens the surface of CB. However, this could be also due to the partial ablation of the impurity layer that covers the CB which could also interfere in the STM measurements. Such effects have not been described in literature and further studies should be carried out to understand the effect of the presence of such compounds during STM measurements on the CB surface. This phenomenon is contrary to other CB and graphite surfaces studied by this technique after plasma treatment at LPP. One example are the results obtained by J.B. Donnet and coworkers where an increase of surface roughness was detected by STM measurements using ammonia, oxygen and nitrogen plasma (J.B. Donnet et al 1994). The same effect had already been observed when HOPG was treated under low pressure argon plasma (H.X. You et al.1992).

5.3.2 .Surface Fractal Dimension (Ds) by Small Angle X-Ray Scattering (SAXS) and Nitrogen Adsorption Isotherms

Further studies related with surface topology were carried out in order to calculate CB surface fractal dimension (d_s). Although several methods have been described till the

moment to obtain such information there is not a clear definition of which are more appropriate and precise to use. In this work two different approaches were evaluated; on one hand Small Angle X-ray Scattering was employed to determine d_s by means of the scattering curve slope, on the other the low pressure nitrogen adsorption data was used in order to calculate d_s by means of the FHH approach. Both methods are presented here briefly.

SAXS measurements were also carried out in collaboration with University of Regensburg (Institut für Experimentelle und Angewandte Physik), Germany although the experiments were carried out in HASYLAB at DESY in Hamburg, under the supervision from Prof. Dr. Göritz. In this case the same N134 treated with nitrogen and nitrogen-ammonia at APP conditions presented as for STM measurements where analyzed.

In a small-angle scattering experiments, a monochromatic beam passes through the investigated sample. The isotropic scattered intensity I(q) is measured as a function of the scattered vector q. The scattering vector is obtained from the scattering angle according to eq. 5.3:

$$q = \frac{4p \sin q}{l} \qquad \text{eq.5.3}$$

From the SAXS measurements the size of the cluster which in this case corresponds to the CB agglomerate can be calculated. The fractal dimension both for mass and surface range can also be obtained as fortunately the two ranges do not overlap as it is shown in Fig.5. 32. In the case of surface fractal dimension surface scattering yields a power-law behavior such as:

$$I(q) a q^{-(6-d_s)} \qquad \text{eq.5.4}$$

where d_s is the surface fractal dimension. The range for the exponent $-(6-d_s)$ is -3 to -4. $d_s=2$ would correspond to a perfectly smooth surface while $d_s=3$ would correspond to infinite fractal surface.

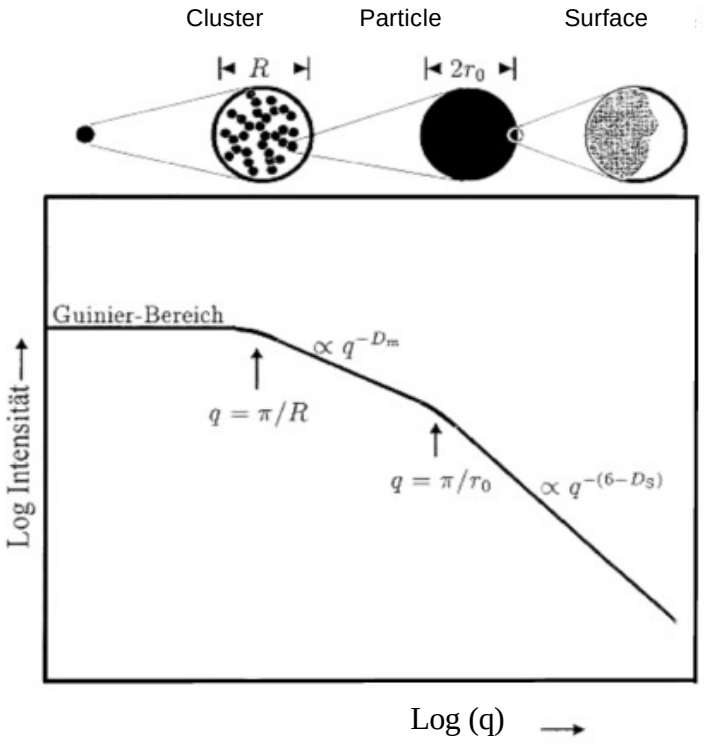

Fig.5. 32 Scheme of the different ranges that can be studied by means of SAXS

Next figures present the SAXS measurements for the N134 treated at APP under nitrogen, nitrogen+ammonia. From this measurements as explained above, the aggregate size as well as the mass fractal dimension and the surface fractal dimension can be obtained.

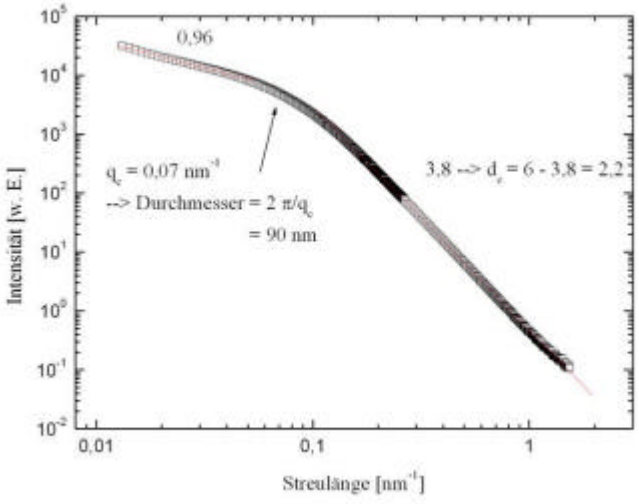

Fig.5. 33 SAXS measurement for N-134

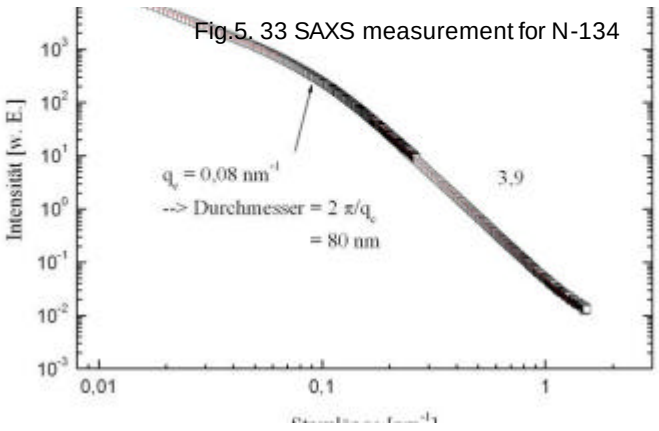

Fig.5. 34 SAXS measurement for N-134_N_2_a

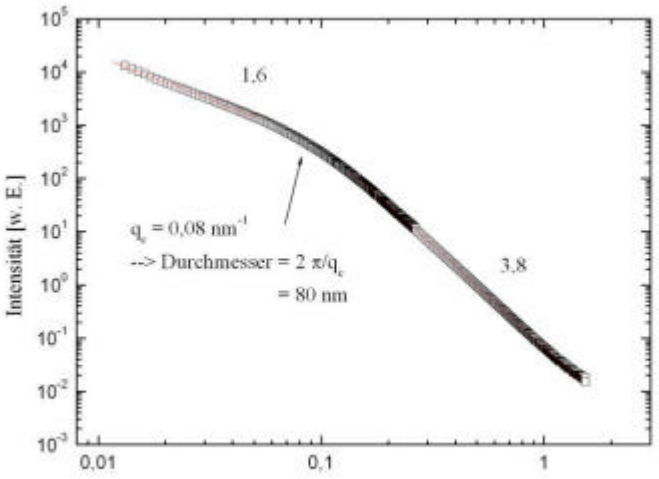

Fig.5. 35 SAXS measurement for N-134_(N_2+NH_3)_a

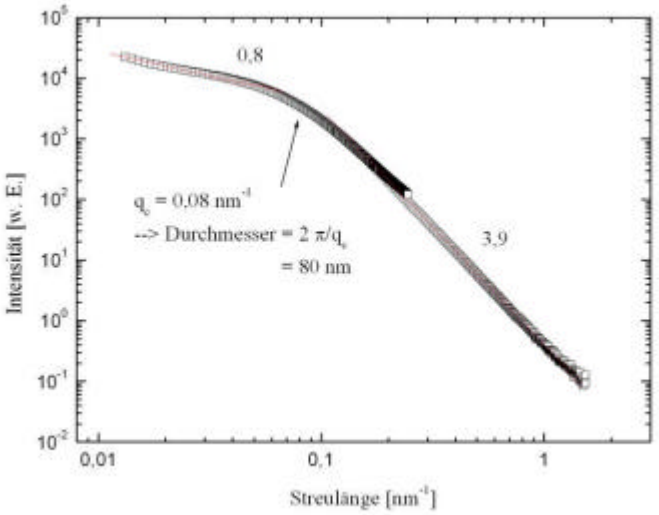

Fig.5. 36 SAXS measurement for N-134_(N_2+NH_3)_a with 5% hydrogen

As it can be observed from the presented results no relevant changes are observed in the SAXS curves for the treated N134 under APP for nitrogen enrichment. As can be seen in table Table 5. 10 were a sum up of he SAXS results is presented, only a slight change of the aggregate size seems to take place during modification. Original CB presents an aggregate size of 90 nm while for all the other APP treated N134 the size is decreased to 80 nm. On the other hand no relevant changes are observed for the fractal surface

dimension d_s which varies between 2,1 and 2,2. As a conclusion it can be said that evident changes on the surface topology using the SAXS results can not be found and therefore the roughness seem to stay constant although the aggregate size seems to decrease slightly.

Table 5. 10 Results obtained from SAXS experiments

CB	Dm	Ds	$2r_o$
N134	**0,96**	**2,2**	**90**
N134_N_2_a	**0,8**	**2,1**	**80**
N-134_(N_2+NH_3)_a	**1,6**	**2,2**	**80**
N-134_(N_2+NH_3)_a with 5% H_2	**1,7**	**2,2**	**80**

When taking into account the mass fractal dimension Dm two of the values are not in the range which would be correct for the parameter which would be between 1 and 3, 1 being a perfect linear structure and 3 a very ramificated one. In this case however, the two first CB's seem to present a higher linearity when compared to the plasma treated samples in an atmosphere containing ammonia.

Surface fractal dimension however, can be determined by several methods as already presented in chapter 2. However, very controversial results are obtained when comparing the techniques. T.W. Zerda et al and A. Schroeder et al. determined that no evident dependence is found between CB grade and particles size when using the Yardistik approach . T.W. Zerda and coworkers described that d_s value found using adsorption of different gas probes was in all cases 2.2 (W.T. Zerda et al. 1992) - On the other hand the results obtained by A. Schroeder and coworkers were higher and always similar to 2.6 (A. Schroeder et al. 1999) . In neither case differences were found when comparing several CB grades but the fractal surface dimension decreased notoriously when CB was graphitized.

Contrary to the described results, the group of D. Göritz et al. determined by using SAXS that the smaller the size of the aggregate the higher the surface fractal was. The values for the fractal surface dimension where in a range of 2.2 for N-115 (similar to the one here obtained and thus coherent), to 2.03 for N-990 which would correspond to an almost perfect flat surface (D. Göritz et al. 1999). In our opinion further research is needed to clarify whether the ranges studied using this two techniques are comparable and information can be equivalent or complementary therefore some further analysis of the obtained data was considered interesting.

As it has been mentioned above another way to calculate the fractal surface dimension is by means of gas adsorption. Because it is a simple way to analyze this phenomenon it has been widely used (A. Schroeder et al., P.Pfeifer et al. 1983 and T.W. Zerda et al

1992). This method can be applied using adsorbates with different cross-sectional area d (molecular yardistick), which allows to calculate the fractal dimension from the slope of a plot representing log (V_{mono}) vs. log (d). where V mono can be obtained using the BET equation for low pressure isotherms already presented earlier in this chapter.

But the fractal dimension can also be calculated from a single adsorption isotherm using a modified FHH theory which was developed around 1950 by Frenkel, Halsey and Hill, and describes the multilayer adsorption where only Van der Waals interactions are considered. In this case the isotherm is described by the following equation:

$$\log(\frac{V}{V_{mono}}) = const + \frac{1}{n}\left[\log \ln\left(\frac{Po}{P}\right)\right] \qquad \text{eq. 5.5}$$

Where V/V_{mono} is the quantity of the molecules adsorbed and n is an empirical constant that describes how fast the substrate-adsorbent interactions decrease with increasing distance from the surface. Although this model is only valid for flat surfaces, several modifications have allowed its extension to surfaces with fractal nature. In this case the one presented by Pfeiffer et al. has been used. In this model the thickness of the layer of molecules adsorbed on a flat surface is used as the characteristic distance scale for the fractal surface. For a flat surface the equidistance surface corresponds to the equipotential surface but this is not true for fractal surfaces. When Van de Waals forces between the gas and solid interactions are dominating and the liquid-gas surface tension forces are negligible, the isotherms can be expressed by means of the following equation:

$$\log\left(\frac{V}{Vmono}\right) = const + \frac{(D-3)}{3}\cdot\left[\log \ln\left(\frac{Po}{P}\right)\right] \qquad \text{eq. 5.6}$$

Where d_s corresponds to the fractal dimension of the surface as presented before. This equation is normally valid for the first stages of the multilayer formation. For higher coverage the interface is controlled by the liquid /gas surface tension forces and the isotherm equation is given by:

$$\log\left(\frac{V}{Vmono}\right) = const + (D-3)\cdot\left[\log \ln\left(\frac{Po}{P}\right)\right] \qquad \text{eq 5.7}$$

However, it should be pointed out that in many cases the selection of the mathematical model can be critical, as in many cases the use of one equation as is the case for eq.5.6. has given erroneous fractal numbers outside the 2-3 interval. The difference between the values obtained from T.W. Zerda and A. Schröeder could be due to a selection of eq. 5.6 and eq. 5.7 respectively as will be presented further on. W. Xu and coworkers also reported the obtaintment of Ds values lower than 2 when using eq. 5.6 that where attributed to the presence of capillary forces during the formation of the first monolayer (W.

Xu et al. 1996). These capillary forces are probably more intense for the materials with higher microporosity.

Using this approach and the data of low pressure nitrogen isotherms obtained from the ASAP 2000 measurements which covers the whole range to perform this calculation, d_s was calculated for the following samples: N134, N134g_NH3, XPB171, XPB171_N_2_a, XPB171_N_2+NH_3_a, XPB171_air_N_2+NH_3_a.

Fig.5. 37 shows the fit for the N134 CB grades, the slope value, very similar for the two represented carbons, is very close to the one obtained by W. Xu and coworkers for a N110 grade (W. Xu et al 1996).

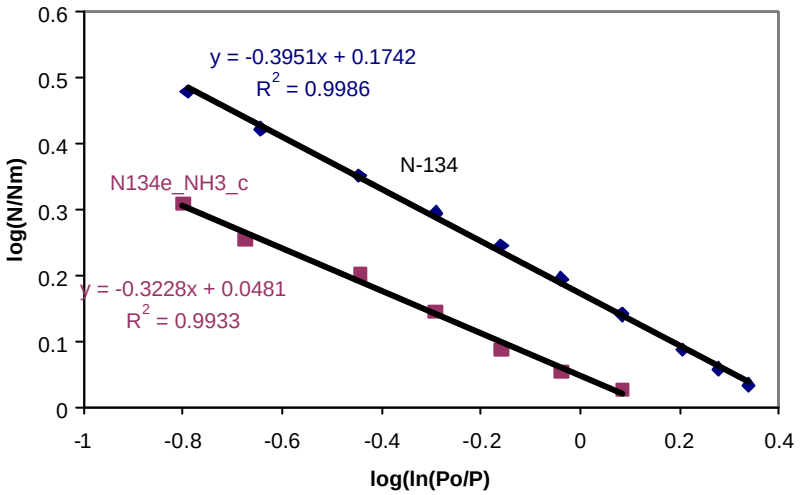

Fig.5. 37 Plot for Ds determination using the modified FHH model for N134 grades

The presented results in the table below Table 5. 11 show indeed a difference when using equation 5.6 or 5.7 for the Ds calculation. In the case of N134 when the Van der Waals equation used (eq.5.6) fractal dimension falls out of the limit for N134 and very close to 2 for the N134_NH_3_c which was also the case for W. Xu et al., as already said this may probably due to the presence of capillary forces. When eq. 5.7 is used, a value between 2 and 3 is obtained which leads to the conclusion that inclusion of capillary forces is necessary for this calculation even for the first monolayer. For the case of N134 and its modified partner, the value is very close to the one obtained by A.Schroeder et al. using the same equation. The two N134 grades present very similar values close to 2.6, however the extracted one presents a slightly larger fractal dimension that could be related to the elimination of the impurity layer.

Table 5. 11 Ds value obtained from the FHH modified method

CB	Ds eq. 5.7	Ds eq. 5.6
N134	**2.60**	**1.81**

N134_NH_3_c	**2.67**	**2.03**
XPB171	**2.89**	**2.69**
XPB171_(N_2+NH_3)_a	**2.72**	**2.16**
XPB171_air_(N_2+NH_3)_a	**2.72**	**2.17**

The case of XPB1 is much controversial, both equations giving values in the fractal region, which makes it difficult to decide which is the correct equation to apply. In both cases however, the modified XPB171 presents a lower surface fractal dimension which confirms the hypothesis about the flattening power presented by the APP treatment. Original XPB1 presents extremely high values when using eq. 5.7 and similar values to N134 for eq. 5.6. On the other hand the APP modified XPB171 grades present fractal dimensions which are in the range of the reported values both using eq. 5.7 and eq. 5.6.

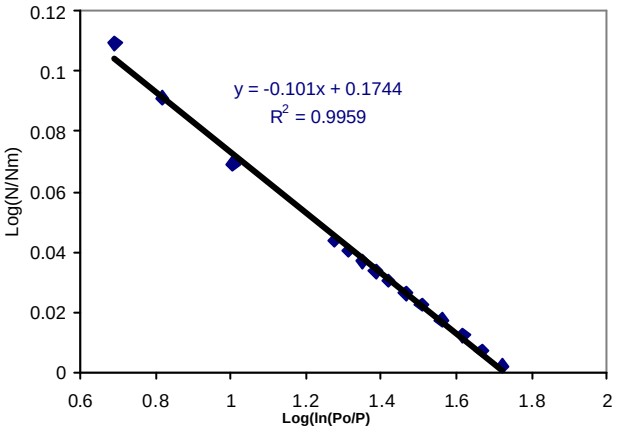

Fig.5. 38 Plot for Ds determination using the modified FHH model XPB171

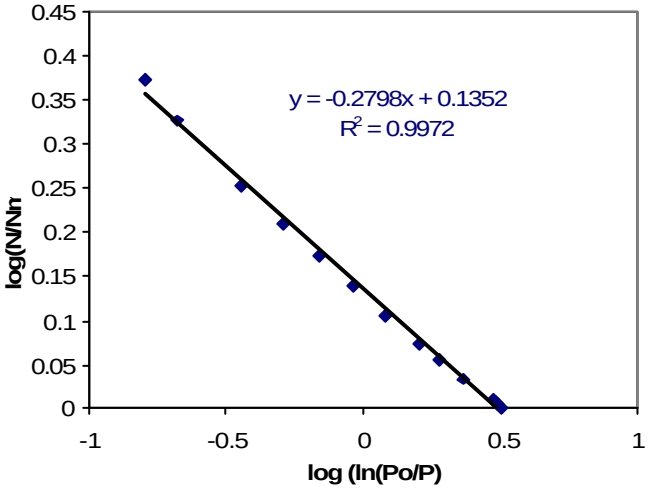

Fig.5. 39 Plot for Ds determination using the modified FHH model XPB171_(N_2+NH_3)_a

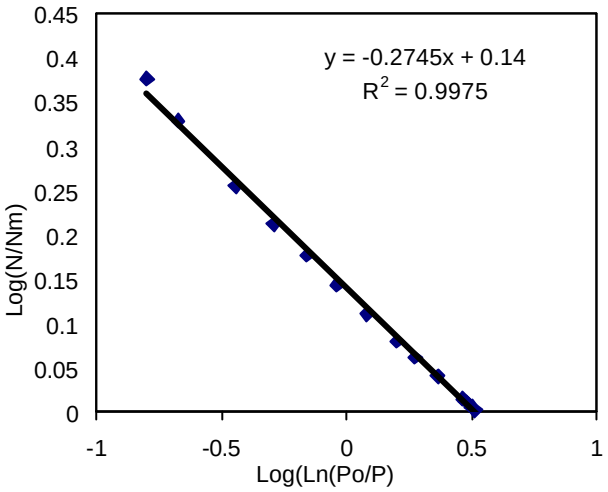

Fig.5. 40 Plot for Ds determination using the modified FHH model XPB171_air_(N_2+NH_3)_a

As summary it can be said that APP seems to probably be able of flattening the surface of CB may be by ablation of lousy C attached structures as was observed by STM but also in the fractal measurements when a high microporosity CB was used. For the case of N134 no changes for d_s were observed, neither by APP modification (using SAXS technique) nor by extraction and posterior LPP modification (FHH method). Although the values obtained from these two techniques are very different, it s believed that a lack of unification in the fractal dimension calculation criteria is present and that methodology can only be used as a comparison technique. In any case the obtained results were in agreement with previous studies done on non-modified fillers.

Up to this point it is possible to say that although very specialized techniques are needed to observe the effect of plasma on CB surface structure and topology, such as XRD or WAXS, it was possible to confirm that CB modification takes place only in the very first layers of this carbon material. Although very subtle, the changes observed could cause very interesting effects in final applications which have already been related to the surface crystallinity and structure of CB such as rubber reinforcement or non-noble metal oxygen catalysis in PEMFC (F. Jaouen et al. 2006, M. Gerspacher et al. 1994) .

5.4 Surface Chemistry

As already presented, the surface morphology including surface crystallinity and roughness are key parameters on the final activity of CB whose changes during plasma treatments have been presented in the previous sections of this work. These presented parameters affect however, mainly the dispersive component of the surface activity which is the one governed by Van der Waals forces. But also the chemical composition can play a very important role in the final activity of the filler. In this case, the energy component affected by changing surface composition is named specific component and is driven by polar interactions.

This section is focused in the analysis of the surface composition of the already presented CB's, and therefore to evaluate the changes produced during the plasma modification.

In Fig.5. 41 a wide accepted model of chemistry on CB crystallites during many years is presented. In this model besides from C some functional groups essentially composed by H and O such as carboxylates, lactones, phenols, aldehydes and quinones among others are present. If the atomic ratios of atoms are calculated the obtained values are 77.7% of C, 9.8% O and 12.5% H.

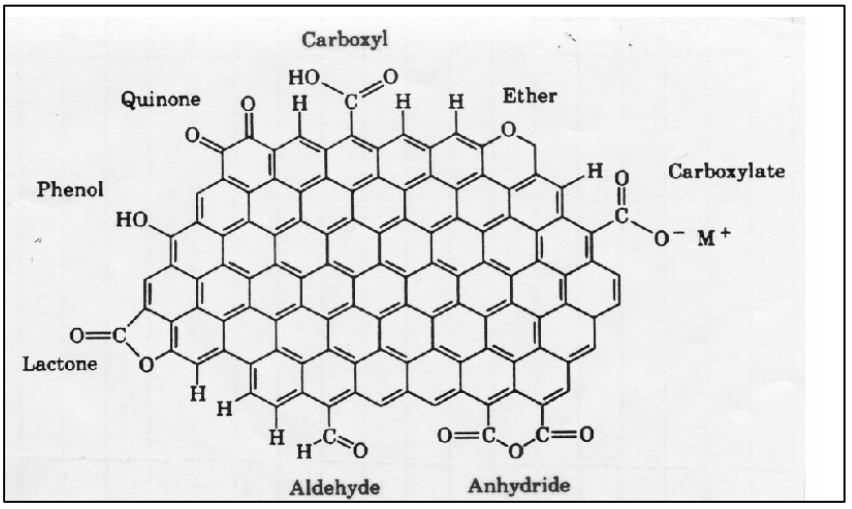

Fig.5. 41 Old Chemistry Model for CB (S. Wolf, 1996)

However, recent studies have shown that the ratios presented in this model are not completely correct (M. Gerspacher i C.P. O'Farrel, 1999). For CB furnace production the carbon content oscillates between a 95 and a 99%. Among the other components present on CB there is sulfur in approximately a 1%- 1.5%. Sulfur is carried over the feedstock oil into the CB, and although it is the largest non-carbon component it is bound to the carbon primarily as an heteroatom that is basically inert and non-extractable. Oxygen is present in

surface groups on CB but their number are small (0.3% - 1.5 %), and they are essentially unimportant for the rubber grade furnace black in influencing compound properties. The last component present on CB surface is Hydrogen. Hydrogen, which is present in a 0.25% - 0.3%, is found at the edge of the aromatic rings that make up the crystallites and in the non-crystallographic (amorphous) areas of the surface. Therefore it can be concluded that the typical literature crystallite does no represent faithfully the surface chemistry of furnace CB, which presents only the 2% of its total surface covered with functional groups.

Many authors consider that the presence of functional groups on CB is almost negligible. However there is an increasing interest for the amount and kind of hydrogen atoms (L. Ballerini, 1990). Following the same direction, there is an accepted hypothesis that describes the edges of crystallites as a region with a high π electron density and a high surface activity. These regions are also the ones with higher hydrogen content and sp^3 unions between carbon atoms, (M. Gerspacher et al. 1999).

Since a long time ago many methodologies gave been used in order to study Carbon black surface chemistry. Specific reactions with aluminum hydride (D. Rivin 1963), and also selective titration with basic reagents which were deeply studied by Bohem and coworkers (H.P. Bohem et al. 1964, 1970 and 1994), were one of the first methods used in order to study CB surface chemistry. They were adopted also by other research groups and are still in use nowadays as will be presented during this section (E. Papier et al. 1977, S.S. Barton 1973, J.P. Boudou et al 2000). Other utilized techniques along the years have included infrared spectroscopy although high radiation adsorption due to carbon black nature make these analysis rather difficult (Studebaker et al. 1972, H. Darmstadt et al. 2003, M.L.).

Newer and more complex techniques such as ToF-SIMS and XPS have also been used to study the chemical composition of CB surface. These two techniques are complementary, while ToF-SIMS offers a very high sensitivity, XPS offers the possibility to perform quantitative analysis than can not be carried out with the other technique. Using these two techniques different CB have been studied. All of them contained a high level of H and aromatic structures while for all of them O content was very low. When the sulfur species were studied it was found that the main sulfur groups present on CB surface are thiolates and sulfates, and their amount were found to be dependent on the manufacturing process (C. Poleunis et al., 2000). Other elements such as F, Cl, N, and Na among others were also detected as impurities of the production process. In the same work, CB thermally treated was also analyzed. The higher the temperature at which CB is exposed the higher graphitization takes place on CB surface; therefore more aromatic ions are detected. However, the intensity for ion with m/Z=407 which is rich in hydrogen also increased (P. Bertrand and L.T. Weng, 1999).

Next the results obtained from several analytical methods such as pH, wettablility and Bohem's titration. Although these two methods are not precise to determine composition,

they do give information about the degree of modification and were conducted mainly to select the most effective modification conditions. Finally, XPS from several CB samples modified by means of low pressure and atmospheric pressure plasma are presented. This information of high value will give a better insight in the type of changes produced on the CB surface.

5.4.1 pH

pH measurements are widely used in the CB industry for quality assurance as well as during research as a first indication of CB surface nature composition (S.J. Park et al. 2000).

Determination of the pH of slurry of CB (1.5g) in pre-boiled water (40ml.) following the ASTM D1512-95 is a quick and common method to analyze CB acidity and basicity. Although it does not give much information about the exact nature of the surface groups it can be very useful to observe trends when changing plasma parameters as plasma power generator and treatment duration.

5.4.1.1 LPP treated samples

Ammonia LPP on N-134

Due to the lack of literature in this particular area of nitrogen and ammonia plasma modification on CB and the will to use this material in such innovation as the reduction of oxygen which will be presented in chapter 7, special attention is given to this type of modification, specially on N-134 due to preliminary results which showed the high activity that this material presented towards the oxygen reduction.

For the reason presented above, several experiments have been carried out in ammonia:argon plasma 3:1, background pressure 0.02mbar, reaction pressure 0.3mbar. Plasma generator power has been varied between 20 and 80W and treatment duration from 10 to 50 minutes.

In Fig.5. 42 changes in pH using the mentioned conditions are presented. As a global result it can be said that slight increase in pH is detected, however the trend is not the same for all used conditions. At low powers such as 20W it seems to have a lower effect on pH at short times, on the other hand for long treatments the pH obtained value is one of the highest presented. On the other hand, for higher powers a maximum can be observed for a duration of 20 minutes, followed by a decrease in the pH value, especially for the 40 and 80W treatment. This effect can be explained by a destruction of the new introduced groups after being some time under the plasma conditions. The decrease of pH could be probably produced by the displacement of the basic groups by the oxygen species in the plasma or a pos-oxidation after the modified CB is put in contact with the atmosphere. This effect was also described by I. Loh et al. after CB treatment with

ammonia nitrogen groups were not stable and an increase of oxygen was also reported, on the other hand they demonstrated that nitrogen on the surface of CB was not due to the adsorption of ammonia (I. Loh et al. 1987)

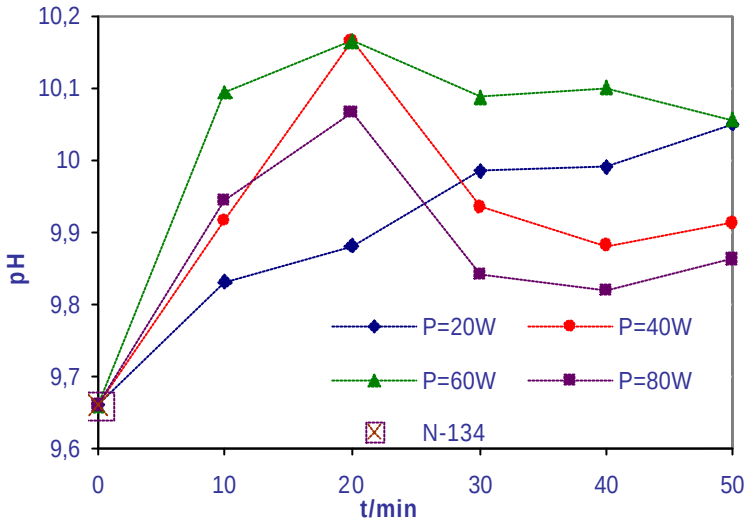

Fig.5. 42 pH measurement for ammonia modified CB at LPP

In order to observe how these changes affect the CB wettability, one of the most interesting properties when CB is in contact with aqueous media such the one in Fuel Cells and Inks, the following test was carried out: approximately 0.1g of CB is deposited on the surface of a water containing beaker (20ml), the vessel is submitted to a 30 seconds stirring in an ultrasonic bath, then the CB on the surface which has not moved to the water phase is separated dried and weighted (Fig.5. 43).

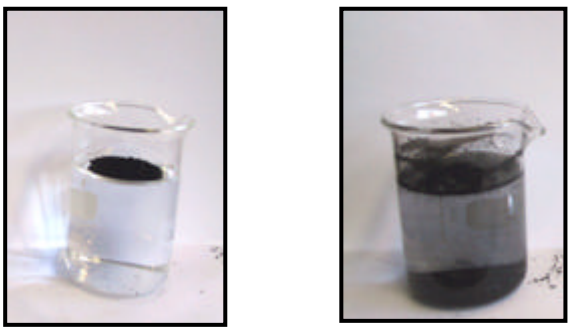

Fig.5. 43 CB wettablility before and after LPP treatment

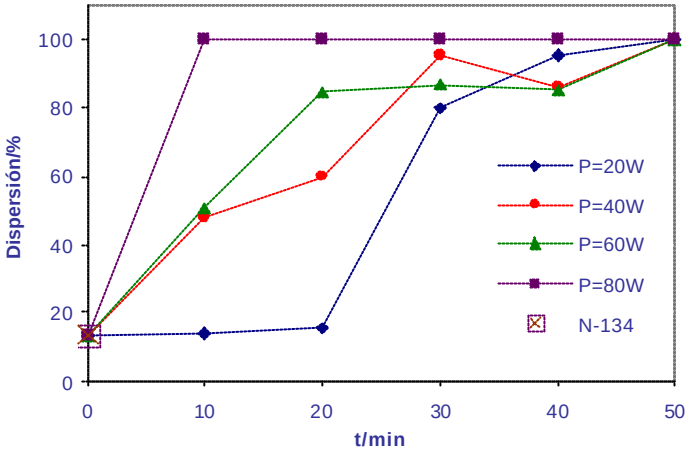

Fig.5.44 CB wettability measurements after ammonia LPP treatment

In the figure above it can be seen how there is an increase in wettability with increasing power and treating time. Contrary to the pH values, although at different rate the increase is present for all treatment conditions. This effect is an indication that although pH may decrease polarity does not decrease for low pH samples. Therefore, the hypothesis of introducing more acidic groups at high power and treatment times seems correct. For a 50 minutes treatment all the CB's present a 100% wettability, this means that all the CB moves into the water phase.

Fig.5. 45 and Fig.5. 46 present a surface response for the presented samples where it can be seen how wettability increases with power and time but there is an optimum for the increase of the pH.

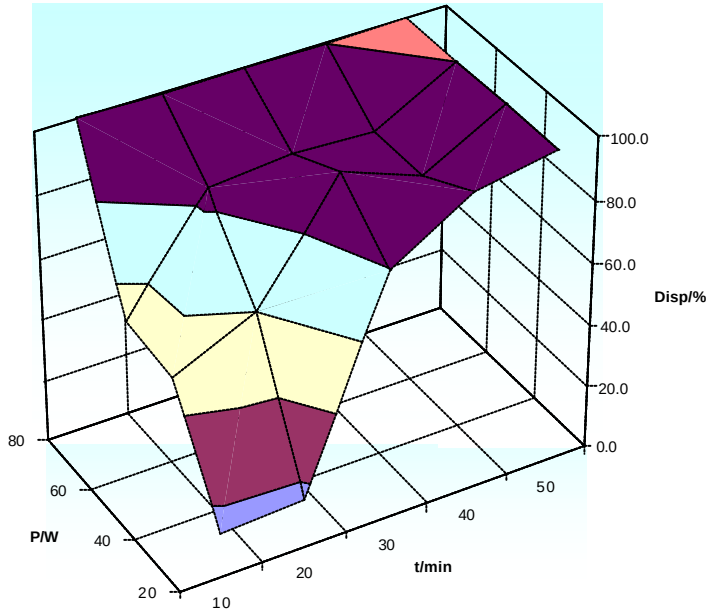

Fig.5. 45 Surface response for wettability as function of Time and Power after Ammonia LPP

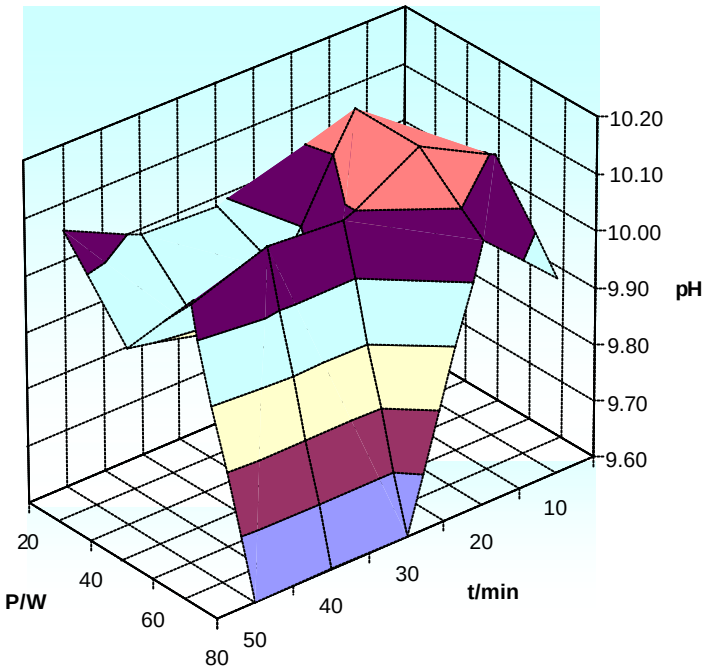

Fig.5. 46 Surface response for pH as function of Time and Power after Ammonia LPP

Therefore, it can be concluded that increasing time and power during ammonia treatment increases CB wettability. However pH does not follow a linear trend probably due to the destruction and replacement of nitrogen groups by more reactive oxygen species for high power and time conditions.

Nitrogen LPP on N134:

As an alternative way to introduce nitrogen atoms on the CB structure pure nitrogen plasma was also tested. In this case also several generator power and treatment duration were evaluated as mentioned in the previous chapter. During these experiments background pressure was held at 0.02mbar and reaction pressure at 0,2mbar.

Fig.5. 47 presents the pH and wettability values for the performed LPP treatment on N134. As it can be observed, in this case pH values do not increase in any of the cases, probably due to the fact that no basic groups are included on the surface. On the other hand both residual oxygen in the reactor or post-reaction with the atmospheric oxygen may lead to the inclusion of some oxygen acidic functionalities. As far as CB compatibility with water is concerned, it is possible to observe also an increase in the CB surface polarity with both increasing power and time, which are the surface groups responsible for this increase, will be discussed later on this section.

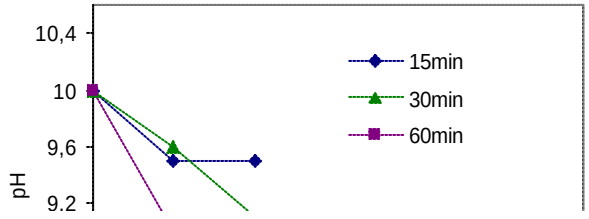

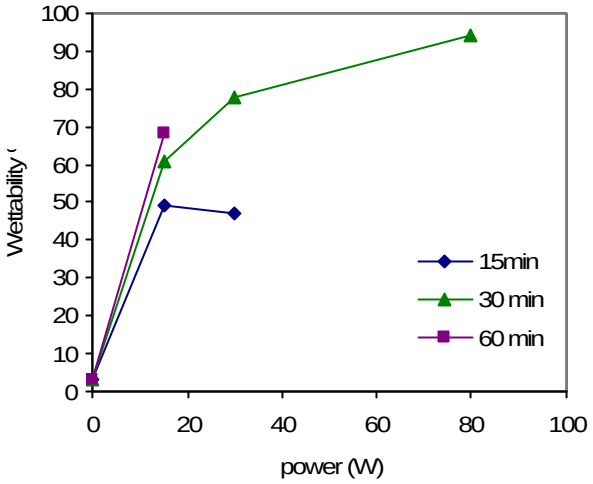

Oxygen LPP on N134

Finally, N134 was also treated in pure oxygen LPP. During these experiments background pressure was held at 0.02mbar and reaction pressure at 0,2mbar.

In Fig.5. 48 the pH values for an oxygen plasma treated N134 series at 40W are presented. Treatment at 60W with oxygen, often damaged the inner tube which carries the active plasma gas, therefore power was limited to 40W which is a common power treatment for oxygen plasma on CB. Because more information can be found on this type of treatments not so much emphasis was given to the study of oxygen plasma on pH values.

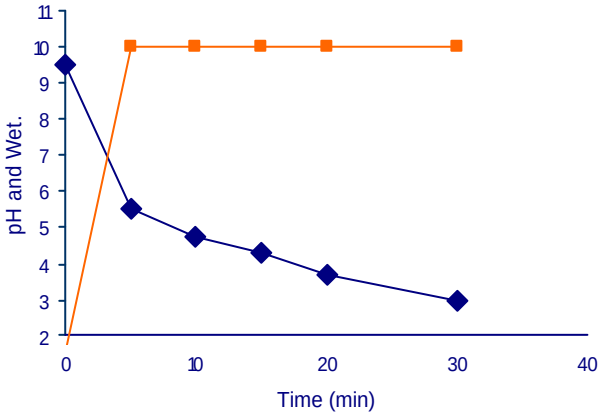

Fig.5. 48 pH and wettability after oxygen LPP treatment for N134

As it can be seen pH decreases dramatically for the first 5 minutes, but follows a decreasing tend for the studied interval up to 30 minutes. Wettability is presented in a

10 basis scale, as it can be observed 5 minute treatment is enough to achieve the maximum wettability at pH 5.5.

LPP on Other CB's

As it has been presented earlier in this work, other CBs were also selected besides N134. Selection was based both on morphological differences but also in final application fields which led to the choice of Vulcan XC-72 (Vulcan) and XPB 171 (chapter 2).

From the studies presented above it was decided to use only one condition to modify the other CB's not only Vulcan and XPB 171 but also N134g, N134e. Conditions are presented in Table 5.12:

Table 5. 12 Used conditions for the study of the effect of LPP on the CB surface (N134, XPB171 and Vulcan)

Plasma Gas	Power	Time	Background P (mbar)	Final P (mbar)
O_2	**40**	**15**	**10^{-2}**	**0.2**
N_2	**40**	**30**	**10^{-2}**	**0.2**
Ar:NH_3 (1:3)	**40**	**30**	**10^{-2}**	**0.3**

Results for pH measurements of the obtained samples are presented in the following Figures.

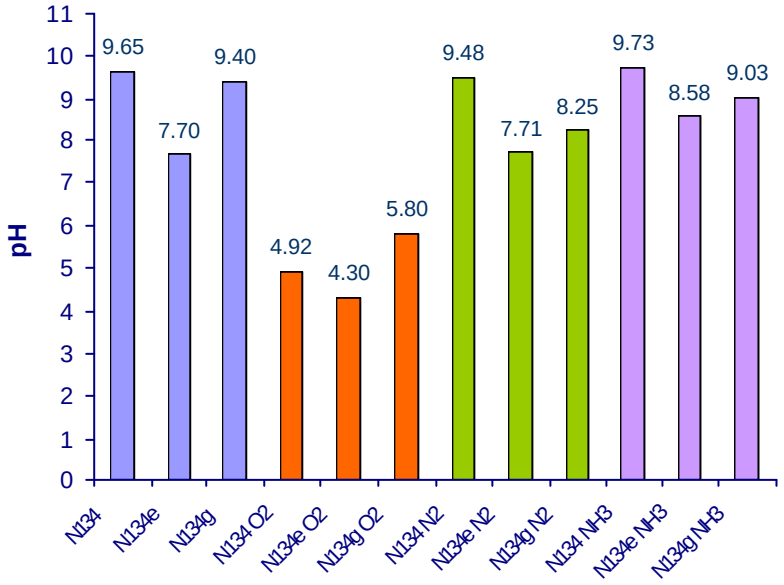

Fig.5. 49 pH for the N134 grades after several LPP treatments.

As it can be observed for N134 grades original pH levels are already different. Original N134 presents the highest value quite close to the N134g CB. Although no explanation was found for the basicity of the graphitized black, inclusion of some heteroatom on the final structure during graphitization could be a possibility. On the other hand the extraction procedure reduces the basicity of the CB surface almost to a neutral value.

After oxygen LPP treatment pH decreases as expected for all the three N134 types. Although the minimum level is obtained for the extracted CB, it is indeed the N134 the one suffering a highest change in pH probably because organic impurities are modified much more easily than the raw carbon surface.

LPP treatment with nitrogen does no produce relevant changes on the CB pH, the most interesting result is presented by the graphitized CB presenting a larger decrease than in for the other CBs. Decrease in pH after nitrogen plasma has been described to be a consequence of high new reactive created sites which react a posteriori with atmospheric oxygen. This effect does agree with the XRD presented results in which ablation and therefore creation of high energetic place was presented.

Finally, the pH results after ammonia LPP show a maximum effect for the extracted CB It is also interesting to notice that ammonia produces not only any increase but even a slight decrease of pH (may be due to formed N_2) for the N134g, which is an indication of the low reactivity of this type of carbon surface towards ammonia LPP species. On the other hand in N134e where more amorphous carbon is present the pH presents a maximum. The result could be an indication of the lack of ammonia plasma reactivity on the graphitic planes or crystalline edges.

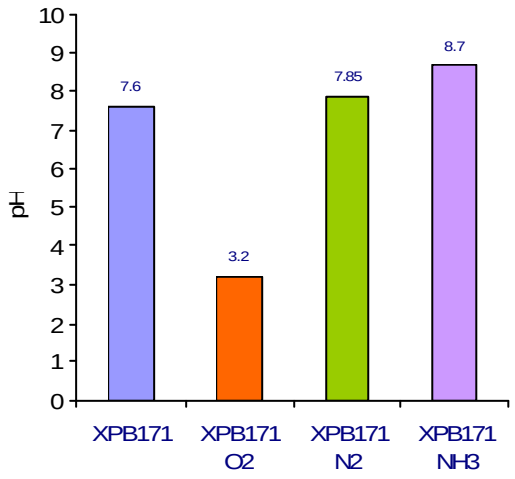

Fig.5. 50 pH for XPB171 after several LPP treatments

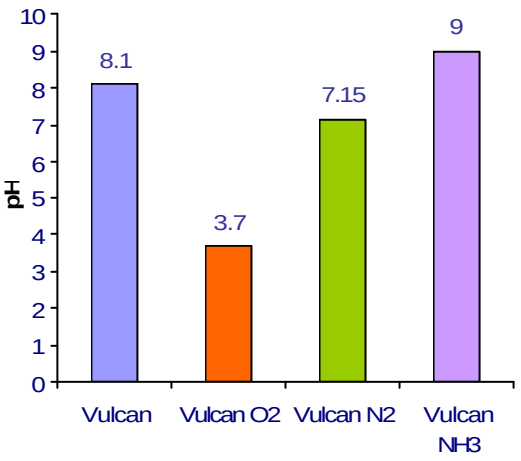

Fig.5. 5 1 pH for Vulcan after several LPP treatments

Last but not least pH for XPB and Vulcan after LPP are presented. Trends are similar than for the presented N134 grades results. Oxygen LPP plasma decreases pH values due to the introduction of acid oxygen functionalities while ammonia plasma does react gently with both surfaces probably due to the presence of the amorphous structure. No evident trend is observed for the nitrogen LPP modified samples.

5.4.1.2. APP treated samples

As a first trial for atmospheric plasma treatments on CB (N134), the pH was measured to observe variations introduced by the number of cycles as well as the position where CB was introduced in the reactor. Finally, also the effect of the cooling system (CS) was checked for both cooling system 1 and 2 presented during the reactor set up in chapter 3. The measurement was repeated for 3 different measurements, standard deviation is also presented in the results table (Table 5.13).

Table 5.13 pH and wettablitity results for configuration trials during the set up of the APP reactor

Treatment	Cooling System	Inlet position (mm)	Number of treatments	pH	Wettability	Standard deviation
Air Plasma	CS1	5	1	3,2	100	0,3
Air Plasma	CS1	5	2	3	100	0,1
Air Plasma	CS1	10	1	3,2	100	0,2
Air Plasma	CS2	5	1	3,2	100	0,2
Nitrogen Plasma	CS1	5	1	7,9	16	0,3
Nitrogen Plasma	CS1	5	2	7,8	20	0,2
Nitrogen Plasma	CS2	5	1	8	14	0,3

As it can be seen neither the inlet position nor the number of cycles seem to have a relevant effect on the final pH or wettability. Therefore it was decided to treat the CB only one cycle to optimize time while the inlet position was established at 10 mm in order to protect the torch from any powder going into the electrodes.

On the other hand the presence of ozone may continue to oxidize the CB black even once collected in the bag. An experiment was carried out in order to check the oxidation capacity of the generator ozone on the collected CB, as well as the thermal effect of the cooling system 1 (at 140ºC). For this purpose, CB was placed directly in the collecting bag and left for a given period of time under reaction conditions. The amount of CB in the bag was increased every 10 minutes by 20 grams to simulate the increasing collected quantity during modification.

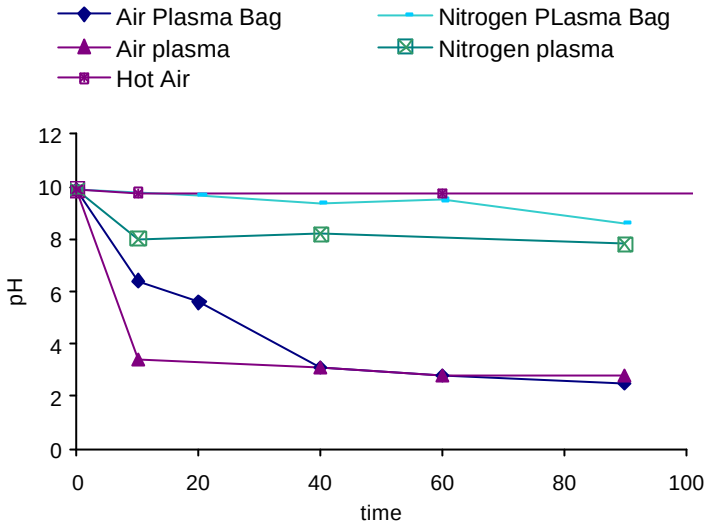

Fig.5. 52 pH of N134 after being submited to different conditions in the APP reactor

In Fig.5. 52 above, “Plasma Bag” indicates CB placed in the collection bag while plasma on its own indicates normal treatment conditions. Hot air simulates the thermal effect at 140ºC for cooling system 1. The results obtained during this experiment indicate that hot air at the presented conditions produces no effect on the CB, thus, thermal effects are minimal compared to the plasma. Looking at the results obtained for nitrogen plasma, although there is an effect due to the chemical species even once the CB is collected, this is also minimal, and it does only take place after 60 minutes collection. On the other hand the effect of chemical species being present and reactive in the collection bag is much more evident for the air APP treated samples. In this case, although pH change occurs much faster when CB is blown through the plasma torch, the effect of the reactive species (probably ozone and NO_x) during the collection stage is also important. As it can be seen after 40 minutes in the collecting bag pH turns to be the same as if CB had gone through the plasma system.

In a second step another inlet situated at 40mm from the end of the plasma nozzle was prepare in order to introduce ammonia as described in the reactor set up in chapter 3. Ammonia was introduced together with nitrogen plasma but also after a pre-oxidizing air plasma treatment. The changes in pH can be observed in Fig.5. 53 while changes in wettablility are presented in Fig.5. 54.

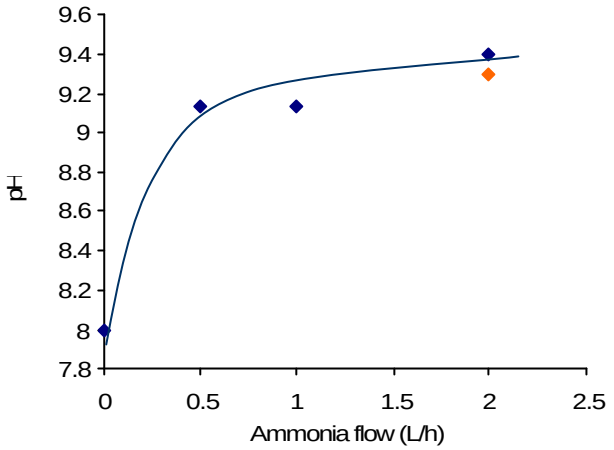

Fig.5. 53 pH after N134 AP modification as function of Ammonia flow

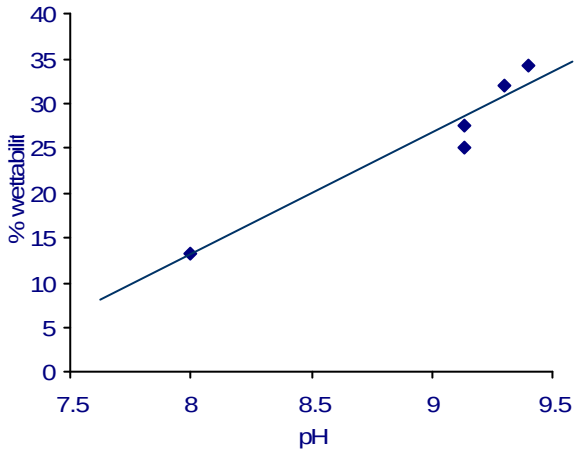

Fig.5. 54 Relation between pH and wettability after Nitrogen and Ammonia AP treatment

It can be observed already at first sight from the presented results, that including ammonia during the nitrogen plasma at APP conditions increased final pH. Maximum pH value was obtained for 2l/h ammonia rate flow. The orange measurement presented in Fig.5. 53 represents a value obtained with a 5% H2 in the carrier gas. Although it could be thought that it could help to the formation of basic groups no evidence was found. Fig.5. 54 shows that the pH increase was also related to an increase in the water compatibility, being maximum also for the highest ammonia flow.

Due to the presented results it was established that the optimal treatment was carried out with 2L/h ammonia inlet and using N_2 as carrier gas on its own. Using these conditions, the treatment was repeated for a pre-oxidized sample. Changes in pH during the different steps are shown in Fig.5. 55.

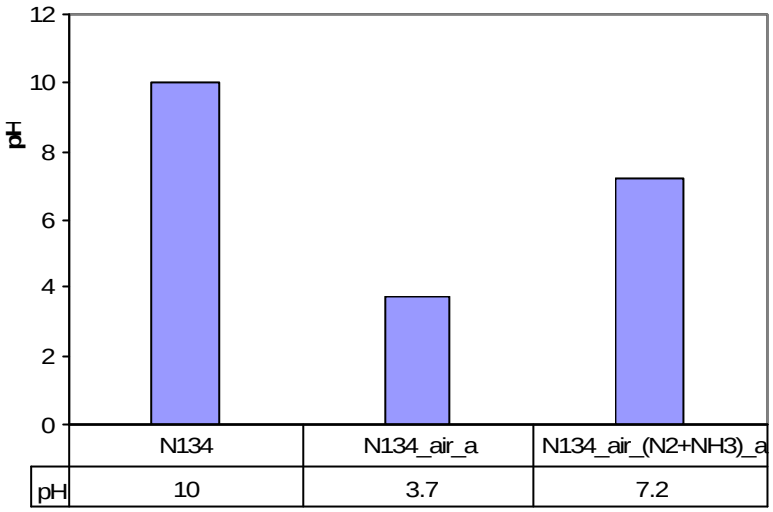

Fig.5. 55 pH for N134 after APP treatment with ammonia with and without pre-oxidation

Besides N134, XPB 171 was also modified using the APP reactor. In this case, table 5.14 shows the pH values for 1 cycle and CB inlet at 10mm. Air, Nitrogen, ammonia post-reaction before and after oxidation pH values are presented. As it can be observed air APP did decrease the pH level below than for N134, and as well as for this CB a post reaction including ammonia as a reactive gas in the system lead to a final pH above neutrality.

Table 5.14 pH values for XPB 171 after APP modification under several conditions.

CB grade	pH
XPB 171	**8.6**
XPB 171_air_a	**2.2**
XPB 171_N_2_a	**8**
XPB171_(N_2+NH_3)_a	**8.5**
XPB171_air_(N_2+NH_3)_a	**7.7**

5.4.1.3 Comparison LPP and APP

As a sum up of this section is possible to say that both oxygen LPP treatments as well as air APP modifications introduce acid groups on the surface of carbon black which provokes a diminishing in the pH values. Focusing on the LPP treatment it was observed that the presence of impurities did favor the pH decrease probably due to a higher modification rate. However, the N134g also presented a very significative pH change allowing to confirm the reactivity of such type of carbon with the oxygen plasma. On the

other hand, for single cycle in the APP system under air plasma a pH of 3.2 equivalent to a 30 min. at 40W in the LPP was achieved, while in the case of XPB 171 the lowest pH value was obtained by means of this treatment.

Nitrogen plasma both at low and APP provokes a slight decrease in the final pH, however this is thought to be a consequence of a post-reaction when the modified CB becomes in contact with the atmospheric oxygen. A special low value was detected for the graphitized CB which could indicate a higher ablation effect when amorphous C is absent on the surface of CB.

Finally, modification produced by ammonia LPP seem to be very dependent on the modification conditions. Low generator powers (up to 40 W) and medium reaction times (up to 30 minute) were found to be optimal in order to obtain the highest basicity retention. In this case it seems that ammonia preferably reacts with the amorphous structures which are absent on the graphitized CB.

When ammonia was introduced in the APP system in order to generate basic structures after the nitrogen plasma activation, it was observed that pH obtained was higher than after pure nitrogen plasma APP modification. An increase in hydrophilicity was also shown as a result of ammonia presence in the APP system. However, pH values in this case did not go beyond than the ones from original N134 as occurred in some cases for ammonia LPP modifications.

5.4.2 Acid/Base Titrations

In order to have a better insight in the final composition of the modified CB's, Bohem's titration was carried out to evaluate quantitatively the acid groups on the surface of CB after both LPP and APP treatments. Acid values were measured for all treated samples while basic values where only obtained for the ammonia treated LPP CB's. Detailed explanation of the sample preparation and procedure for evaluation of this parameter can be found in annex 5. Measurements were repeated 3 times.

5.4.1.1 LPP treated samples

First, the results for LPP treated CB's are presented. Fig. 5.57 presents the acid equivalents present on the surface, the small figure at the right angle shows the values per gram of CB, however more importance was given to the value normalized by the specific surface are as will be described in detail next.

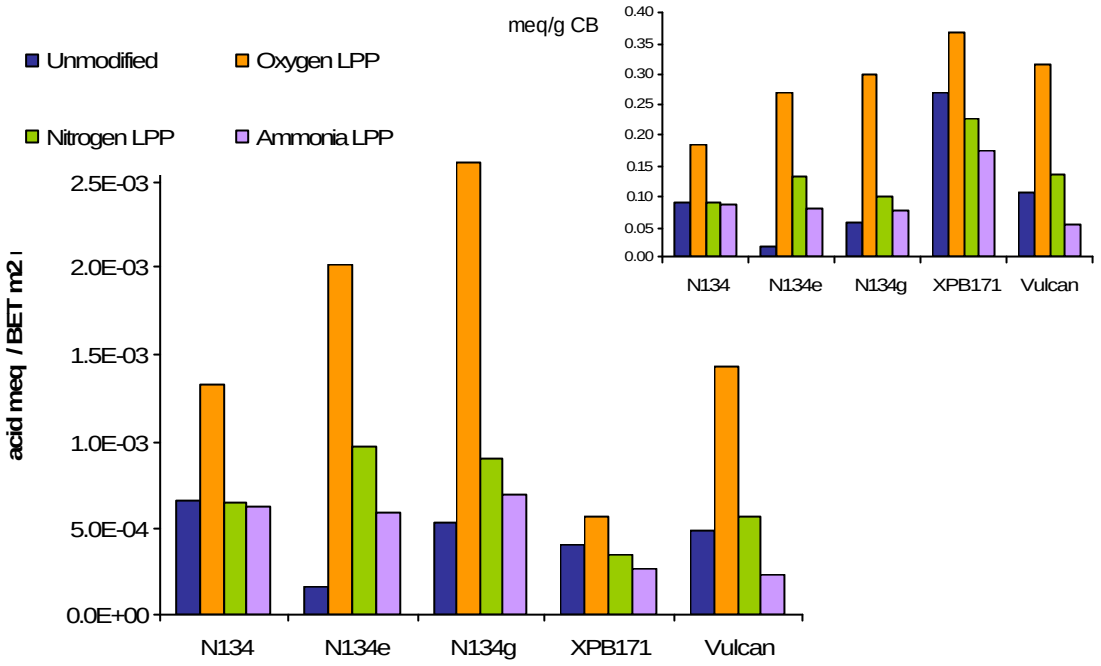

Fig.5. 56 Obtained acid meq./ m^2 CB surface after oxygen, nitrogen and ammonia LPP modification. Small figure right above, shows acid meq. per gram of CB.

Although when looking to the obtained meq. per gram of CB, XPB 171 seems to have a higher number of acidic groups both before and after LPP treatment, it has been considered that the amount of acidic groups per square meter would give a better idea of the reactivity of the carbon surface towards the plasma. When values are normalized using their specific surface area calculated previously in this chapter, a very different trend can be observed.

The results are in good agreement with the effect observed by the group of J.P. Boudou et al, where they observed that modification of active carbon by using a microwave plasma reactor with oxygen as active media, the inclusion of oxygen groups took place at the outer surface of the carbon powder (J.P. Bodou et al. 2000). Looking at the above results, the hypothesis seems also to be acceptable for CB powders. As it was shown previously in this chapter, microporosity on the surface of the studied CB's followed the next order: XPB171> Vulcan> N134 > N134e > N134g. If the amount of acidic groups on the surface is normalized by the specific surface area (including microporous) the amount of acidic groups per square meter follows the same order described above. On the other hand as it shown in fig. X there is not a linear relationship between the acidic groups and the microporosity. Although for low microporosties the trend is rather lineal, at high

microporous levels (as the ones presented by XPB 171), it seems to reach a plateau. Finer measurements about the microporous diameter should give more information about the oxygen attack mechanism. A possibility could be that due to their proximity the attack by the oxygen species may provoke the conversion of two or more microporous in a larger area which can be then attacked by the reactive oxygen species. When the microporous area for XPB171 is analyzed after the oxygen plasma treatment a slight decrease is observed about the 3% of the initial value, it is also possible to observe how the whole adsorption isotherm presents lower levels than the rest as presented also previously in this chapter. Because this is such a small change studies in this field should be followed to positively confirm this hypothesis.

However, the idea above is also supported by the studies performed by J.I. Paredes and coworkers about the mechanism for oxygen plasma attack on HOPG. It was observed that oxygen activated species could attack the HOPG surface creating vacant positions, in a first step vacancies were created apart of each other but as time increases new attacks are concentrated around the already formed vacancies (J.I. Paredes et al. 2002).

A slight increase in the acid value after nitrogen APP modification is also observed in accordance with the pH registered values. Increased acid values were also detected by S.J. Park et al. after N_2 cold plasma (S.J. Park et al. 2001).

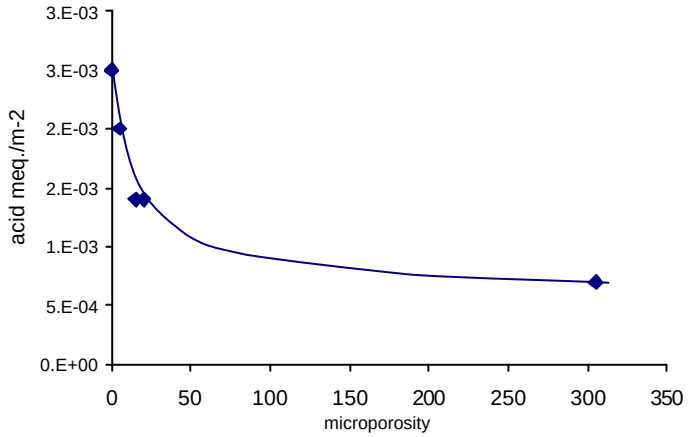

Fig.5.5 7 acid meq/m ^{2} as function of the microporosity

Finally, a relation between the acid meq. presented per gram of CB and the measured pH was found as shown in Fig.5.5 8. An exception is found for the values presented for N134g after oxygen LPP which does not follow the same trend. Results indicate that this CB presents a higher meq. acid value than the one that should correspond for its pH. A reason could be found in the type of acidic groups introduced in each type of structure (graphitic, edges and amorphous carbon). Nevertheless, more detailed experiments should be performed in order to confirm this result.

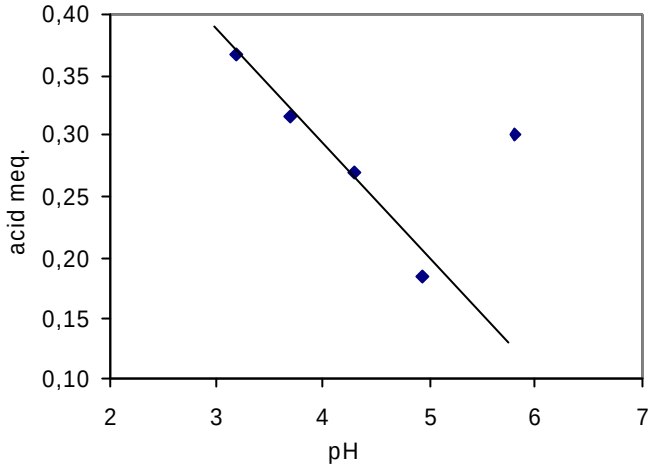

Fig.5.5 8 Linear relation found between acid meq and pH

It is also worth to mention that acid values similar to those obtained by acid (HNO_3) and air oxidation but preventing changes in specific surface (Y. Otake et al. 1993).

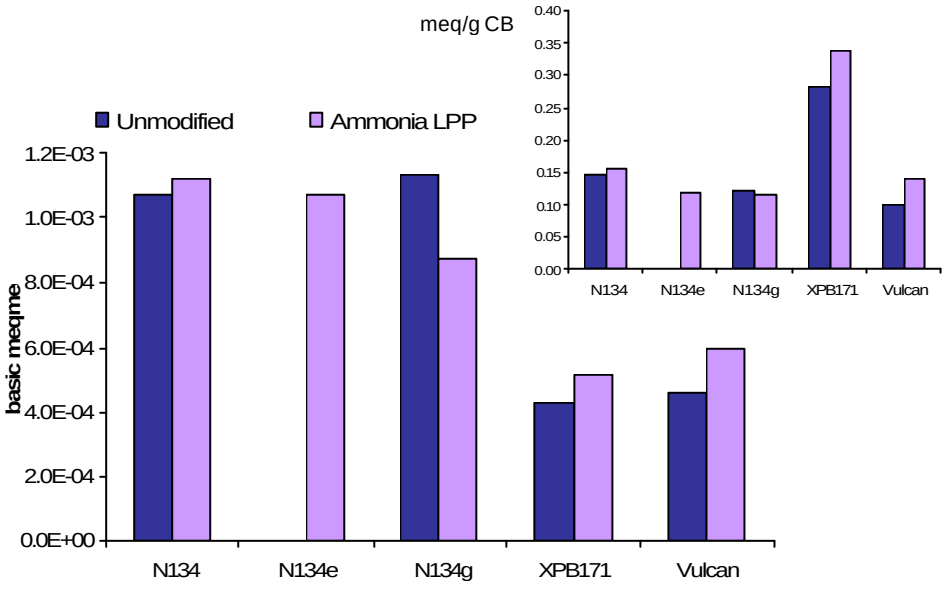

Fig.5.5 9 Obtained basic meq. per square meter of CB surface after ammonia LPP modification. Small figure right above, shows acid meq. per gram of CB.

When looking in Fig.5.5 **9** to examine the final basic miliequivalent after the ammonia plasma treatment the same trend is not observed as for oxygen LPP, which indicates that

the mechanism for ammonia reactive species is different than the one proposed for the LPP oxygen species.

As a first result it can be observed that the inclusion of basic groups is produced at a much lower level than for acidic groups indicating a lower activity for this type of plasma. When looking more in detail to the basicity values it is also observed that as it was already presented during the pH results, ammonia plasma does not introduce basic groups on more graphitic structures as the ones presented by the N134g. On the other hand maximum variation is observed for the N134e which is thought to present higher amorphous structures than any other presented CB. The result is also in accordance with the pH measurements for which N134e presented also the highest increase.

5.4.1.2 APP treated samples

In the case of APP treated CB's acid meq. were determined both after air and nitrogen treatments. Moreover, the proportion of weak and strong acids was also evaluated after N134 APP treatment. Bohem's titration using NaOH gives a result for the total acidity, $Ba(OH)_2$, has been reported to give a hint for the acidic positions and $HNaCO_3$ gives a value just for strong acids (mainly carboxylic groups). The results for N134 are presented in Fig.5. Important changes can be observed for surface total acidity (NaOH). The results with $Ba(OH)_2$ indicate that probably the acidic groups are adjacent so that one molecule of the base is able to neutralize two acidic groups at the same time. Other studies have reported that this proximity could be due to the fact that these two acidic adjacent groups come from the hydrolysis of carboxylic anhydride (P.F. Fanning et al. 1993). Finally, the result for the weak base indicate that more than one different type of acidic groups are present at the surface of the filler, being the most likely carboxylic acids, quinones and lactones. It was also found that nitrogen plasma presents a lower percentage of weak acids on the surface of carbon black 13% of the total acidity while for the air treated the weak acid represent a 27% of the total acidity. The same results were obtained for the filler two cycle treated CB through the plasma torch.

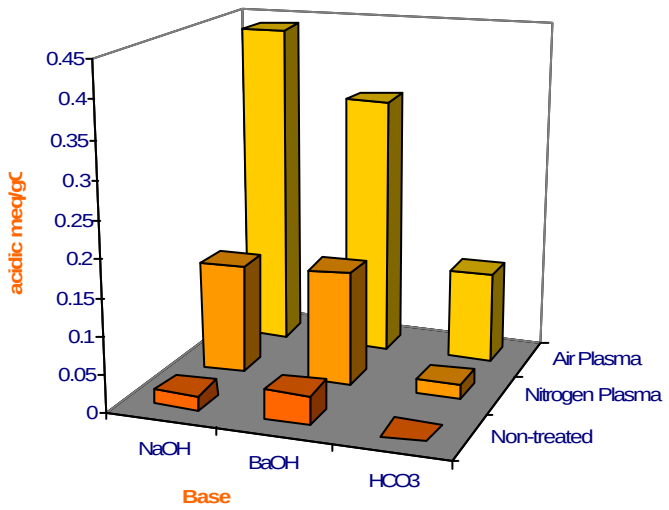

Fig.5.60 Acid meq. after nitrogen and air APP N134 treatment using several base titrating reagents.

Next figure presents a relation between the obtained acid meq. with the pH values for both total and strong acids. It is possible to observe that total acidity presents a linear relation with pH values, however the higher the pH the lowest also the amount of strong acid groups.

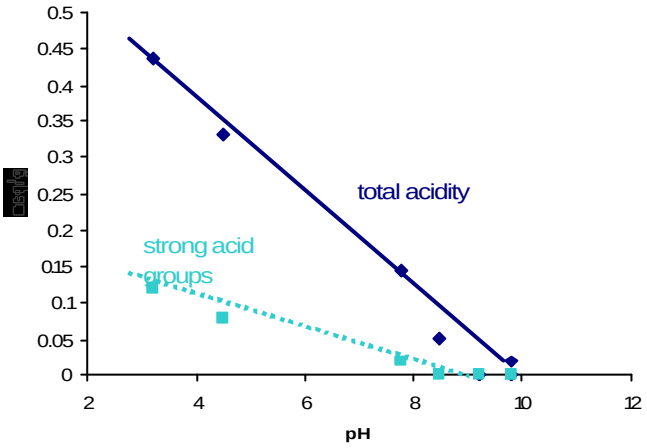

Fig.5.6 1 Relation between strong acid groups and total acid groups and pH after APP N134

Total acidity measurements were also carried out for XPB 171 after air and nitrogen APP. Obtained results are presented in table 5.15. A linear relationship was also found between total acidity and pH values as observed in Fig. 5.62.

Table 5.15 . Obtained acid meq. After XPB 171 APP treatment

CB	Acid meq/g CB
XPB 171	**0.197**
XPB 171_ air_a	**0.769**
XPB 171_ N_2_a	**0.245**

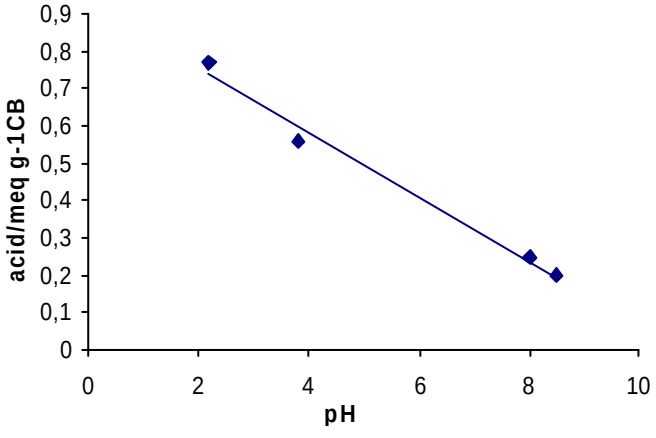

Fig.5.6 2 Linear Relation between Acid meq and pH for XPB 171 APP treated

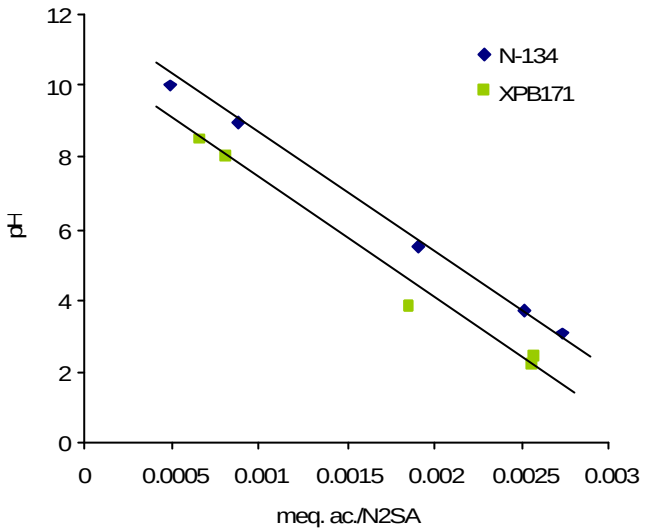

Fig.5.6 3 Linear relation for N134 and XPB171 after specific surface normalization.

Finally figure Fig.5.6 3 presents also a relation between pH and acid meq. However, in this case acid meq. are normalized by the specific surface area. As it can be observed, although XPB 171 presents lower pH sue to the higher surface area and therefore higher number of acid groups for the same CB amount, it is possible to observe that both CB's present parallel trends after APP treatments. This indicates that contrary to the trend for the LPP where N134 presented a higher reactivity, for APP treatments the reactivity of both CB surfaces is equivalent. It is worth to remember that impurities on N134 during APP are eliminated to a large extend (about 80%) which confirms that impurities are mainly modified during LPP treatment giving a higher reactivity.

5.4.2.3 Comparison

The acid/base values have been presented both for LPP and APP. The results obtained mainly confirmed the ones obtained by means of the pH values and it was normally possible to obtain a linear relation between the total amount of acid groups and the pH value. However, N134g presented a very high acid value showing once again its reactivity toward oxygen plasma. At the same time basic miliequivalents diminished on the surface of N134g after ammonia LPP which confirms the absence of reaction between the ammonia active species and the structures present on the N134g. On the other hand

N134e presented a very intense reaction in such media although the number of introduced milieqivalents was always lower than for oxygen plasma.

On the other hand, it was show that air APP modification is not so much dependent on surface structure as LPP treatments. For the LPP higher activity in oxygen plasmas is obtained for N134, especially when impurities are on the surface. However, in APP conditions the surface nature does not seem to be relevant as it is shown by the parallel slope of the pH vs $Meq \cdot g^{-1} * m^{-2}$. In this case the larger the surface the higher the final number of acid meq. and the lower the pH.

5.4.3 X-Ray Photoelectron Spectroscopy (XPS)

In order to study more in detail de surface composition of the plasma treated CB's, XPS studies were conducted on some specimen's both treated at LPP and APP for some of the presented CB's.

XPS measurements were carried out at the INRS-Energie, Matériaux et Télécommunications, Varennes, Québec, Canada by the group of Prof. J.P. Dodelet. Surface analysis was performed by X-ray photoelectron spectroscopy (XPS) using a VG ESCALAB 200i instrument. Some measurements were carried out in the Universitat de Barcelona using. XPS experiments were performed in a PHI 5500 Multitechnique System (from Physical Electronics) with a monochromatic X-ray source (Aluminium Kalfa line of 1486.6 eV energy and 350 W), placed perpendicular to the analyzer axis and calibrated using the 3d5/2 line of Ag with a full width at half maximum (FWHM) of 0.8 eV3 measurements were carried out in order to ensure comparable results between the two apparatus. Differences were smaller than 0,2% in composition.

Fig.5.6 4 presents the XPS spectrum for N134. The same feature is obtained for all CB's, not only the ones studied here but also for CB's produced using the furnace method. As said in the introduction of this work, in some cases similar XPS results can be obtained although some evident behaviour differences exist, such as the curing rate during the vulcanization reaction (J. Clotet 2005). Therefore, although XPS may give very useful information it can not considered as a unique method to obtain information about CB surface. Worth to mention is that the Hydrogen amount can not be detected by using this technique; therefore the impurities can not be differenced from the real carbon surface belonging to the first's layers of the CB structure.

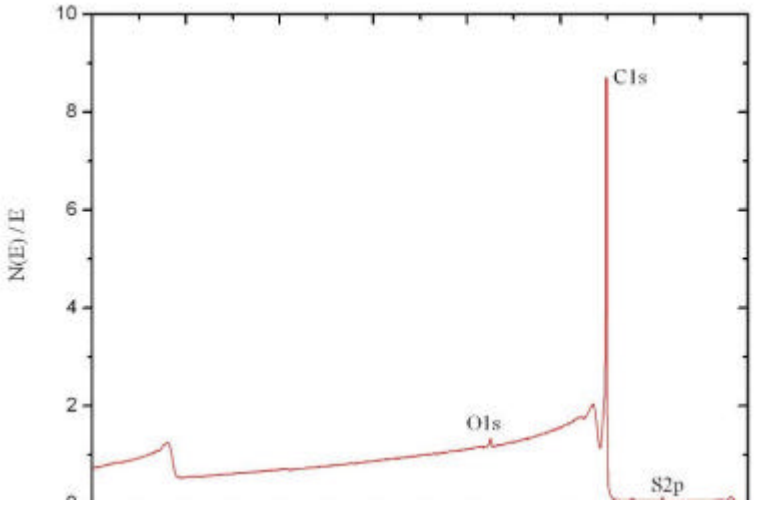

Fig.5.6 4 XPS spectrum for unmodified N134

In the XPS spectrum for not modified CB's, usually three elements can be detected, carbon as the most present, oxygen and also sulphur traces. Oxygen comes from oxidation processes after the CB obtainment while sulphur comes from the utilized feedstock during the CB production. C. Poleunis and co-workers studied the presence of sulphur on CB and determined that main sulphur groups were thiolates and sulphates (C. Poleunis et al. 2000). The study included also Vulcan XC-72 for which very similar values to the ones presented here are reported. Contrary, XPB 171 which is used manly as pigment in inks and coatings did not present any sulphur on its surface. Oxygen content also is variable depending on the final application and CB grade but is normally present between 0,3 and 1,5%. As it can be observed also in the table below in any of the unmodified CB's nitrogen was detected.

Table 5.16 Composition for the unmodified CB's

CB grade	C%	O%	S%	N%
N134	**98.09**	**1.35**	**0.56**	**---**
XPB 171	**100**	**----**	**----**	**---**
Vulcan	**99.23%**	**0.3**	**0.47**	**---**

On the other hand Fig.5.6 **5** shows the spectrum after a CB treatment in a nitrogen containing plasma. This type of spectrum is common for all plasmas containing some nitrogen precursor, nitrogen or ammonia, both at low and atmospheric pressure. However, the amount of nitrogen introduced on the surface of CB was different depending on the system.

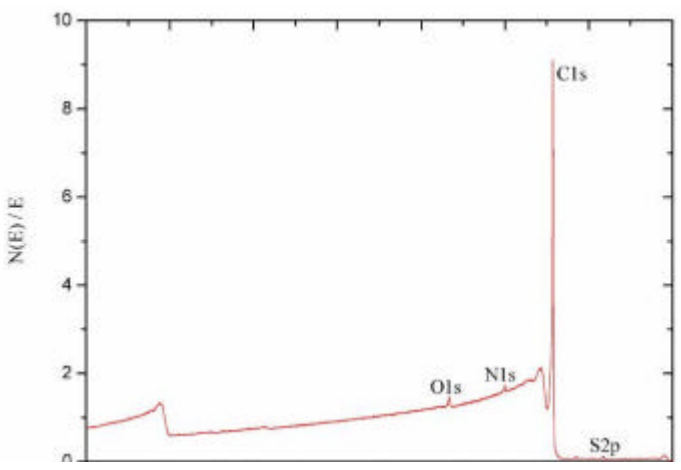

Fig.5.6 5 XPS spectrum after modification in a nitrogen containing plasma, in the present case N134_N2_ a

Deconvolution of the nitrogen peak envolvent was carried out in the cases were the Nitrogen peak was large enough to ensure a reliable result (above 0.3%). The deconvolution allowed to study the different nitrogen functionalities present on the CB surface. The importance of such information will be further explained in chapter 7. Fig.5.6 6. shows an example of the deconvoluted nitrogen peak. For some cases the same procedure was also done on the oxygen peak. Table 5.15 and 5.16 show the binding energy that was attributed to each nitrogen and oxygen functionality.

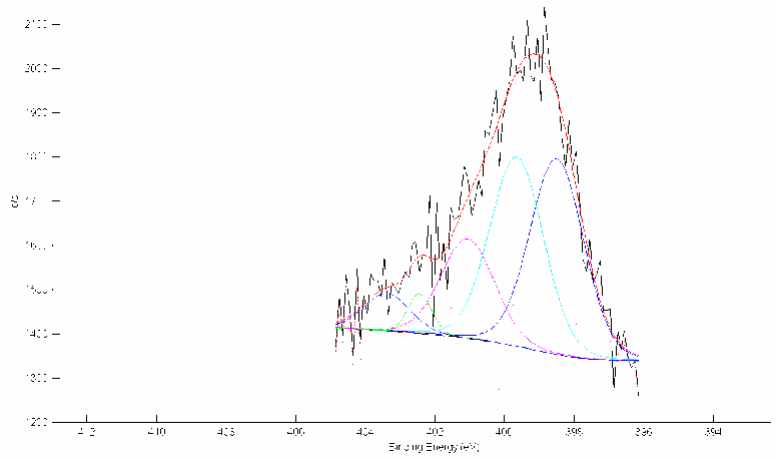

Fig.5.6 6 Deconvolution of the N1s Nitrogen Peak in order to study the nitrogen Funcionalities

Table 5.17 Binding energies for N functionalities

N_{1s}	E/Ev	FWHM
Pyridinic	398↔399	1↔2

Table 5.18 Binding energies for O functionalities

Nitrile	400↔400,5	1↔2
Pirrolyc	400,2↔400,9	1,5↔2,5
Graphitic	401↔402	0,5↔2
Oxide	402↔405	0,5↔4
Others	405↔410	0↔5

O_{1s}	E/eV	FWHM
C=O	531↔531,85	1↔2,5
C-O	532↔533	1↔2,5
C-OOH, C-O-C	533↔534	1↔2,5

Following detailed composition is given for several LPP samples for the three CB grades: N134, XPB171 and Vulcan. Nitrogen containing plasma was again given more emphasis for the already presented reasons, being mainly lack of information in this field as well as very interesting applications in the field of fuel cells. Composition in % of atomic element after LPP modification is given in Table 5.17

Table 5.19 Chemical composition determined by XPS for several LPP treatments

CB Reference	Gas	t (min)	P(W)	N%	O%	S%
N134_NH_3_c	NH_3:Ar (3:1)	60	20	0.29	1.25	0.52
N134_NH_3_c	NH_3:Ar (3:1)	30	40	0.35	1.34	0.58
N134_NH_3_c	NH_3:Ar (3:1)	30	80	0.3	1.23	0.49
N134_N_2_c	N_2	60	15	0.36	1.56	0.51
N134_N_2_c	N_2	30	60	0.4	2.5	0.52
N134_N_2_c	N_2	15	80	0.34	2.5	0.46
Vulcan_NH_3_c	NH_3:Ar (3:1)	30	80	0.1	2.7	0.45
Vulcan_NH_3_c	NH_3:Ar (3:1)	30	40	0.2	2.3	0.47
Vulcan_N_2_c	N_2	30	40	0.22	3	0.49
XPB 171_ NH_3_c	NH_3:Ar (3:1)	30	40	0.23	2.6	---

As it can be observed in the table above, maximum nitrogen content on the N134 surface when using ammonia LPP treatments was achieved after treating the material at 40W for 30 minutes. As before stated, medium power and time range seem to be the more beneficial conditions to obtain maximum nitrogen retention. On the other hand, maximum nitrogen content was not obtained by ammonia treatment but when using nitrogen LPP modification. Up to 0.4 % was obtained for 60W at 30 minutes. It is possible to observe however, that nitrogen LPP treatment also increased the amount of oxygen on the final CB surface.

When treating however both Vulcan and XPB171 under similar conditions, the amount of final nitrogen on the carbons was lower than for N134. Therefore, the nature of carbon surface seem to be an important parameter when trying to introduce nitrogen in the C structure, probably in a higher extend than for oxygen functionalization.

On the other hand, sulphur species seem not to be altered by the plasma conditions. Variation o this element is almost negligible. Sulphur being covalently linked to the Carbon structure does not disappear during the LPP modification.

In most cases for LPP treated CB's the amount of N was too low to perform a reliable deconvolution of the nitrogen peak. Only for the nitrogen treated N134 presenting a 0.4% of this element was acceptable and composition is Fig.5.6 7.

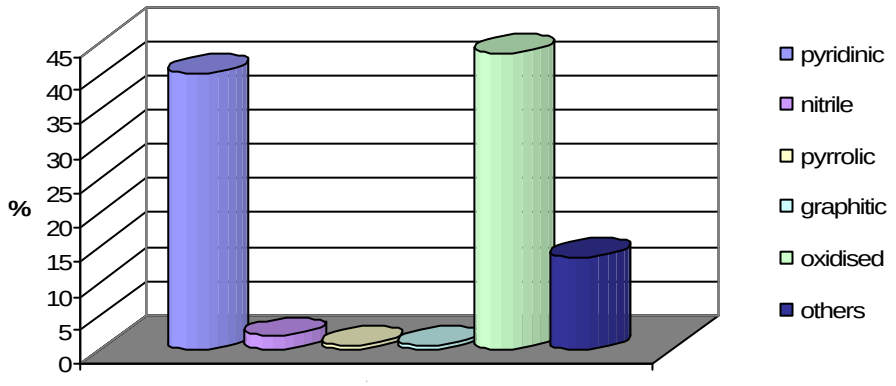

Fig.5.6 7 Nitrogen functionalities determined by N_{1S} peak deconvolution for N134 treated with N_2 at LPP conditions (60W/30 min)

As it can be observed in the figure above mainly N was introduced in pyridinic positions and oxidated groups which also is in agreement with an increase in the oxygen atomic composition. The main oxygen functionalities are also presented in Fig. 5.68 showing that carboxylic groups are the most relevant species among the oxygen containing groups.

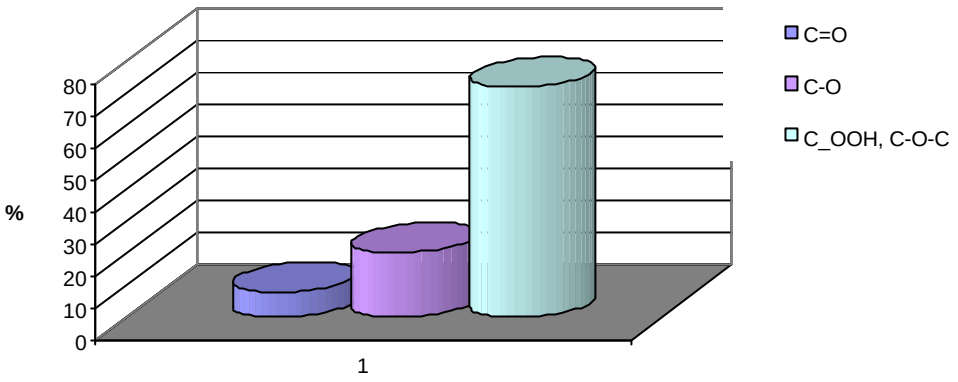

Fig.5.6 8 Oxygen functionalities determined by O1S peak deconvolution for N134 treated with N2 at LPP conditions (60W/30 min)

XPS was also used to study the final composition of some APP modified CB presented in table 5.18 (one cycle treatment was only applied).

As first interesting result it can be observed that air plasma on N134 not only introduced oxygen but also nitrogen on the final composition. Worth to mention that air plasma having 20% nitrogen may also create some nitrogen active species which are not formed in pure oxygen LPP plasma. The second interesting information is that for all presented APP treatments final nitrogen atomic concentration was higher than the one presented for the LPP nitrogen precursor plasmas. Highest value was found for nitrogen APP treatment on N134 which at the same time presented also high oxygen content. Ammonia containing treatment presented very close results to the pure nitrogen APP treatment with slightly lower oxygen content.

Table 5.20. Composition determined by XPS for APP treated CB's

CB Reference	Carrier gas	Plasma Gas	CB inlet (mm)	NH_3 inlet (mm)	N%	O%	S%
N134_air_a	N_2	air	10	----	0.7	6.1	0.52
N134_N_a	N_2	N_2	10	----	1.7	2.86	0.56
N134_(N_2+NH_3)_a	N_2	N_2_NH_3	10	40	1.67	2.23	0.55
N134_(N_2+NH_3)_a	N_2/H_2(5%)	N_2_NH_3	10	40	1.21	1.98	0.50
*N134_air*_(N_2+NH_3)_a	N_2	Air_(N_2_NH_3)	10	40	0.9	5.34	0.48
*XPB171*_(N_2+NH_3)_*a*	N_2	N_2_NH_3	10	40	0.4	1.2	---
*XPB171_air*_(N_2+NH_3)_a	N_2	N_2_NH_3	10	40	0.5	3.9	---

In this case the amount of nitrogen detected on XPB 171 although higher than for LPP treatment was still far for the ones obtained on N134.

Next figure shows the proportion of nitrogen functionalities for the N134 APP treated samples. Although for all samples pyridinic functionalities are the most relevant, a higher functionalities diversity than for LPP treatments is found. Nitrogen APP treated N134 is the one presenting a higher content of pyridinic structures, followed by nitrile and oxidated species. When ammonia is present in the treatment both nitrile and pyrrolic functionalities

seem to increase while the hydrogen presence trends to increase the oxidative species which is in agreement with a higher final oxygen content.

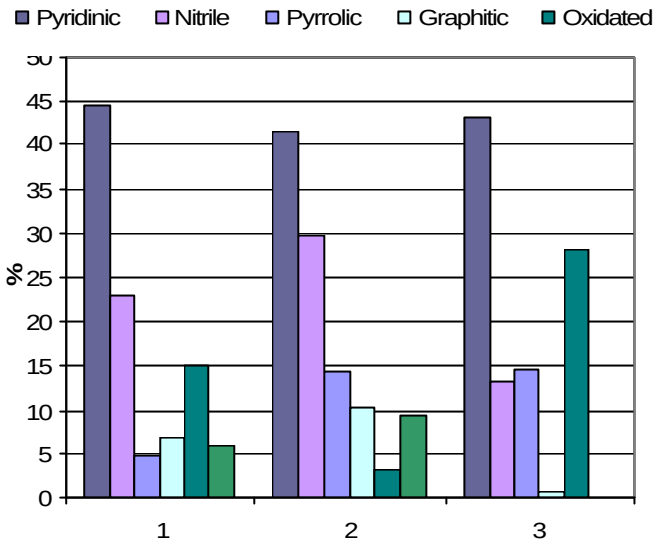

Fig.5.6 9 Nitrogen Functionalities for several APP treatments on N134: Sample 1 corresponds to N_2 APP treatment, 2. (N_2+NH_3), and 3 (N_2+NH_3) with 5% H_2 in the carrier gas

Next figure presents the distribution for oxygen functionalities. In all cases the higher proportion is presented by the carboxylic and ether groups with slightly higher values in the hydrogen containing treatment.

.

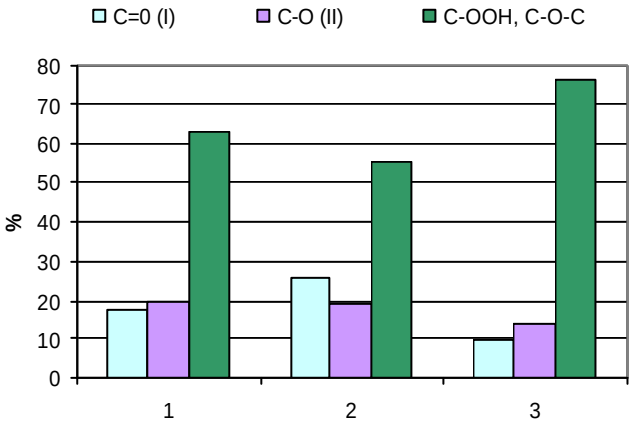

Fig.5.70 Oxygen Functionalities for several APP treatments on N134: Sample 1 corresponds to N_2 APP treatment, 2 to N_2+NH_3, and 3 N_2+NH3 with 5% H2 in the carrier gas.

XPS
results have shown that nitrogen has been included on the CB surface composition both by LPP and APP. Surface nature has been shown to be a relevant factor for final nitrogen

levels being N134 the one with higher nitrogen content after LPP an APP treatments. On the other hand, nitrogen levels have been observed to be higher after APP than after the studied LPP treatments.

5.4.4 Impurity level and GC-MS from extracted Matter after Plasma modification

As it has been presented during the discussion of the obtained results, surface impurities may play an important role in the modification of CB by means of plasma techniques. In order to obtain some information, CB's were selected and extracted after being submitted to different plasma treatments. As for the original CB grades, impurities were quantified and analysed by GC-MS (procedure described in annex. 2 and 3)

Results for LPP treated CB's are presented in Table 5.21. As it can be observed and as it was already introduced earlier in this work, no difference in the impurity level was found after LPP treatment. Nor the vacuum conditions or the attack by the active species provoked the ablation of the adsorbed impurities on the CB. Therefore, it can be concluded that in the case of high impurity content as for N134, the modification takes place mainly on the impurity layer.

Table. 5.21 Impurity level after LPP reatments

CB	LPP Treatment	Impurities (mg/g)
N-134	---------	10,4
N-134	O_2 (40W, 15 min)	10,2
N-134	N_2 (40W, 30min)	10,3
Vulcan	----------	0,3
Vulcan	O_2 (40W, 15 min)	0,31
Vulcan	N_2 (40W, 30min)	0,27
XPB171	----------	0,34
XPB171	O_2 (40W, 15 min)	0,4
XPB171	N_2 (40W, 30min)	0,36

It could be expected then that if impurities are modified, some changes could be observed on the GC-MS chromatograms. Contrary to this statement, no new peaks were found for the analyzed extracted compounds. A possible reason is that because modification takes place only on the most outer surface, quantities are not enough to be detected by this technique. Analysis by ToF-SIMS could be an alternative to study this effect with more sensitivity as only the outer molecules are studied.

Next table indicates the amount of impurities after APP treatment. In this case different amounts before and after treatment are observed. The larger difference is observed for N134 after air APP treatment for which impurity level is decreased in a 70%. The effect was not observed by the nitrogen plasma, and can be concluded that oxygen active species are the ones responsible for this surface “cleaning” effect. Moreover, in this case a small difference was detected in the GC-MS analysis where a new oxidized specie (naphtalic anhydride) was detected (fig 5.71). As already stated during the acid value determination anhydride was very likely to be in the surface of the air APP treated carbon due to the proximity detected by means of $Ba(OH)_2$ titration of the acid groups.

Table 5.22 Impurity levels after APP treatments

Mostra	APP Treatment	impurities (mg/g)
N-134	---------	10,4
N-134	Air (1 cycle)	3,2
N-134	N_2	10
XPB171	----------	0,34
XPB171	Air (1 cycle)	3,2
XPB171	Air (2 cycles)	6
XPB171	N_2	0,4

Contrary to the effect caused by the air plasma on the N134, the level of impurities increased after the air APP treatment of XPB 171. It is also observed that the final level of impurities after air APP (3,2mg/g) is very similar to the final value obtained for N134. It is also possible to see that the level increases with increasing cycle number through the system. The results indicate that APP acts as a surface cleaner from non covalent attached structures but it also provokes the formation of macrocyclic oxidized structures as the one mentioned above, which are eliminated from the surface during the extraction procedure. To test this hypothesis pH was measured after drying in a vacuum oven at 160ºC the extracted CB’s. the results presented in table 5.23 show a real increase of the pH after the extraction of air APP treated samples.

Table 5. 23. pH after air APP treatment previous and after extraction

	pH before extraction	pH after extraction
N134_air_a	**3.2**	**5.5**
XPB 171_air_a	**2.2**	**4.1**

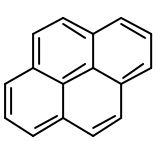

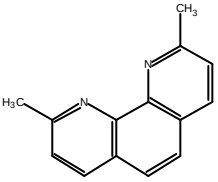

2- 1,10-phenatroline

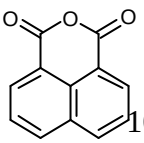

5- 1,8-Naphtalic anhydride

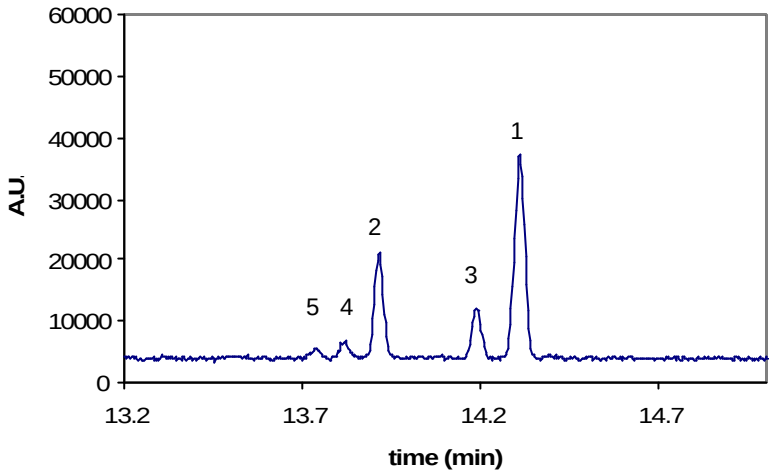

Fig. 5.71 GC Chromatogram for extracted matter after APP air treatment on N134. Identification of compunds was done by means of Mass Spectrometer detector

The formation of high weight aromatic compounds which include a high number of oxidized groups has already been described during the CB oxidation by means of nitric acid (K. Kamegawa et al. 2002) The structures detected are presented in Fig. 5.72, Further studies should be carried out in order to confirms this hypothesis.

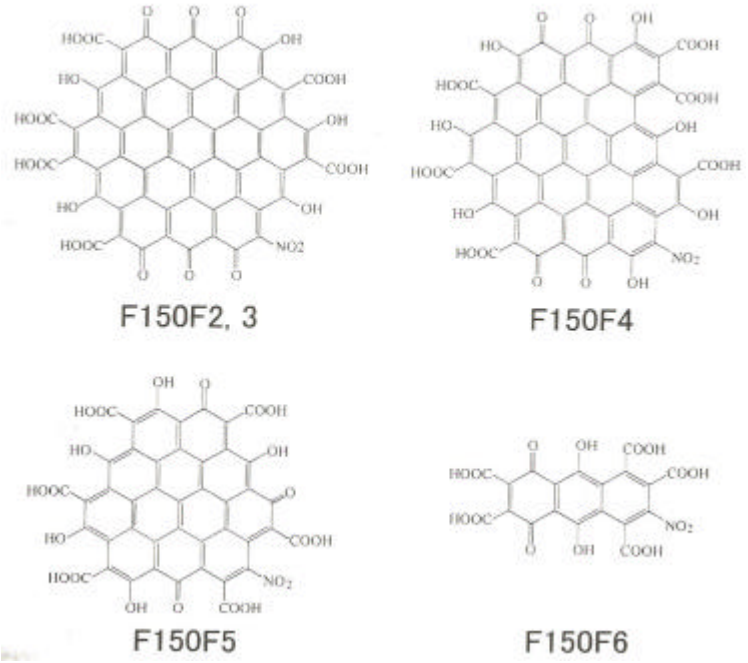

Fig.5.7 2. Structures detected by K.Kamegawa et al. during surface oxidation of CB with acidic acid.

As a sum up of CB surface chemistry composition alter plasma treatment it can be said that oxygen introduction seem to be more carbon structure dependent when using LPP plasmas, on the other hand APP seems to attack with the same reactivity all carbon structures.

When introducing nitrogen on the carbon surface, APP both with air and nitrogen seem to be an effective method, however in this case final nitrogen presence seem to depend on the reactivity of the carbon. In the present case N134 was the CB presenting a higher N content followed by XPB 171 and Vulcan.

5.5 Surface Energy

So far in this work morphologic, surface structure and chemical studies on the surface of CB before and after plasma treatment have been carried out in order to evaluate the changes produced both by LPP and APP treatments. As last part of CB characterization surface energy determination is presented.

Surface energy of CB and other carbon fibers and powders, also known as surface activity has been studied by several methodologies such as capillary tension methods (K. Tsutsumi et al. 1990 and 1996), contact angle (S. J. Park et al 2001), Thermo Gravimetric Analysis, Inverse Gas Chromatography and adsorption gas isotherms (J. Donnet et al. 1993 and 2002, A. Schroeder et al. 2000) and even by using XPS (R.H. Bradley et al 2002). Almost all of them divide the surface energy in two different components as already presented, one is known as dispersive and is related to the Van der Waals interaction of the carbon with the surrounding molecules or surfaces, the second corresponds to the polar. Usually several probes of different polarity are used in order to get information about the two presented components. This is the case for capillary systems, contact angle, and inverse gas chromatography. However, some energetic information can also be obtained from the nitrogen adsorption curves, mainly about the dispersive component, or by studying the decomposition of the carbon surface under controlled conditions (TGA) (F.M. Fowkes 1980 and T. I. T Okpalugo et al 2005).

In this section the suitability of some methods to determine the surface energy of CB is evaluated. Capillary and contact angle measurements were chosen as method to obtain information about the two different energetic components. In some cases the results were compared with the ones obtained by IGC a much more tedious and time consuming method.

5.5.1 Surface Capillarity and Contact Angle

Capillary methods are based on the study of the weight uptake velocity from a column of powder situated in a glass cylinder. The glass cylinder which is hanged from a precision balance, has a porous bottom which allows the solvent below to get in contact with the powder. A picture of the system can be observed in Fig.5.73. In order to avoid the effect of surface morphology such as particle size and porosity hexane is used as a blank probe to normalize all samples, as hexane is assumed not to interact with any of them, or at least to a very little extent, due to its low polarity.

The measurements where carried out in a K100MK2 tensiometer from Krüss company. In order to have consistent results a good packing reproducibility of the powder has to be ensured. For the samples used in this study the column was filled with an amount about 0.1g. Tapping of the cylinder while filling it is necessary in order to try to obtain reproducible conditions.

In order to obtain the energy parameters a modified Washburn following the next equations was used:

$$t = \frac{h}{c r^2 s \cos q} \cdot m^2 \qquad \text{Eq. 5.8}$$

were
t= time
? = probe liquid viscosity
m= mass uptake
? = probe liquid density
s = probe liquid surface energy
? = Contact angle between the liquid and the powder
c = Constant for the measured powder

C, can be calculated using hexane as probe liquid, as it is assumed to wet all apolar surfaces and contact angle is taken as zero value. Once c is known contact angles can be calculated for other probe liquids with different polarities.

This measurement has been successfully applied when measuring the surface energy of Carbon single fibers, as K. Tsutsumi and Coworkers did after oxidation both with wet (HNO_3) and dry ($O_2/N_{2\ gas}$) techniques. They determined that although the dispersive components were more or less stable to the treatment, the polar component increased with the number of oxygen containing groups on the surface (K. Tsutsumi et al. 1990). Later on, they also modified the carbon fibers using plasma at low pressure for mixtures of CF_4 and O_2. The specific energy component increases with increasing oxygen content in the mixture (40 to 60% of O_2 range), while the dispersive component stays stable as for the already presented treatments. When CF_4 is present in the plasma composition above 60 % than both components trend to decrease, although the decrease is more noticeable for the specific component (K.Tstutsumi et al. 1996)

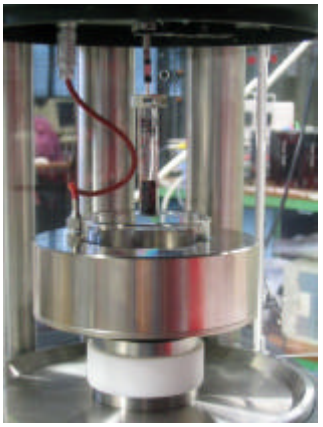

Fig.5.73. Tensiometer picture

However, as it can be seen in fig. 5.74, in the case of the present fluffy CB it was not possible to obtain a smooth reproducible curve from which the c value could be calculated. Fig. 5.74 at the bottom shows the smooth desired curve obtained for a silica test. In the case of CB and due to its low apparent density (CB was used in fluffy state) the powder column starts to break apart when the liquid starts to rise throw the powder. Consequently the weight uptake does not present a constant velocity and the curve was not valid to calculate the energy levels. In an attempt to pack the powder more compactly to avoid the breaking, a flow of nitrogen was used to press the powder, although a visible decrease of the height of the powder column was observed, the test was in this case unsuccessful. This method has only been described for carbon fibers or carbon pellets.

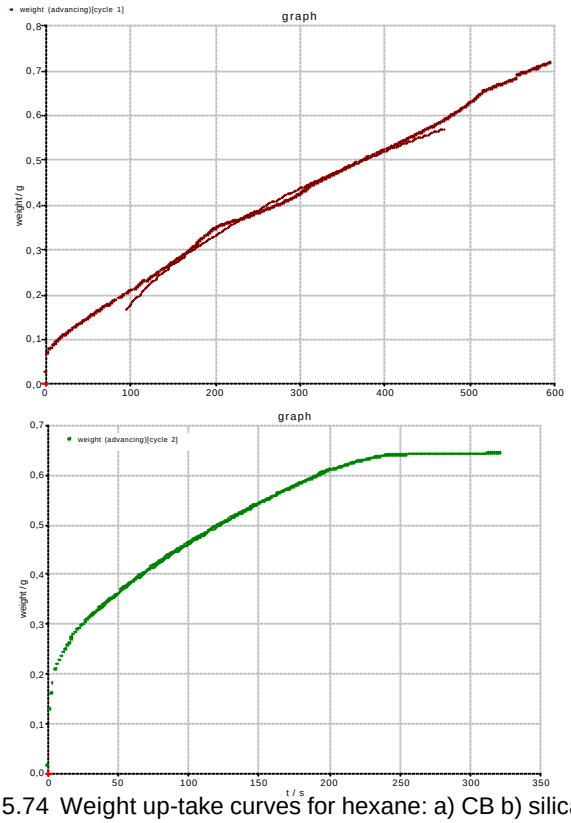

Fig. 5.74 Weight up-take curves for hexane: a) CB b) silica

As a conclusion it can be said that the use of capillary technique in order to measure the surface activity of very low density powders is not convenient due to the breakage of the powder column during the measurement and alternative methods need to be explored.

In order to find a solution for the exposed problem, contact angle was selected as alternative method in order to perform surface energy studies. The surface energy can be measured from the angle formed between the surface and a drop of a liquid probe as shown in fig. 5.75 following the Young equation. The angle itself is measured with the help of a CCD camera. Indices s and l stand for “solid” and “liquid”; the symbols s_s and s_l describe the surface tension components of the two phases; symbol ?sl represents the

interfacial tension between the two phases, and ? stands for the contact angle corresponding to the angle between vectors s_l and $?_{sl}$.

$$s_s = g_{sl} + s_l \cdot \cos q \qquad \text{Eq. 5.9}$$

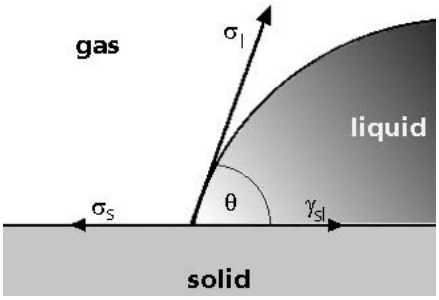

Fig.5.7 5 Scheme for the contact angle measurement (www.Krüss.com)

According to Owens, Wendt, Rabel And Kaelble (OWRK) which was the methodology used for the calculations of the presented experiments the surface tension of each phase can be split up into a polar and a disperse fraction:

$$s_l = s_l^D + s_l^P \qquad \text{Eq. 5.10}$$

$$s_s = s_s^D + s_s^P \qquad \text{Eq. 5.11}$$

OWRK method takes the empirically equation developed by Fowkes to calculate the dispersive component of a surface energy and extends it with the polar component (Fowkes 1964 and Fowkes 1980):

$$g_{sl} = s_s + s_l - 2\left(\sqrt{s_s^D + s_l^D} + \sqrt{s_s^P + s_l^P}\right) \qquad \text{Eq. 5.12}$$

Combination of the above equation with the Young equation (eq.5.9) is used to solve the system transposing the obtained equation to the one for a straight line the result being eq. 5.13:

$$\frac{(1+\cos q)\cdot s_l}{\sqrt{s_l^D}} = \sqrt{s_s^P}\cdot\sqrt{\frac{s_l^P}{s_l^D}} + s_s^D \qquad \text{Eq.5.13}$$

An example of the represented graphic in order to obtain the solid surface energy by means of using the OWRK approach is presented in fig.76.

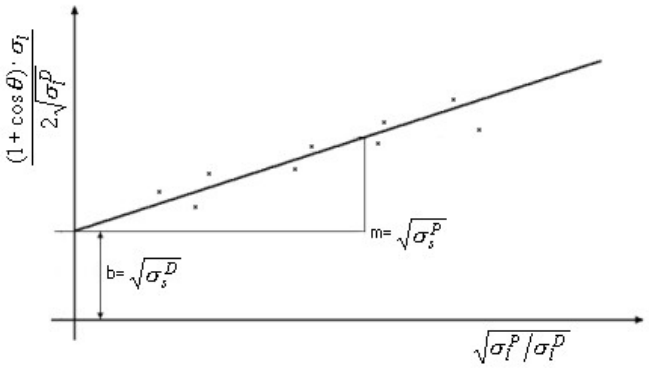

Fig.5. 76 Determination of the polar component by using the OWRK approach

A minimum of two liquid probes therefore are needed to be able to obtain an energy value for the dispersive and specific energy components of a surface, but more accurate values are obtained as the number of probes is increased. For this study water and glicerine where used. Although in some studies for CB surface energy diiodmethane is used as very apolar probe, in our case and probably once again to the fluffy state of the powder, the liquid was spread completely in all samples and it was not possible to measure the contact angle value. Values for energy parameters of the used liquids are presented in table 5.24

Table.5.2 4 Energy components for the liquid probes as determined by Ström et al.:

Liquid probe	g_l^D (mJ/m^2)	g_l^P (mJ/m^2)	g_l (mJ/m^2)
Water	**21.80**	**72.80**	**72.80**
Glicerine	**37.00**	**26.40**	**63.40**
Diiodmethane	**50.80**	**0**	**50.80**

The measurements were carried out in a from Krüss DSA100 which determines the contact angle ? by means of a CCD camera. The energy components were determined by the OWRK method explained above. In a first attempt a pellet of the fluffy CB was made by pressing it in a KBr press with a little amount of methanol. The pellet was dried for 3 hours at 100ºC. Also in this case the fine powder did not allow to make a correct measurement as the drop of the probe liquid was very rapidly adsorbed into the bulk without allowing a correct measurement of the contact angle. Although this method has been used by some research groups mixture of CB with some binding agent such as KI had to be used which probably could alter the obtained energy values (L.E. Cascarani de Torre et al. 1998).

Another approach was decided to be used to perform the contact angle measurements on the modified carbons. In this case CB was placed on a double side tape which was sticked on a glass surface. The CB powder was pressed on the tape and the powder which did not stick on the tape was removed by shaking the glass holder. When using

normal TESA tape on to stick the CB no uniformity was achieved and the tape surface had a very high influence. On the other hand, when using double side carbon adhesive tape, as the one used to obtain SEM images, a very homogeneous coating of the tape surface was observed. A minimum of 10 measurements in 5 different sample preparation (2x sample preparation) were obtained for each investigated sample. 5 µl of liquid were used to generate the drop on the sample surface.

As a first step, complete coverage of the tape by the CB powder was ensured by comparing the measurement of contact angle of the tape before coating and after coating with N-134 with both water and glicerine. The results are given in table 5.25 where it can be observed that while water gave a determined contact angle for the uncoated surface (116.6º) it was impossible to place a water drop on the surface of N-134 due to its high hydrophobicity. Therefore the influence of the tape after coating it with the CB powder can be considered minimal or absent. On the other hand the contact angle measurements for glicerine also show different value for the uncovered tape and the initial tape surface. It is also worth to notice that diiodmethane could be used in order to measure the contact angle on the tape surface, which could not be done once the tape was covered with CB as the liquid spread instantaneously.

Table.5.2 5 CA measurements and energetic components for the Carbon Tape

	Carbon Tape	N-134
CA water	**116.6**	**------**
CA glicerine	**122.1**	**130.4**
CA diiodemethane	**80.9**	**-------**
Dispersive component (mJ/m^2)	**149.26**	**-------**
Polar component (mJ/m^2)	**400.72**	**-------**
Total surface energy (mJ/m^2)	**549.98**	**-------**

Table 5.25 shows also the determination of the energy values for the uncoated tape surface. In this example, the surface energy of N134 could not be determined by using the OWRK method as no value for water contact angle could be obtained on N134 due to the impossibility to place a water droplet on its surface.

CA measurements were obtained for cold plasma treated plasmas on N-134, N134e and N134g, for oxygen (40W/15 min) nitrogen (40W/30 min) and ammonia (40W/30min) treatments. A picture of the obtained drops after placing CB on the tape can be observed in fig. 5.77.

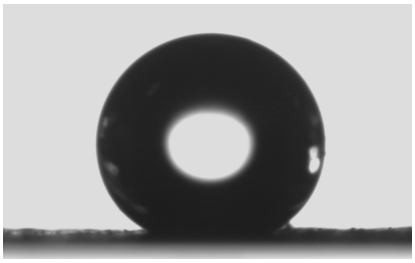

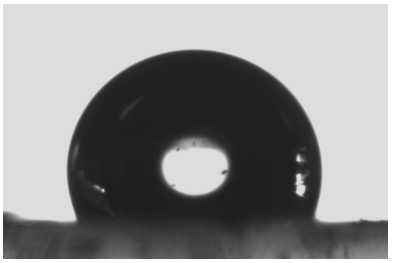

Fig.5.76 Contact angles (water right side and glicerine left) after APP treatment (N134_air_a)

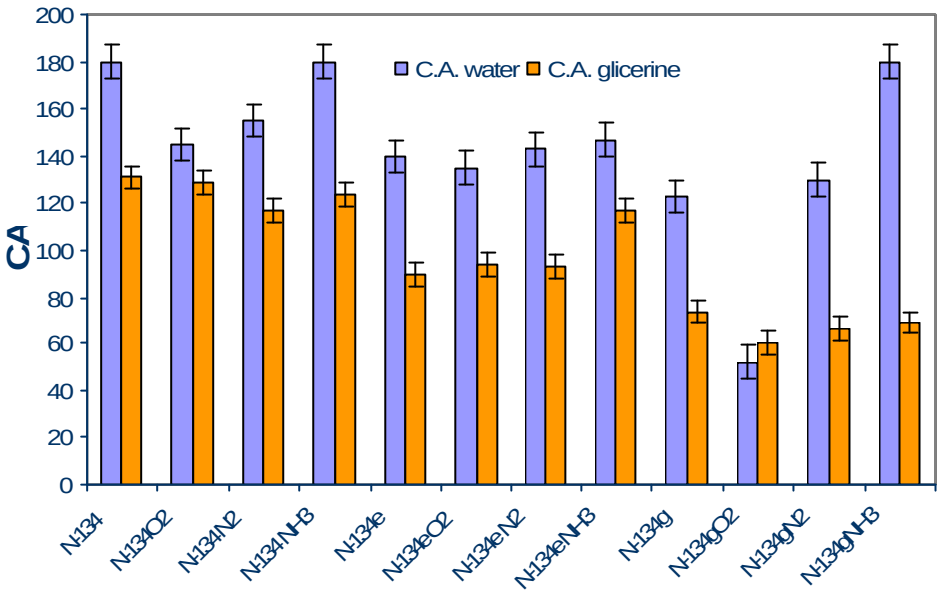

Fig.5.78 Contact angle measurements for N134 grades after LPP treatments

Fig.5.78 shows the obtained contact angles for N134 and its variation grades N134e and N134g. CA equal to 180 are shown when deposition of the water droplet was not successful due to the high hydrophobicity of the sample. In the case of original N134, the high hydrophobicity could be related to the impurities present on the surface of CB, as the form an oily coating which does not allow the contact of water with the CB surface.

Because both the extraction and graphitization pretreatments could have produced aggregation phenomena which could give some alteration of the CA measurement, it seems difficult to compare the results among the three different N134 types. In order to minimize this effect the CB samples where grinded before the CA measurements after both graphitization and extraction as they were also before plasma modification.

In order to compare the size of the final material the particle size was analyzed by means of a particle size analyzer (Saturn from Micromeretics). Because this system uses preferably water to disperse the powder during the analysis, the oxidized blacks where used to compare de size of N134, N134g and N134e. In order to ensure a good dispersion of the CB some tensoactive was added to the dispersing media. In annex 6 more information about the experiment can be found as well as the results for these CB's.

As summary it can be said that for N134 all particles (probably aggregates and agglomerates) where found to be smaller than 10 microns. On the other hand for N134e and N134g all particles were found to be larger than 40 microns. Due to this difference in particle size it seems difficult to compare the CA results as the particle size difference could cause some changes in roughness and surface coverage.

One of the first observed results is that after oxygen and nitrogen LPP treatments it is possible to measure the water CA. This is a first indication that the plasma treatment has affected the surface energy of the original N134. However, ammonia LPP did not produce such effect.

As general trend it can be observed that all oxygen low pressure plasma treatment caused a decrease of CA, especially in the case of N134g where this difference is much larger. This result shows once again the capacity of the oxygen plasma to attack the graphitic structures on the surface of CB as was already presented in the previous section. On the other hand, although may be not so evident, the CA measurement after NH_3 seems to increase specially for N134g or at least does not diminish the value for the water CA. Similar results were described after low pressure ammonia modification for CNF which are probably more similar to the structure of graphitized CB than to the one for regular CB (V. Brüsser et al. 2004).

Glicerine CA did not present such remarkable variation, being more or less constant after all presented treatments, the only case where a slight increase is shown is after ammonia plasma treatment for N134e which also showed previously a much higher modification from pH and basic equivalents values.

Using the above information, the energetic components where calculated by means of the OWRK approximation which has been already presented. In fig. 5.78 the values of both can be observed. As it can be seen N134, N134_NH_3 and N134g_NH_3 are missing as a result of having only one CA value which did not allow to make the corresponding calculations. As it has already been discussed this figure does not pretend to compare all CB's but the ones coming from the same N134 grade. As it can be seen when taken all CB's the total energy varies from 20 to 250 mJ/m^2. Although this variation could seem incorrect, it is possible to find in the literature values for CB energy covering all this range. Probably this does not indicate that the values are accurate but that much care has to be taken when comparing energetic values without taking into account the type of CB and morphological state.

For the N134 cold plasma treatments energy levels could only be calculated for oxygen and nitrogen plasma treatments. In this case, surface energy is not very different among these two samples although slightly lower values are detected for the oxygen plasma treated sample. On the other hand Table 5.26 presents the percentage of polar component referred to the total surface energy were it can be seen that slightly higher values are obtained for the oxygen LPP treated sample.

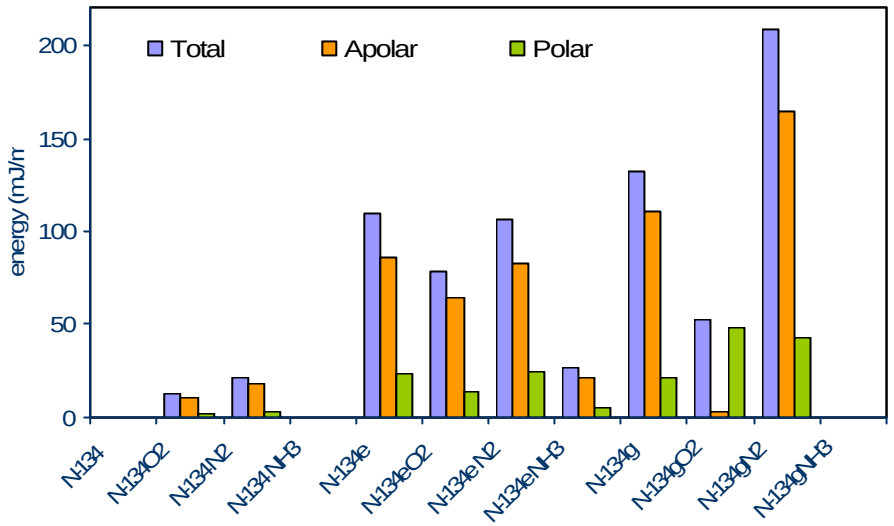

Fig.5.7 9 Surface energy components for N134 grades after LPP treatment

It is worth to mention that an increase for the dispersive energy component of CB surface was found by using C.A. after nitrogen modification by S.J. Park et al after nitrogen RF LPP (100% increase after 30min treatment), in our case it is difficult to compare due to the lack of energy values for the unmodified CB, but N134g does present a very high apolar energy which could be related to the mentioned fact. It is worth to remember that it has already been proposed from the results obtained in previous sections that nitrogen species could attack by ablation the surface of CB producing new high energy sites.

Table 5.26. Percentage of specific energy component

CB	% polar surface energy
N134_O_2_c	**10**
N134_N_2_c	**7.7**
N134e	**12.2**
N134e_O_2_c	**10.0**
N134e_N_2_c	**12.8**
N134e_NH_3_c	**10.1**
N134g	**8.6**
N134g_O_2_c	**86.7**

N134g_N_2_c	**11.5**
N134g_NH_3_c	**10.0**

In the case of extracted N134, ammonia total energy components present an abnormal behavior when compared to the rest of the values. Worth to remember that the ammonia LPP N134e was also the sample for which an increase of basic groups and pH increase was detected. However, these results did not translate in a higher specific energy component but in a total diminishing of the surface energy.

Finally for N134g it is observed that once again, the oxygen plasma treatment although presents a lower value for total surface energy, the percentage of the polar component versus total energy increases up to an 86%. Therefore it seems that oxygen plasma does affect the polar component of graphitic structures in a much higher extend than for amorphous or crystallite edges. On the other hand nitrogen treatment seems to cause an increase of the total surface energy with much influence on the apolar component of the surface energy which is also in accordance with the creation of new active sites due to ablation.

In order to determine whether there exists a relation between the surface crystallinity and the final surface dispersive energy a plot representing the dispersive component versus Lc before and after LPP for N134g is presented in Fig. 5. 80. It can be shown that a linear correlation was found between the increase in L_c and the dispersive surface energy.

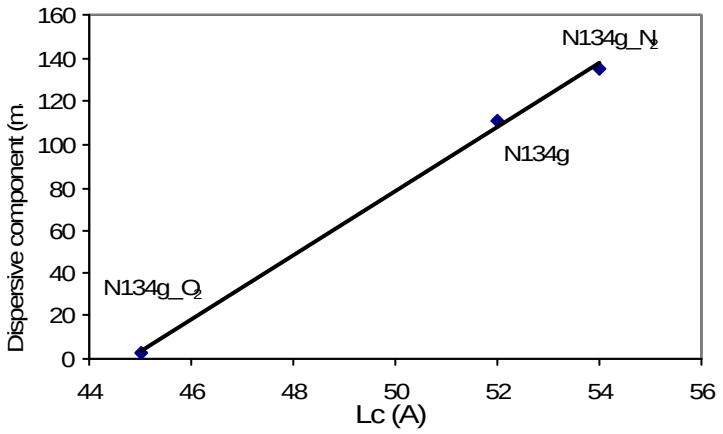

Fig.5.80 Relation between the surface energy dispersive component and the crystallite dimension Lc

An opposite relation was found by Wang and coworkers for dry-pelletized regular CB-grades, for which increasing Lc gave decreasing dispersive component. The effect is explained due to a lower crystallite edge number present on the CB surface which are considered the high active dispersive sites. However, Lc is not related to the dimension of crystallite but to their stacking height and therefore a higher stacking height may represent a larger vertical area for dispersive interactions. (Wang et al. 1991). Although it is more difficult to present the results for N134 as its dispersive component could not be calculated due to its high hydrophobicity, the trend followed by the low pressure plasma with oxygen and nitrogen also follow the same trend (Fig. 5.80)

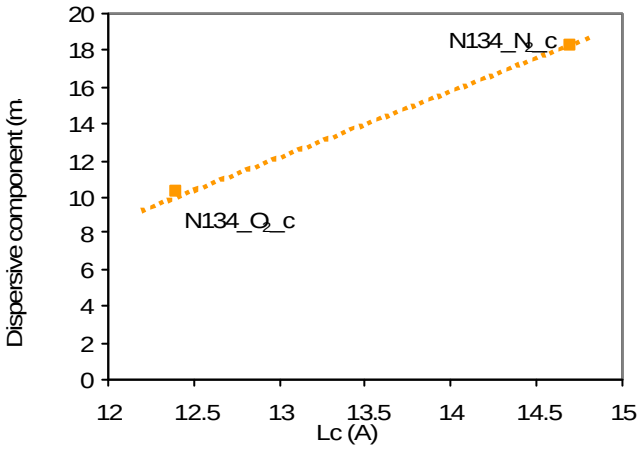

Fig. 5.80 Relation between the surface energy dispersive component and the crystallite dimension Lc

As it has been shown contact angle was able to reveal energetic changes on the surface of N134. Once more the effect of cold plasma was observed to be dependent on the initial carbon surface and composition. The presence of the impurity layer prevented the water CA to be measured on CB, however, the measurement could be done after treating with oxygen and nitrogen LPP.

Once again relevant changes were observed for oxygen treatment on N134g indicating the high reactivity of oxygen plasma species on this surface. Nitrogen plasma treatment was observed to change the dispersive component of the surface energy which is probably related to the ablation processes and formation of new microporous as shown in previous results.

5.5.2 Inverse Gas Chromatography (IGC)

As it has been presented, wet energy measurements involving contact angle measurements are difficult to implement reproducibly on free flowing powders since they usually involve a compression of the powder, which can change its surface characteristics or an irregular packing of columns when using tensiometer measurements. They can also be strongly affected by the particle size and pore geometry. Moreover, only a limited number of probe molecules can be used by either wettability method since the formation of a contact angle is required and many potentially interesting probe molecules spread on the relative highly energetic surfaces as is the case of CB. Another problem of wettability methods is the absorption of liquid in the bulk which would lead to an overestimation of the surface energy.

As an alternative, Inverse Gas Chromatography was shown in the literature to be a versatile and extremely sensitive technique for the determination of surface thermodynamic properties such as the surface energy. This approach inverts the conventional relationship between mobile and stationary phase found in analytical chromatography. The stronger the interaction, the more energetic the surface and the longer the retention time. For this reason thermodynamic parameters can be derived from the retention behaviour. In contrast to wetting methods this technique involves neither liquid wetting nor compression of particles.

Inverse Gas Chromatography (IGC) is a very sensitive and accurate way of determining dispersive and specific interactions and has several benefits over common wettability techniques. In this study two different concepts (van Oss and Gutmann) have been applied to study the acid-base properties of three different types of XPB 171 modified with atmospheric plasma techniques. Samples were selected due to the improvement observed after such treatments for oxygen reduction catalyst as it will presented in chapter 7. The dispersive energy component was also studied. For these purposes IGC measurements have been carried out under infinite dilution conditions. In this low concentration range only a few probe molecules interact with the high-energy sites on the surface of a solid. Parameters obtained under these conditions are highly sensitive and can reflect small changes on the surface.

Determination of the dispersive component by IGC

The free energy of adsorption for a given probe can be related to the net retention volume of the probes inside the column with the following equation.

$$\Delta G_A = -R \cdot T \cdot Ln(V_N) \qquad \text{Eq.5.14}$$

Were R corresponds to the ideal gases constant (8.31451 $JK^{1}mol^{1}$) and T is the column temperature (K). The net retention volume (V_N), the volume of mobile phase to elute the probe from the column, is given by:

$$V_N = F \cdot D \cdot (t_R - t_0) \qquad \text{Eq.5.15}$$

Where F corresponds to the mobile phase flow ($cm^3 \cdot min^{-1}$), t_R is the retention time of the probe, t_0 the retention time of an inert probe co-injected with the sample probe and D is the Jeams-Martin correction factor due to the gases compressibility given by:

$$D = \frac{3 \cdot \left[\left(\frac{P_i}{P_0} \right)^2 - 1 \right]}{2 \cdot \left[\left(\frac{P_i}{P_0} \right)^3 - 1 \right]} \qquad \text{Eq.5.16}$$

Where P_i and P_0 are the pressure at the inlet and outlet of the column respectively.

Usually, the adsorption free energies variations of n alkanes (given by equation 5.17), versus the number of C atoms they contain are lineal, and allow to define the so-called “alkane line”. The slope of this line corresponds to the free energy of adsorption of the methylene group, $\Delta G_A(CH_2)$, given by equation:

$$\Delta G_A(CH_2) = -R \cdot T \cdot Ln\left(\frac{V_N[n]}{V_N[n+1]} \right) \qquad \text{eq.5.17}$$

Where $V_N[n]$ and $V_N[n+1]$ are the retention volumes of two alkanes with n and n+1 carbon atoms in their chain.

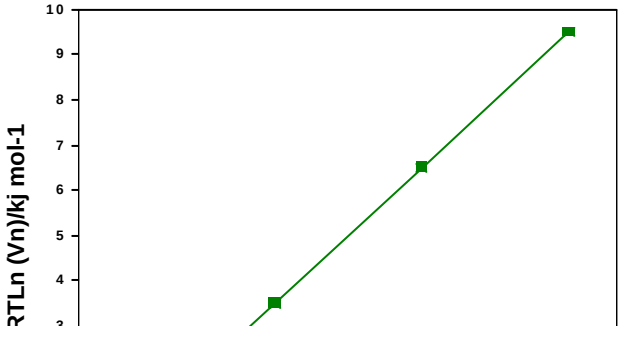

Fig. 5.8 1 Correlation to obtain the dispersive energetic component

The methylene adsorption energy, from Doris & Gray correlation (D.M. Doris and D.G Gray, 1980) can also be defined as:

$$\Delta G_A = 2 \cdot N_A \cdot a[CH_2] \cdot \sqrt{g_S^D \cdot g_S[CH_2]} \qquad \text{eq.5.18}$$

Where N_A is the Avogadro's number, a[CH_2] is the surface area covered by one methyl group (0.06nm^2) and $g_s[CH_2]$ is the free surface energy of a surface consisting of methylene groups, i.e. polyethylene, given by:

$$g_s[CH_2] = 35.6 + 0.058 \cdot (20 - T) \quad \text{in mJ/m}^2 \qquad \text{eq.5.19}$$

Where T is the column temperature in ºC.

Thus, using the experimentally determined values of V_N[n] and V_N[n+1], the dispersion component of the surface free energy g_s^d may be calculated.

In the present case the following apolar probes have been used in order to determine the apolar component: hexane, heptane, octane, nonane. In order to study the specific component: acetonitrile, ethanol, dichlormethane, acetone and ethyl acetate. A 30cm c 4mm ID column was filled with 1,5-5mg CB. Before measurement, samples were pre-conditioned for 2 hours at 200ºC and 0% humidity under nitrogen to remove physisorbed water. Experiments were carried out on an SMS-iGC 2000 instrument.

Column temperature was set at 110º C. Two samples of each CB were analyzed, reproducibility was found to be always higher than 3%.

The dispersive component obtained from the alkane probes injection is presented in Fig.5.82:

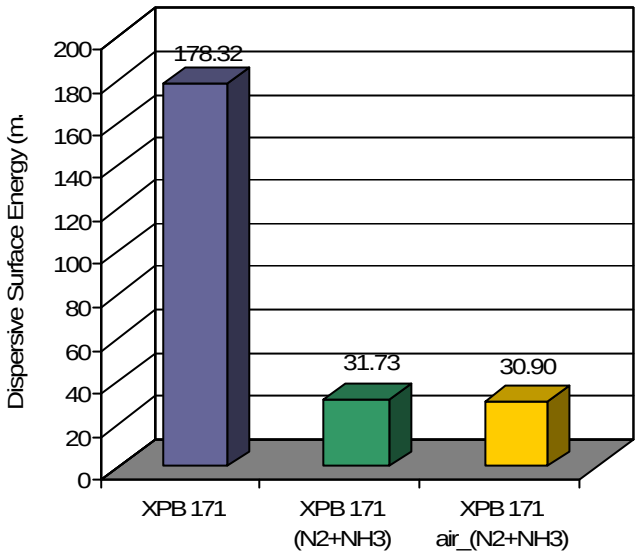

Fig. 5.8 2 Dispersive surface energy for XPB171 APP treated grades

As it can be seen in the figure above, the dispersive component for the presented XPB171 samples decreases dramatically after the treatment with atmospheric plasma, both with nitrogen plasma and ammonia post injection, as well as when the former treatment is preceded from an air plasma oxidation.

Specific Energy Component determination by IGC

If polar probe molecules are also injected in to the column, then specific interactions can be measured. The experimental points for the polar probe molecules are located above the alkane straight line in the surface energy plot. The distance between each point and the straight line represents the specific contribution of the interaction, which is expressed as the specific free energy (fig.5.83).

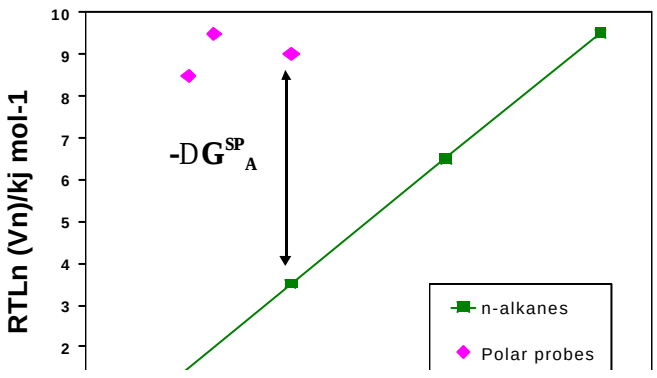

Fig. 5.8 3 Determinationof the polar surface energy by IGC

The specific component can be converted into acid-base parameters if acid-base concepts are applied. Several approaches have been suggested over the years, most of them based on the Lewis acid-base concept, where the base is the electron-donating part while the acid is accepting electrons. These concepts assume that certain orbitals are shared and interactions do not involve complete electron transfers. Two of the most used approaches to describe this kind of interaction are the Gutmann and van Oss concept.

The Gutmann approach involves a simple four-parameter equation, with an acid and base term for each interaction partner according to the following equation:

$$\Delta G \approx \Delta H = K_A * DN + K_B * AN \qquad \text{eq.5.20}$$

K_A is the acceptor (acid) number and K_B is the donor (base) number of the solid surface. DN and AN* are the donor and acceptor numbers of the vapour probe molecule, which are available from the literature. A detailed description how DN and AN* have been determined can be found elsewhere (P. Mukhopadhyay et al. 1995). By representing $\Delta G/AN$ *vs.* DN/AN, K_A and K_B can be determined as the slope and the intercept of a straight line.

On the other hand Van Oss subdivided this specific term of the surface energy into two non-additive parameters γ^+ and γ^- representing the electron acceptor and donor properties, respectively:

$$g_{SP} = 2 \cdot \sqrt{g^+ \cdot g^-} \qquad \text{eq.5.21}$$

The acceptor and donor parameters are related to the specific free energy by equation 5.22:

$$\Delta G = N_A * a * 2 * ((\gamma_L^+ * \gamma_S^-)_{1/2} + (\gamma_L^- * \gamma_S^+)_{1/2}) \qquad \text{eq.5.22}$$

Where a corresponds to the cross-section area of the injected probe and N_A the Avogadro number. When the γ_L^- and γ_L^+ values are known the acid-base parameters of the surface

can be calculated. A detailed description how γ_{L^-} and γ_{L^+} have been determined can be found at the work performed by C. van Oss and coworkers (C. van Oss et a. 1988).

Fig. 5.84 presents the values for the free energy of desorption (-?G_A) for several probes: acetonitril, dichloromethane, ethanol, ethylacetate and acetone for the three XPB171 samples.

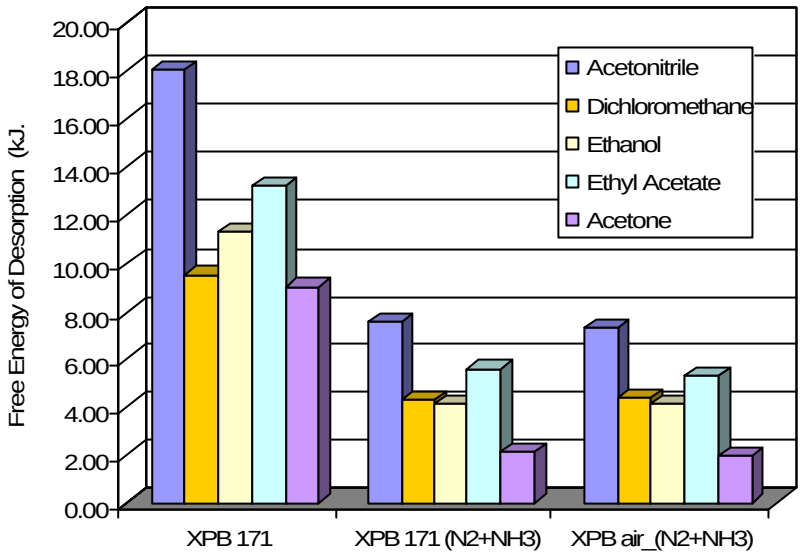

Fig.5.84 free desoption energy for polar probes

As it can be shown in fig.5.84 the free energy of desorption for polar probes decrease very significantly after the plasma treatment due to a lower retention of the polar probes on the CB surface. This is an indication that, as it was observed for the dispersive component also the specific energy of the surface has decreased. It is however interesting to notice that the results are very similar for the two treated samples, the one including air plasma pretreatment and the one without, which indicates that the final surface have similar polarity. In this case is very interesting worth to calculate the acid-basic properties by means of the Van Oss and Gutman approaches that have been presented.

K_A and K_B have been calculated using eq 5.20. and the AN and DN values for the presented probes in fig.5.84. which are presented in table 5.27.

Table.5.2 7 AN and DN values fort he used probes to obtain Gutman numbers

	AN	**DN**	
Acetonitrile	**4.7**	**14.1**	**Amphoteric**
Dichloromethane	**1.8**	**----**	**Acidic**
Ethanol	**10.3**	**19**	**Amphoteric**

Ethyl acetate	**1.5**	**17.1**	**Amphoteric**
Acetone	**2.5**	**17**	**Amphoteric**

Gutman obtained acid-base numbers

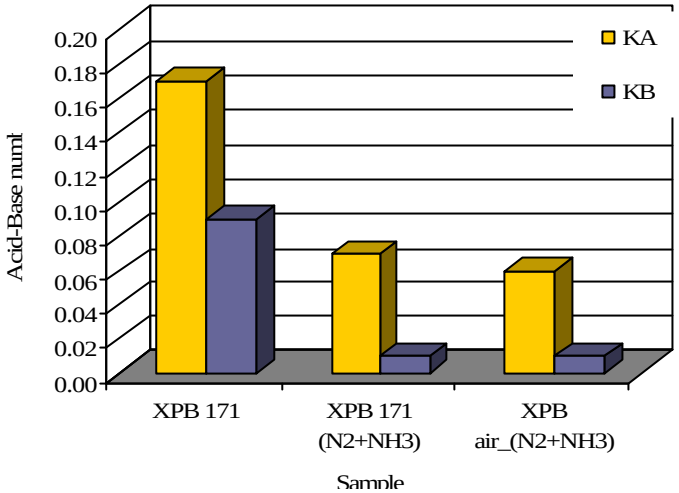

Fig.5.85 Gutman acid-base numbers

The results show that the initial surface, although mainly acidic also presents an important number of basic sites, therefore it could be said that is a rather amphoteric surface. On the other hand, the surface of the plasma modified XPB171 seem to have a much important acidic component even when the sample is not pretreated with air plasma. This effect can also be seen in table 5.28 where the percentage of acidity on the total specific component is presented.

Table.5.2 8 Percentage of KA vs. KB

CB	KA/(KA+KB) *100
XPB171	65.38
XPB 171_(N_2+NH_3)_a	87.50
XPB 171_air_(N_2+NH_3)_a	85.71

Any type of probe, acid, basic or amphoteric can be used in order to calculate the acid-base Gutman's number presented above, however, that is not the case when calculating the donor-acceptor numbers for the van Oss concept and amphoteric molecules should be avoided. For this reason, values for γ_S^- *and* γ_S^+ have been obtained with the monopolar probe molecules dicholomethane and ethyl acetate.

Literature parameters for calculation of Van Oss donor/acceptor values are presented in Table 5. 29

Table.5.29 Van Oss donor acceptor values (C.Della Volpe et al. 2000)

Literature Values		
Probe	DCM	Ethyl Acetate
γ^+_l (mJ/m^2)	124.58	0.00
γ^-_l (mJ/m^2)	0.00	475.67
γ^t_l (mJ/m^2)	28.60	23.90
γ^d_l (mJ/m^2)	26.50	20.50
γ^p_l (mJ/m^2)	2.10	3.40
x-sectional area (m^2)	2.45E-19	3.30E-19

Using the parameters above the following values were obtained by means of Eq.5.22 :

Table.5.30 Van Oss values for surface energy components

CB	g^+_s (mJ/m^2)	g^-_s (mJ/m^2)	g^P_s (mJ/m^2)
XPB 171	**2.32**	**8.41**	**8.84**
XPB 171 (N2+NH3)	**0.41**	**1.70**	**1.68**
XPB air_(N2+NH3)	**0.37**	**1.77**	**1.62**

In this case also a decrease of both parameters donor and acceptor is observed for the atmospheric plasma treated samples. However, it can be seen that for the XPB171 pre-treated with air plasma the donor component is slightly higher probably due to the presence of more acid groups, while for the sample without pretreatment the acceptor number is slightly higher indicating the presence of more basic type groups.

The advantage of the van Oss approach is that a value for the specific component can be calculated by means of eq. 5.22 while the acid-base number of Gutman's approximation have no units and only are used to compare the properties without absolute value. A final figure where both the dispersive and the polar component are shown is presented, it is once again observed that both atmospheric treated samples present lower surface energy than the original CB with very similar levels for both treatments.

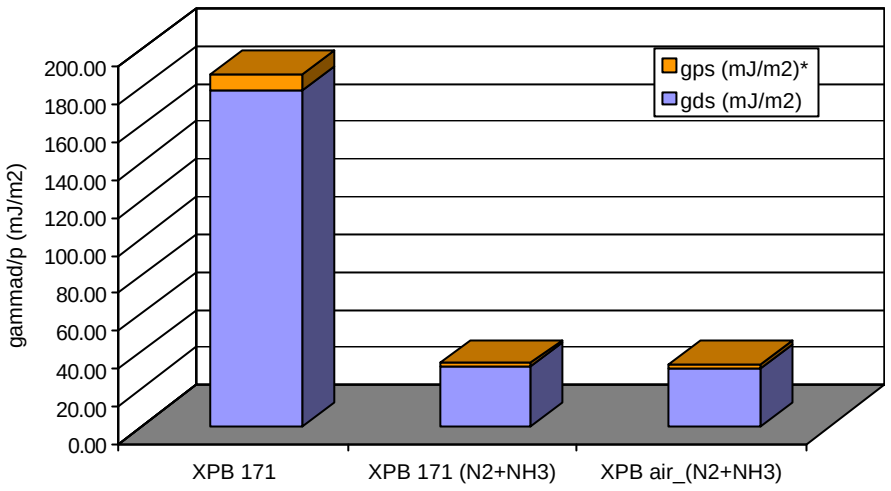

Fig.5.86 Surface Energy determined by Van Oss theory for XPB171 APP modified CB

Although no previous measurements have been found in literature for APP treated CB by IGC measurements it was found that after microwave plasma treatment on N550g, the dispersive component is decreased after ammonia plasma treatment, for argon stays the same and for air increases (180 to 300mJ/m^2). In the same study N was detected for the ammonia treated sample (W.Wang et al.1993). Therefore a decrease in surface energy does not mean that CB surface composition may not include nitrogen species after the treatment as it has also been shown in this work. The dispersive component of CB was also not modified when using n-butyl alcohol and n-butyl-amine as reactive species in a microwave plasma at 50W for 30min. All measurements were found around 130 and 138mJ/m^2. In the same study K_A and K_B were also determined, only butyl-alcohol plasma was able to increase K_A, no increase of K_B was found for any of the treatments (J.B. Donnet et al. 1992)

Concluding the chapter for CB characterization after LPP and APP treatments, it has been shown that both structure and chemical composition have been changed during both treatments. While LPP are more dependent on CB initial properties such as impurity presence, crystallinity or microporosity, APP seem not to present such relation. This difference is probably attributed to a higher reactivity of the present species in and to a higher temperature during modification in the APP system. In both cases modification did not cause relevant changes in surface morphology such as specific surface area which indicates that the effect of the treatment is located in the very first layers of the CB. Such low range modifications can be very interesting in order to improve the behavior of CB in final applications as will be evaluate din the next two chapters.

REFERENCES:

- V.Brüser, M.Heintze, W. Brandl, G.Marginean, H.Bubert, Surface modification of carbon nanofibres in low temperature plasmas. Diamond and Related Materials 13 (2004) 177

- J.B.Donnet, E. Custodero, T.K. Wang, G. Hennebert, Energy site distribution of carbon black surfaces by inverse gas chromatography at finite concentration conditions. Carbon 40 (2002) 163

- J.B. Donnet, S.J. PArk and M. Brendle, The effect of microwave plasma treatment on the surface energy of graphite as measured by inverse gas chromatography, Carbon 30 (1992) 263

- G.M. Doris and D.G. Gray , títol Journal of Colloid and Interface science 71 (1979)93

- J. F. Evans and Th. Kuwana, Introduction of Functional groups onto Carbon Elctrodes via treatment with Radiofrequency Plasmas, Analytical Chemistry 51 (1979) 358

- P.F. Fanning and M.A. Vannice A Drifts study of the formation of surface groups on carbon black by oxidation carbon 31 (1993) 721

- P. Favia; N. De Vietro,; R. Di Mundo,; F. Fracassi,; R.d'Agostino, Tuning the acid/base surface character of carbonaceous materials by means of cold plasma treatments. Plasma Processes and Polymers 3 (2006) 66

- F.M. Fowkes, Atractive forces at interfaces, Industrial ENgineering CHemistry 56 (1964) 40

- F M. Fowkes Surface effects of anisotropic London dispersion forces in n-alkanes. *J. Phys. Chem* 84 (1980) 510

- R.E. Franklin, Influence of the bonding electrons on the scattering of X-rays by carbon. Nature 165 (1950) 4185

- J. Froehlich, ; S. Kreitmeier, D.Goeritz, Surface characterization of carbon blacks. Kautschuk Gummi Kunststoffe 51 (1998) 370

- Y. Gao, I. Kueaots, X. Chen, R. Aggarwal, A. Mehta, E.M. Suuberg, R.H. Hurt, Ozonation for the chemical modication of carbon surfaces in ash Fuel 80 (2001) 765

- M. Gerspacher, C.P. O'Farrel, L. Nikiel and H.H. Yang Furnace Carbon Black Characterization: Continuing Saga, Rubber Chemistry and technology 69 (any) 569

- M. Gerspacher C.P. O'Farrell and H.H. Yang, A Proposed Mechanism for the Reinforcement of Elastomers of elastomers in the Rubbery Plateau by Carbon Black Kautschuk Gummi Kunststoffe 47 (1994) 349

- M. Gerspacher , C.P. O'Farrel and W. A. Wampler, Alternate Approach to study Carbon Black Rubber World 26 (1995) 212

- M. Gerspacher and C.P. O'Farrel, Filler-Filler and Filler- Polymer Interactions as a Function of On-Rubber Carbon Black Dispersion, Kautschuk Gummi Kunststoffe 51 (1997) 488

- M. Gerspacher, C.P. O'Farrell, Energy at the Interface Tire Technology International, June (1999)

- V Gomez-Serrano, C. M. Gonzalez-GarciaM. L Gonzalez-Martin,. Nitrogen adsorption isotherms on carbonaceous materials. Comparison of BET and Langmuir surface areas. Powder Technology 116 (2001) 103

- V. Gomez-Serrano , P. M. Alvarez, J. Jaramilloa, Fernando J. Beltran Formation of oxygen complexes by ozonation of carbonaceousmaterials prepared from cherry stones I. Thermal effects Carbon 40 (2002) 513

- V. Gomez-Serrano ,P. M. Alvarez, J. Jaramillo,F. J. Beltran Formation of oxygen structures by ozonation of carbonaceousmaterials prepared from cherry stones
- II. Kinetic study Carbon 40 (2002) 523

- Goritz, H. Raab, and J. Frohlich and P.Maier Surface structure of carbon black and reinforcement. Rubber Chemistry and Technology 72 (1999) 929

- Graham Physical Adsorption on Low Energy Solids. II. Adsorption of Nitrogen, Argon, Carbon Tetrafluoride, and Ethane on Polypropylene Journal of Physical Chemistry 68 (1964) 2788

- T.C. Gruber, T.W. Zerda and M. Gerspacher, Raman studies of heat-treated carbon blacks , Carbon 32 (1994) 1377

- V. Gutmann Coordination chemistry of certain transition-metal ions. The role of the solvent *Coordination Chemistry Reviews*, *2, (1967*) *239*

- W.M Hess and C.R. Herd Carbon Black Science and Technology 2nd Edition ch. 3 p. 120 1993

- K. Huang, Q. Gao, L. Tang, Li-hua; Z. Zhu, C. Zhang, A comparison of surface morphology and chemistry of pyrolytic carbon blacks with commercial carbon blacks. Powder Technology 160 (2005) 190

- P. Izhik and N.B. Uriev, Surface properties and Specific features of structurization of disperse carbon black with different degrees of oxidation, Colloid Journal 5 (2002) 623

- J. Janzen Physicochemical Characterization of Carbon Black Rubber Chemistry and Technology 55 (1982) 668

- F. Jaouen, JP. Dodlet, M. Lefèvre, M. Cai, Heat-Treated Fe/N/C Catalysts for O_2 Electroreduction: Are Active Sites Hosted in Micropores? J. Phys. Chem. B110 (2006) 5553

  F. Jaouen, F. Charreteur and J.P. Dodelet Fe-Based Catalysts for Oxygen Reduction in PEMFCs Importance of the Disordered Phase of the Carbon Support Journal of The Electrochemical Society, 153 (2006) A689

-

- K. Kameagwa, K. Nishikubo, M. Kodama, Y: Adachi and H. Yoshida, Oxidative degradation of carbon blacks with nitric acid II. Formation of water soluble polynuclear aromatic compounds, Carbon 40 (2002) 1447.

- N. Krishnankutty abd M.A, Vannice Effect of pre-treatment of surface area, porosity and adsoption properties of carbon black, Chem Mater. 7 81995) 754

- M . Kurk M. Jaroniec and Y. Berznitzki Adsorption study of porous structure development in Carbon Blacks Journal of Colloid and Interface Science 182 (1996) 282

- M. Kruk, Z. Li, M. Jaroniec, W. Betz, Nitrogen Adsorption Study of Surface Properties of Graphitized Carbon Blacks. Langmuir 15 (1999)1435

- S. Kwon, R. Vidic, E. Borguet Enhancement of adsorption on graphite (HOPG) by modification of surface chemical functionality and morphology, Carbon 40 (2002) 2351

- A.Lapra E. Custodero N.Simon Characterization of Surface Organization by Nitrogen Adsorption Kautshuk Gummi Kunststoffe 57 (2004) 52

- Z. Li and M. Jaroniec, Comparative Studies od CB's by thermogravimetry and Nitrogen Adsorption, Journal of Colloid and Interface Science 210 (1999) 200

- I.H. Loh, R.E. Cohen, R.F. Baddour, Modification of carbon surface in cold plasmas, Journal of Materials Science 22 (1987) 2937

- P. Mukhopadhyay and H. P. Schreiber Aspects of acid-base interactions and use of inverse gas chromatography *Colloids and Surfaces A: Physicochemical and Engineering Aspects*, *100* (*1995*) *47*

- S. O'Kell, S. Pringle and C. Jones A study of the effects of Low Power Plasma Treatment on the graphite and highle oriented pyrolytic graphite (HOPG) Surfaces, Journal of Adhesion 56 (1996) 261

- T. I. T Okpalugo, P.Papakonstantinou, H.Murphy, J.Mclaughlin,; N. M. D. Brown, Oxidative functionalization of carbon nanotubes in atmospheric pressure filamentary dielectric barrier discharge (APDBD). Carbon 43 (2005) 2951

- Y. Otake and R. Jenkins, Characterization of oxygen-containing surface complexes created on microporous carbon by air and nitric acid treatment carbon 31 (1993) 109

- D. Pantea, H. Darmstadt, S. Kaliaguine, S. Blacher, Ch. Roy, Christian. Surface morphology of thermal, furnace and pyrolytic carbon blacks by nitrogen adsorption - relation to the electrical conductivity. Rubber Chemistry and Technology 75 (2002) 691

- Pantea, H. Darmstadt, S. Kaliaguine, Ch. Roy Electrical conductivity of conductive carbon blacks: influence of surface chemistry and topology Applied Surface Science 217 (2003) 181

- E. Papier and E. Guyon Contribution to the study of the surface goups on Carbons: acidimetric methods and formation of derivatives, Carbon 16 (1977)127

- Papirer, J. Dentzer, Sh. Li, J.B. Donnet, Surface groups on nitric acid oxidized carbon black samples determined by chemical and thermodesorption analyses. Carbon 29 (1991) 69

- E. Papier, R. Lacroix, and J. B. Donnet, Chemical modifications and surface properties of carbon blacks, Carbon 34 (1996)1521

- J.I. Paredes, A. Martinez-Alonso and J.M.D. Tascón Characterization of Microporosity and Mesoporosity in Carbonaceous Materials by Scanning Tunneling Microscopy Langmuir 17 (2001)474

- J. I. Paredes, A. Martinez-Alonso and J.M.D. Tascón, Early stages of plasma oxidation on high oriented pyrolitic graphite: Nanosclae Physicochemical Changes as Detected by Scanning Probe Microscopies, Langmuir 18 (2002) 4314

- J. I. Paredes, A. Martinez-Alonso and J.M.D. Tascón High resolution imaging of functional group distributions on carbon surface by tapping mode atomic force microscopy Chemmical Communications vol (2002) 1790

- S.J.Park, J.S. Kim, Role of Chemically Modified Carbon Black Surfaces in Enhancing Interfacial Adhesion between Carbon Black and Rubber in a Composite System. Journal of Colloid and Interface Science 232 (2000) 311

- S.J. Park and J.S. Kim Influence of Plasma Treatment on Microstructures and Acid-Base Surface Energetics of Nanostructured Carbon Blacks: N_2 Plasma Environment. Journal of Colloid and Interface Science 244 (2001) 336

- S.J. Park,; J.-S. Kim, Surface energy characterization of modified carbon blacks and its relationship to composites tearing properties. Journal of Adhesion Science and Technology), 15 (2001) 1443

- S.-J Park and J.-S Kim Modifications produced by electrochemical treatments on carbon blacks. Microstructures and mechanical interfacial properties. Carbon 39 (2001) 2011

- S.J.Park and M.Brendle London Dispersive Component of the Surface Free Energy and Surface Enthalpy Journal of Colloid and Interface Science, 188 (1997) 336

- S.J. Park, K.S. CHo, S.K. Ryu, Filler-elastomer interactions: influence of oxygen plasma teatment on surface and mechanicla properties of carbon black/rubber composites, Carbon 41(2003)1437

- S.J. Park, Ki-Sook Cho, Seung-Kon Ryu, Filler-Elastomer interactions: influence of oxygen plasma treatment on surface mechanical properties of carbon black/rubber composites, Carbon 41 (2003) 1437

- W. G: Peng, M. Strauss, T.Pieper, H.G. Kilian, X-ray diffraction and model calculation on carbon blacks 80 (1993) 419

- P. Pfeifer D. Avnir Chemistry in noninteger dimensions between two and three. I. Fractal theory of heterogeneous surfaces, Journal of Chemical Physics 79 (1983) 3558

- Poleunis, X. Vanden Eynde, e. Grivei, H. Smet, N. Probst and P. Bertrand, ToF-SIMS stydy of sulphur on Carbon Black surface, Surface and Interface Analysis, 30 (2000) 420

- H Raab,.; J Frohlich,.; D Goritz, Surface topography and its influence on the activity of carbon black. .Kautschuk Gummi Kunststoffe 53 (2000) 137

- Rivin, Surface Properties of carbons, Rubber Chemistry and Technology 44 (1971) 307

- D. Rivin, Use of lithium aluminum hydride in the study of surface chemistry of carbon black. Rubber Chemistry and Technology 36 (1963) 729

- M. A. Short and P. L. Walker Measurement of interlayer spacings and crystal sizes in turbostratic carbons Carbon, 1 (1963) 3

- G. J.; Schneider, A.Weigert,; A.Bergmann,; , H Raab.; D Goeritz, Surface and bulk structure of carbon black studied by scanning tunneling microscopy and wide angle scattering. . KGK, Kautschuk Gummi Kunststoffe 58 (2005) 570

- A.Schroder, M. Kluppel and R.H. Schuster.Characterization of the surface activity of furnace blacks. Part 1. Determination of the surface roughness by static gas adsorption monolayer regime. Kautschuk Gummi Kunststoffe 52 (1999) 814

- A.Schröder, M. Klüppel and RH. Schuster, Characterization of surface activity. Part 2. Determination of furnace blacks surface roughness by means of static gas adsorption multilayer regime Kautsch. Gummi kunststoffe, 53 (2000) 257

- M.L. Studebaker and R.W. Rinehart, Infrared studies of oxygen-containing groups on the surface of Carbon Black, Rubber Chemistry and Technology, 45 (1972) 106

- Stoeckli, A.Guillot, A.M. Slasli and D. Hugi-Cleary Microporosity in Carbon Blacks Carbon 40 (2002) 211

- K. Tsutsumi, S. Ishida and K. Shibata Determination of the surface free energy of modified carbon fibres and its relation to the work of adhesion, Colloid and Polymer Science 268 (1990) 31

- K. Tsutsumi K. Ban and K. Shibata, S. Okazaki and M. Kogoma Wettability and Adhesion Characterisctics of Plasma – Treated Carbon Fibres, Journal of Adhesion 57 (1996) 45

- V. Tvardovski and A. A. Fomkin Theory of Adsorption in Microporous Adsorbents *Journal of Colloid and Interface Science*, *198 (1998*) *296*

- T. Ungar, J. Gubiczaa, G. Ribarika, Cr. Panteab, T. W. Zerda Microstructure of carbon blacks determined by X-ray diffraction profile analysis Carbon 40 (2002) 937

- J. Van Oss, R. J. Good, M. K. Chaudhury Additive and nonadditive surface tension components and the interpretation of contact angles *Langmuir; 4 (*1988)884

- A.Vidal, W. Wang, J.B. Donnet, Study of surface activity of carbon black by inverse gas chromatography. Part I. Evolution of the surface properties of carbon blacks upon extraction Kautschuk Gummi Kunststoffe 46 (1993) 770

- M.J. Wang, S. Wolff, J.B. Donnet, titol, Rubber Chemistry and Technology 65 (1991) 714

- W.Wang, A.Vidal and J. -B Donnet, M.J. Wang, Study of surface activity of carbon black by inverse gas chromatography, Part III. Superficial plasma treatment of carbon black and its surface activity. Kautschuk Gummi Kunststoffe 46 (1993) 933

- W.D. Wang, B. Haidar, A.Vidal and J.B. Donnet, Study of Surface Activity of Carbon Black by Inverse gas Chromatography, Part IV: Effect of Mechanical Aaction on Surface Activity of Carbon Black, Kautschuk Gummi Kunststoffe 47 (1994) 238

- P.A. Webb and C. Orr, Analytical Methods in Fine Particle Technology, Micromeretics 1997
- S. Wolff, E.H. Tan, and J.B. Donnet, The effect of Filler Surface Energy on Dynamic Properties. Kautschuk Gummi Kunstoffe 47 (1994) 485

- S. Wolff, M. J. Wang E.H. Tan, Surface Energy of Fillers and its effect on Rubber Reinforcement Part 1 Kautschuk Gummi Kunststoffe 47 (1994) 873

- S. Wolff, M. J. Wang E.H. Tan, Surface Energy of Fillers and its effect on Rubber Reinforcement Part2 Kautschuk Gummi Kunststoffe 47 (1994) 780

- S. Wolff, Chemical aspects in rubber reinforcement by fillers, Rubber Chemistry and Technology, 69 (1996) 325

- Y. Xie, P. Sherwood, X-ray photoelectron-spectroscopic studies of carbon fiber surfaces. Part IX: the effect of microwave plasma treatment on carbon fiber surfaces. Applied Spectroscopy 43 (1989) 1153

- W. Xu, T. W Zerda, H. Yang and M. Gerspacher, Surface fractal dimension of graphitized Carbon Black particles, Carbon 34 (1996) 165

- H.X. You, N. M.N. Brown and K.F. Al-Assadi, The surface modification using argon radio-frequency plasmas of high oriented pyrolitic graphite: a sacanning tunnelling microscopy study Surface Science 279 (1992) 189

- T. W. Zerda, W. Xu h. Yang, M. Gerspacher The effects of heating and cooling rates on the structure of carbon black particles, Rubber Chemistry and Technology 71 (1998)1

- T.W. Zerda, H. Yang and M. Gerspacher, Rubber Chemistry and Technology 64 (1992)130